Supporting Information

Mechanistic insights into amine borane dehydrocoupling using dinuclear zirconocene complexes

Kevin Lindenau[a], Nora Jannsen[a], Mirko Rippke[a], Hanan Al Hamwi[a], Carmen Selle[a], Hans-Joachim Drexler[a], Anke Spannenberg[a], Matthias Sawall[b], Klaus Neymeyr[a,b], Detlef Heller[a], Fabian Reiß[a]*, and Torsten Beweries[a]*

[a] Leibniz-Institut für Katalyse e.V., Albert-Einstein-Str. 29a, 18059 Rostock, Germany,
fabian.reiss@catalysis.de, torsten.beweries@catalysis.de

[b] Universität Rostock, Institut für Mathematik, Universitätsplatz 1, 18055 Rostock, Germany

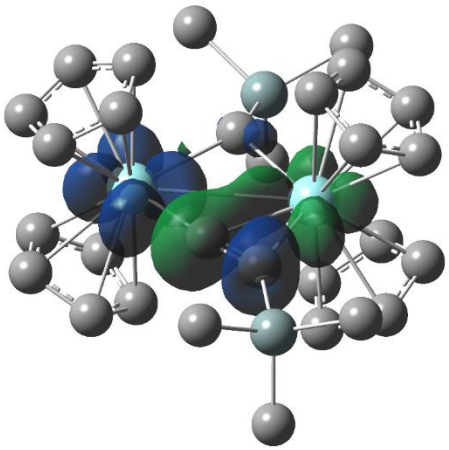

Content

1. Catalytic tests 2
2. Crystallographic details 5
3. Details of NMR spectroscopy 7
4. Details of UV/Vis spectroscopy 41
5. Details of vibrational spectroscopy 46
6. Computational details 52
7. References 69

1. Catalytic tests

1.1. Dehydrocoupling of $H_3B{\cdot}NMe_2H$ with 1/MeLi, variation of catalyst concentration

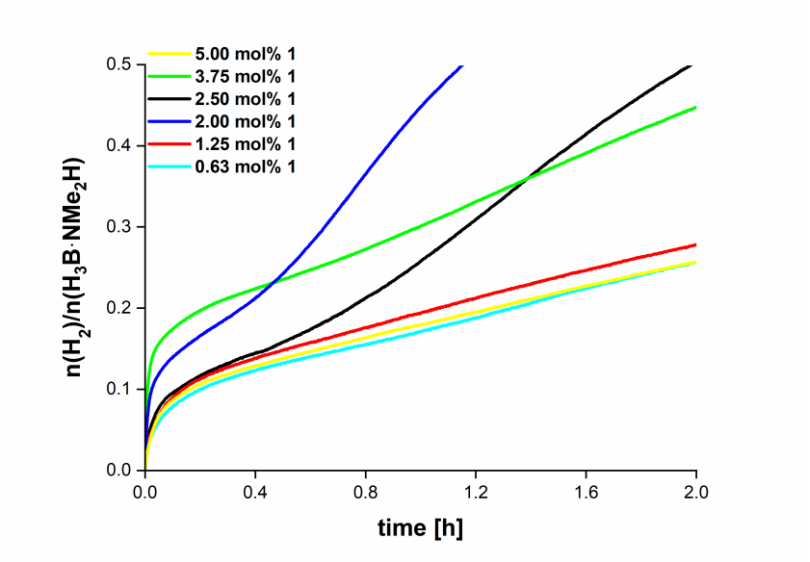

Figure S1. Enlargement of the volumetric curves (Figure 1) of dehydrocoupling of $H_3B{\cdot}NMe_2H$ with complex **1**/MeLi. Conditions: room temperature, toluene, [$H_3B{\cdot}NMe_2H$] = 0.33 M, 2.5 mol% **1**, 5.2 mol% MeLi.

1.2. Dehydrocoupling of $H_3B{\cdot}NMe_2H$ with 1/MeLi, colour changes

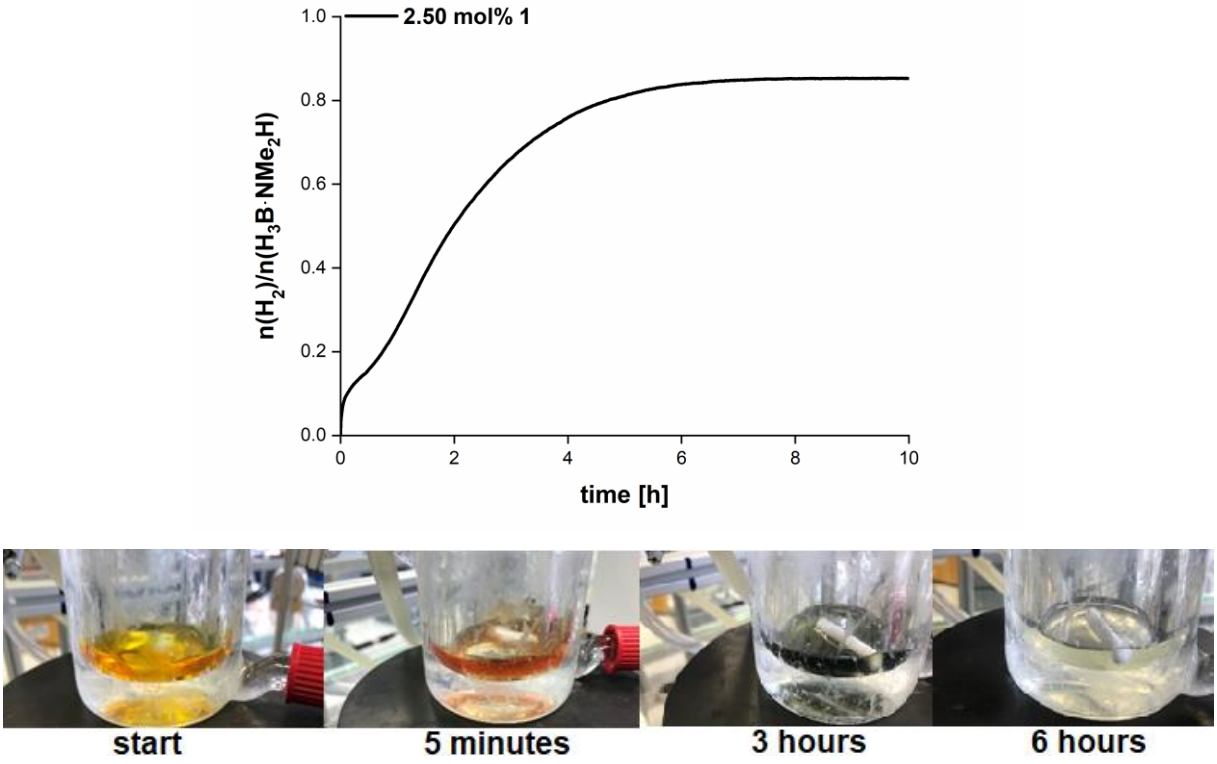

Figure S2. Observed colour changes in the dehydrocoupling of $H_3B{\cdot}NMe_2H$ with complex **1**/MeLi. Conditions: room temperature, toluene, [$H_3B{\cdot}NMe_2H$] = 0.33 M, 2.5 mol% **1**, 5.2 mol% MeLi.

1.3. Dehydrocoupling of $H_3B{\cdot}NMe_2H$ with 1/MeLi, variation of substrate concentration

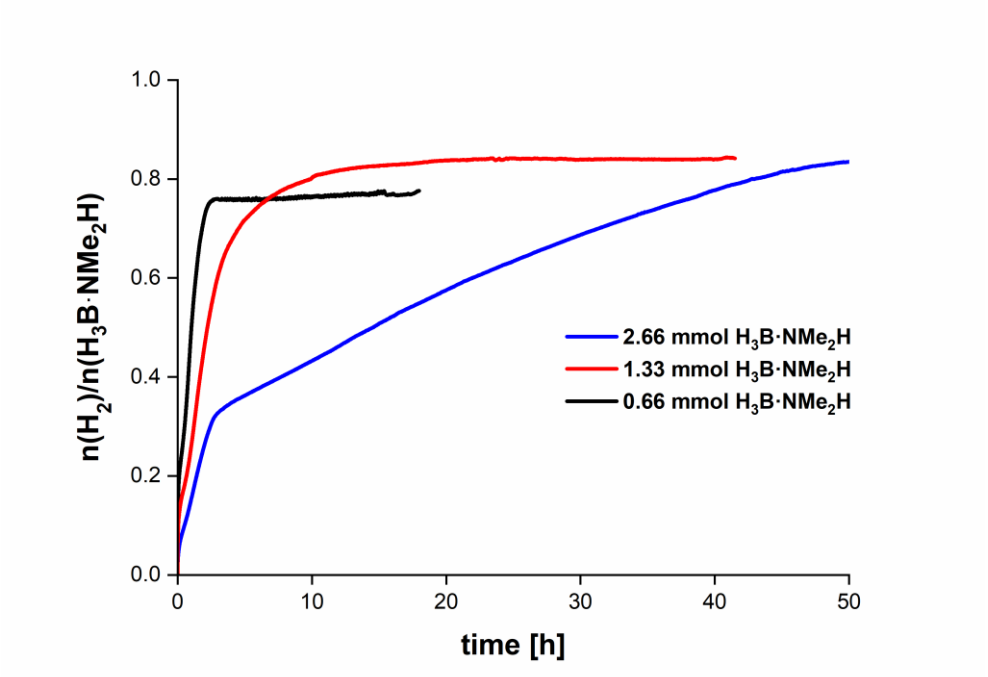

Figure S3. Volumetric curves of dehydrocoupling of $H_3B{\cdot}NMe_2H$ with complex **1**/MeLi using different substrate concentrations. Conditions: room temperature, toluene, 2.5 mol% **1**, 5.2 mol% MeLi.

1.4. Dehydrocoupling of $H_3B{\cdot}NMe_2H$ with 1/MeLi; THF inhibition experiments

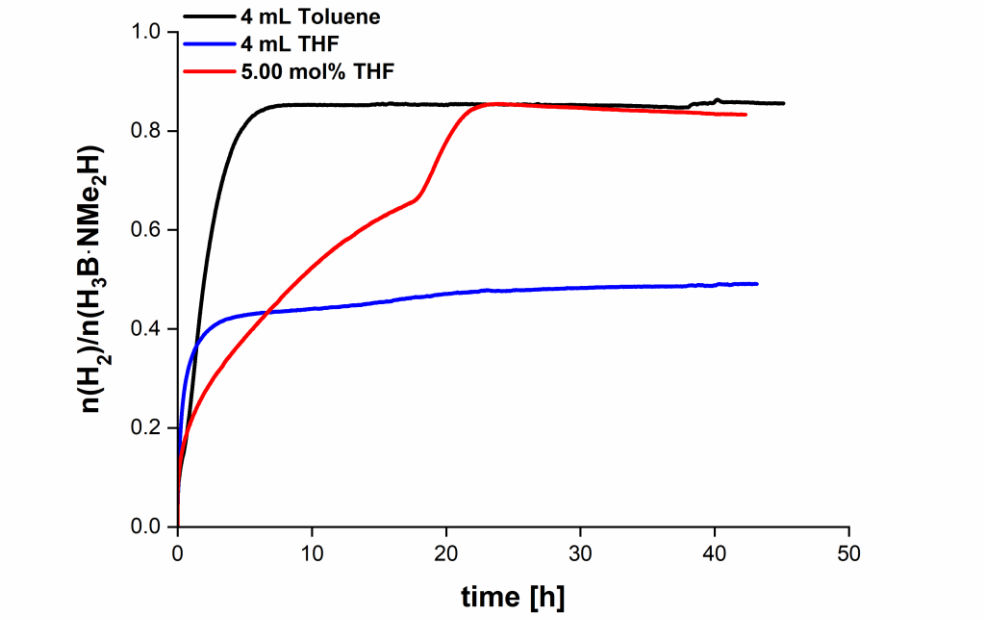

Figure S4. Volumetric curves of dehydrocoupling of $H_3B{\cdot}NMe_2H$ with complex **1**/MeLi. Conditions: room temperature, toluene, 2.5 mol% **1**, 5.2 mol% MeLi.

1.5. Comparison of dehydrocoupling of deuterated amine boranes with complex 1/MeLi

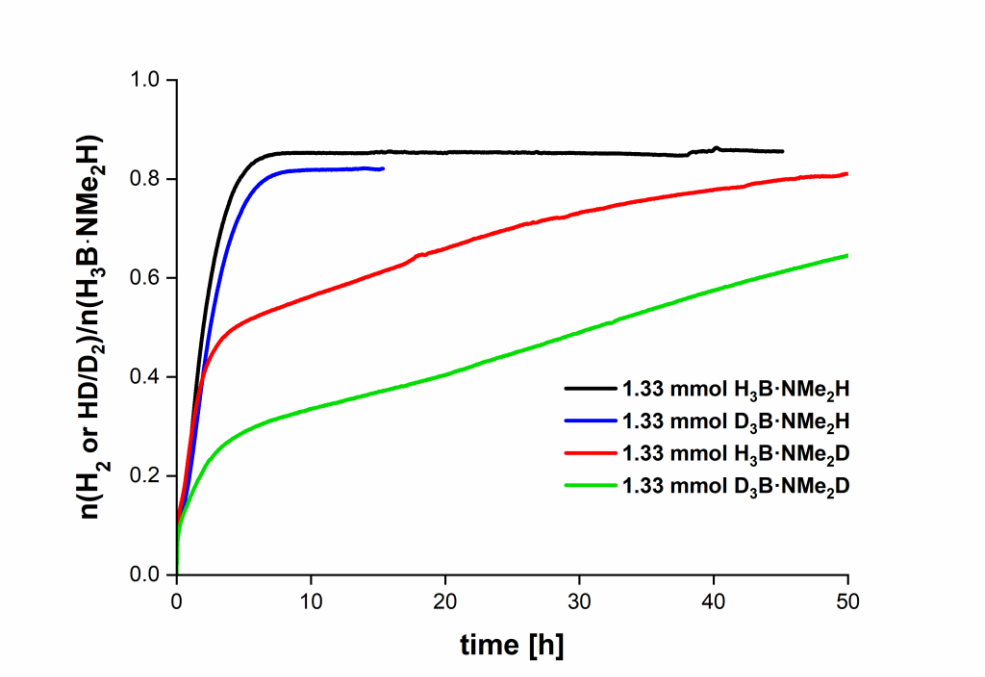

Figure S5. Volumetric curves of dehydrocoupling of deuterated amine boranes with complex **1**/MeLi. Conditions: room temperature, toluene, 2.5 mol% **1**, 5.2 mol% MeLi, [substrate] = 0.33 M.

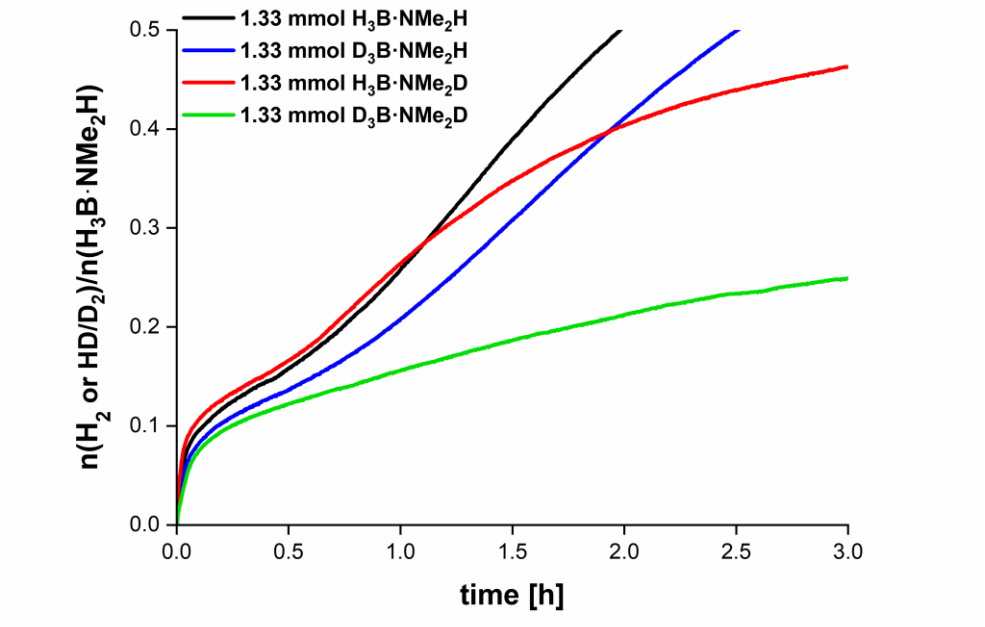

Figure S6. Enlargement of the volumetric curves (Figure S5) of dehydrocoupling of deuterated amine boranes with complex **1**/MeLi. Conditions: room temperature, toluene, 2.5 mol% **1**, 5.2 mol% MeLi, [substrate] = 0.33 M.

2. Crystallographic details

Table S1. Crystallographic details of **4** ,**5** ,**7** and **10**.

	4	**5**	**7**	**10**
Chem. Formula	$C_{33}H_{50}N_2Si_2Zr_2$	$C_{30.11}H_{41.33}C_{10.89}Si_2Zr_2$	$C_{29}H_{40}Si_2Zr_2$	$C_{33}H_{40}SiZr_2$
Form. Wght [g mol^{-1}]	713.37	673.45	627.23	647.18
Colour	yellow-orange	orange	red	red
Cryst. system	monoclinic	triclinic	triclinic	monoclinic
Space group	$P2_1/c$	$P\bar{1}$	$P\bar{1}$	$P2_1/n$
a [Å]	16.1662(15)	12.9147(8)	8.4309(6)	8.3405(2)
b [Å]	12.7556(12)	16.0454(11)	8.6096(6)	25.5764(6)
c [Å]	16.3557(15)	16.0971(10)	10.3197(8)	14.2103(4)
α [°]	90	73.455(3)	89.1575(17)	90
β [°]	96.7815(18)	74.142(3)	78.2307(18)	100.188(2)
γ [°]	90	82.668(3)	74.7766(17)	90
V [Å^3]	3349.1(5)	3071.4(3)	706.99(9)	2983.54(13)
Z	4	4	1	4
$\rho_{calc.}$ [g cm^{-3}]	1.415	1.456	1.473	1.441
μ [mm^{-1}]	0.718	0.851	6.955	0.758
T [K]	150(2)	150(2)	150(2)	150(2)
radiation type	Mo Kα	Mo Kα	Cu Kα	Mo Kα
reflections measured	55376	159799	15302	54638
independent reflections	8075	14071	2475	7938
observed reflections with $I > 2\sigma(I)$	7008	12879	2467	6546
$R_{int.}$	0.0295	0.0284	0.0401	0.0255
F(000)	1480	1380	322	1328
R_1 ($I > 2\sigma(I)$)	0.0449	0.0274	0.0327	0.0265
wR_2 (all data)	0.1216	0.0706	0.0890	0.0712
GOF on F^2	1.040	1.174	1.096	1.028
Parameters	549	682	163	365
CCDC number	2046121	2046122	2069777	2069778

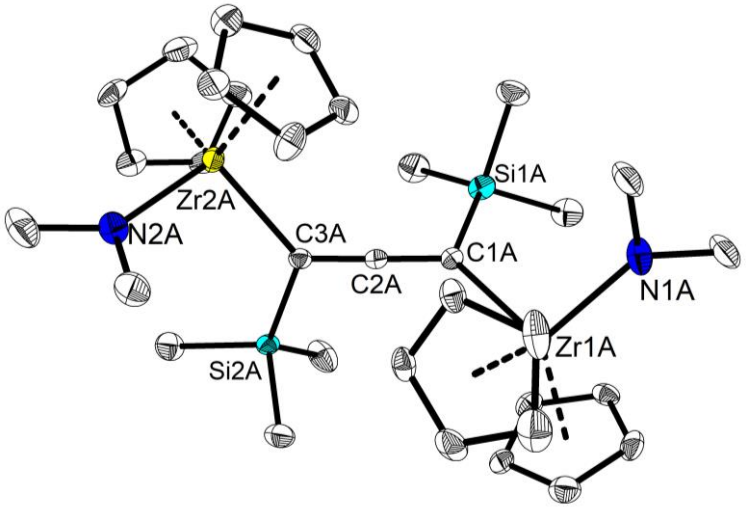

Figure S7. Molecular structure of complex **4**. Thermal ellipsoids correspond to 30% probability. Hydrogen atoms and the second position of the disordered part are omitted for clarity.

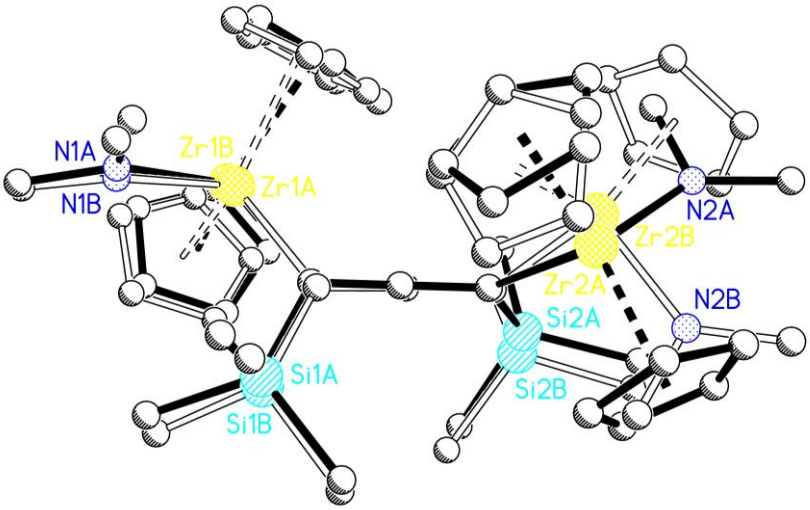

Figure S8. Ball and stick model of the molecular structure of complex **4**.

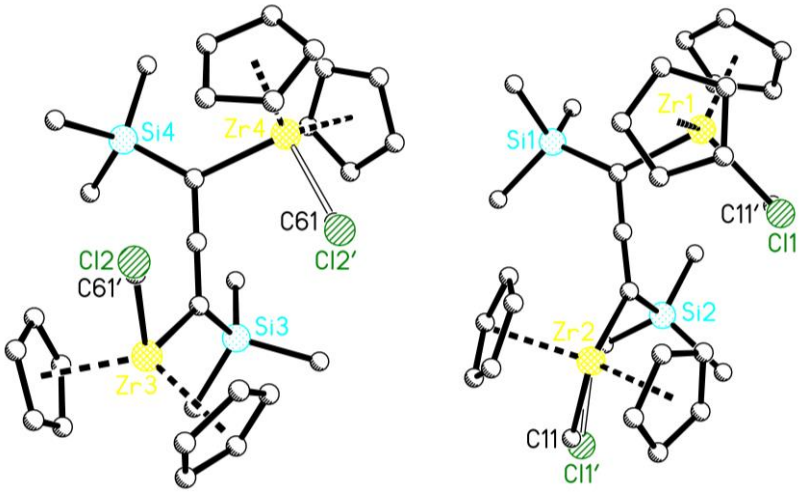

Figure S9. Ball and stick model of the molecular structure of complex **6**.

3. Details of NMR spectroscopy

3.1. NMR spectra of complex 2

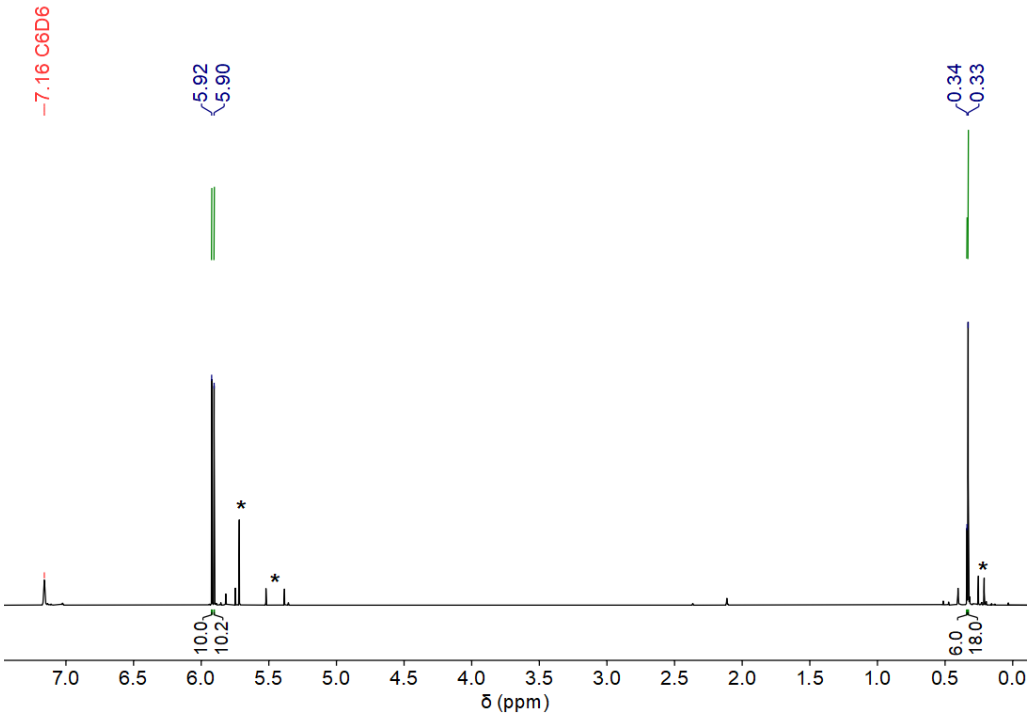

Figure S10. ^{1}H NMR spectrum of **2**, asterisk marks decomposition products (25 °C, benzene-d_6, 300.20 MHz).

3.2. NMR spectra of complex 4

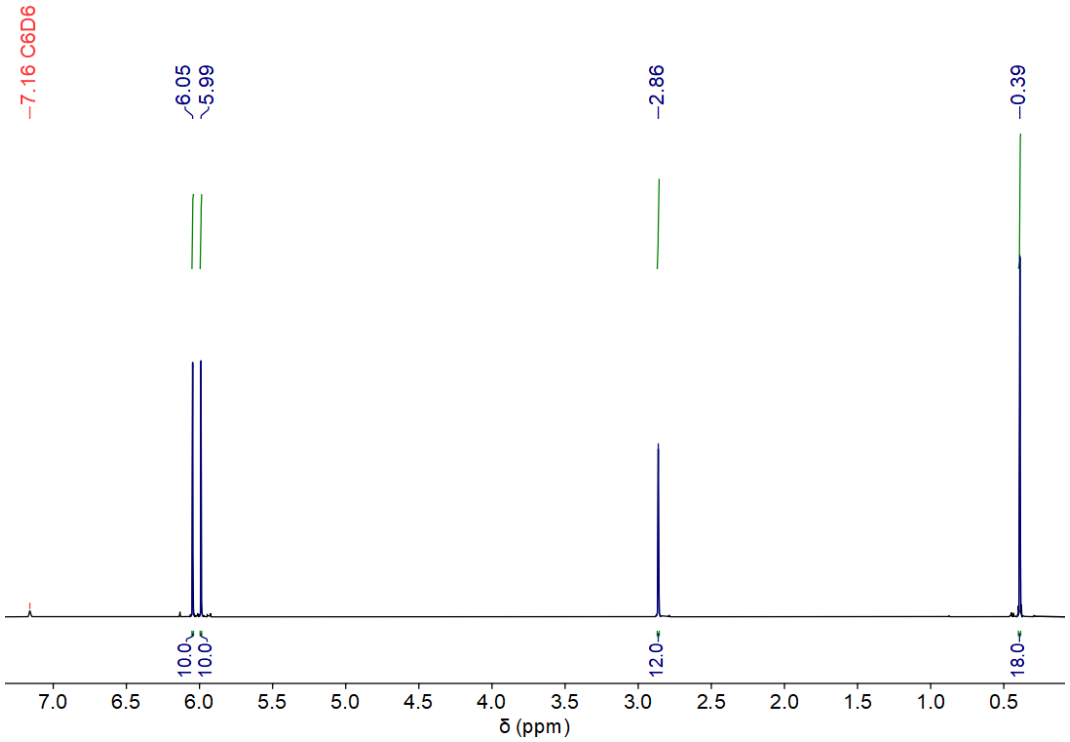

Figure S11. ^{1}H NMR spectrum of **4** (25 °C, benzene-d_6, 300.13 MHz).

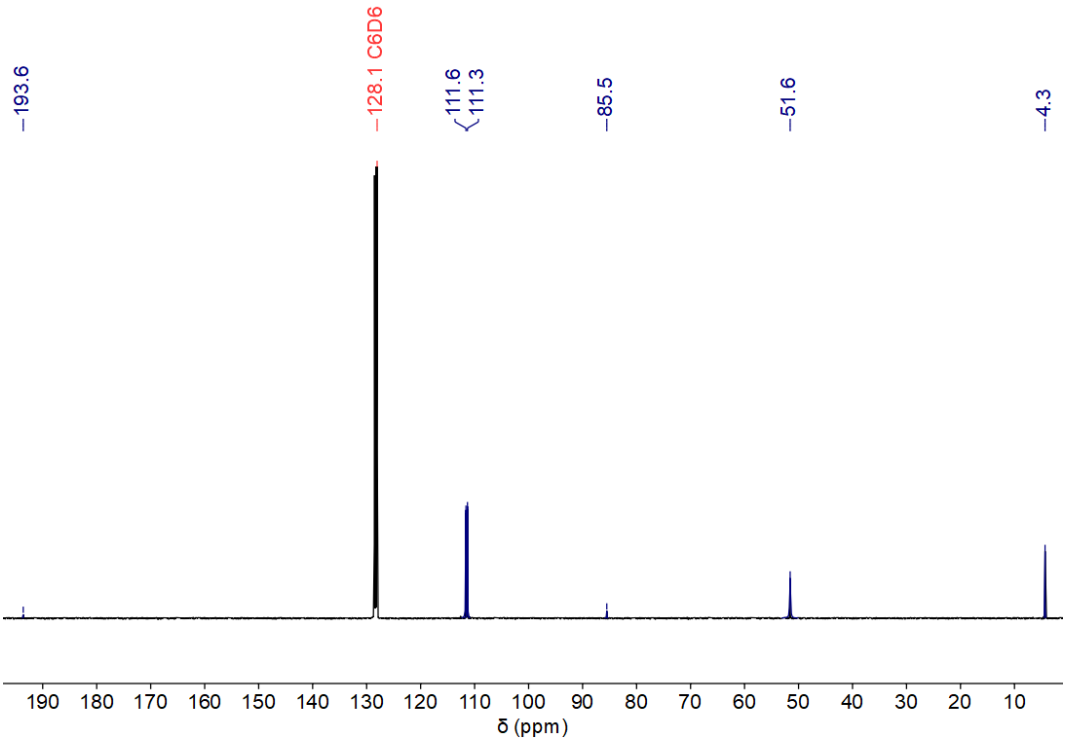

Figure S12. ^{13}C NMR spectrum of **4** (25 °C, benzene-d_6, 100.03 MHz).

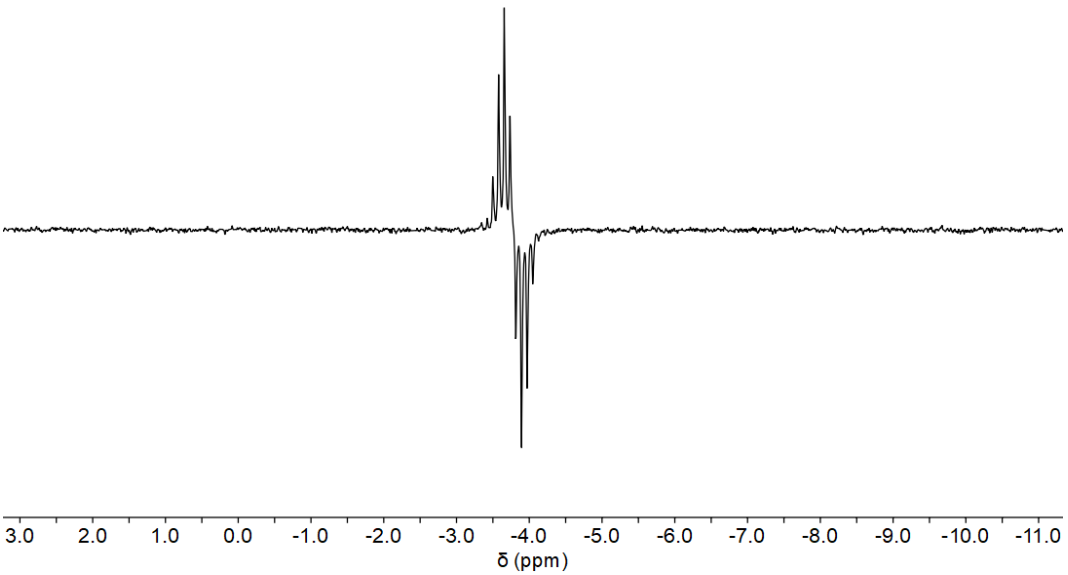

Figure S13. ^{29}Si INEPT NMR spectrum of **4** (25 °C, benzene-d_6, 79.5 MHz).

3.3. NMR spectra of complex 5

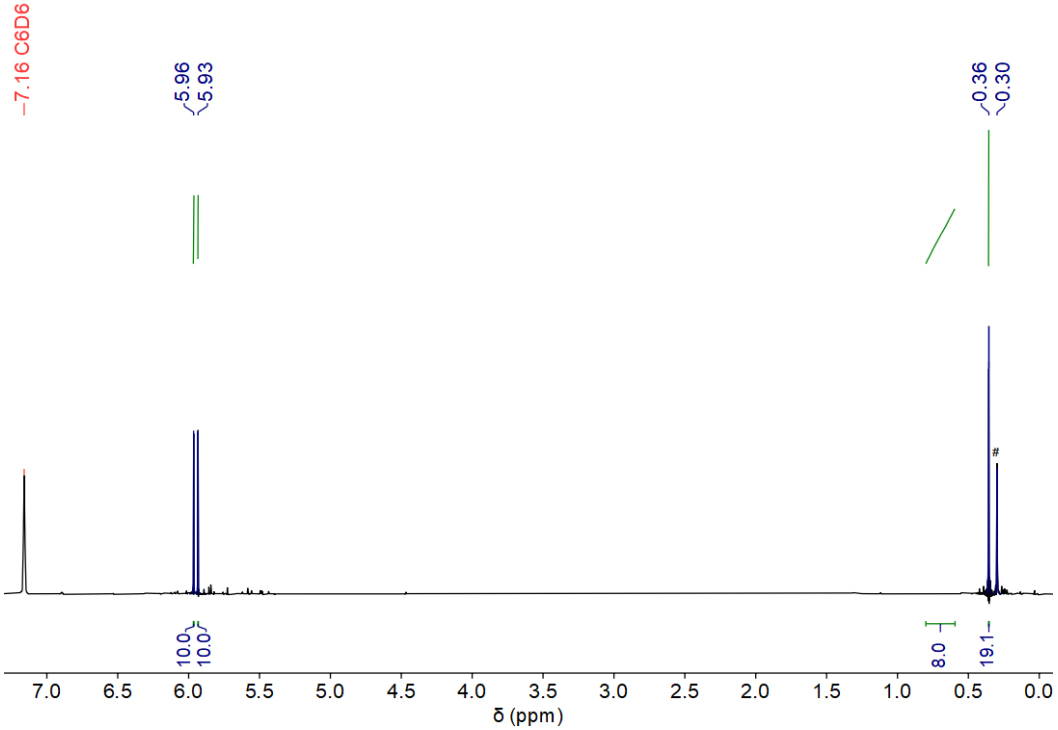

Figure S14. ^{1}H NMR spectrum of **5** (25 °C, benzene-d_6, 300.19 MHz). # indicates silicon grease.

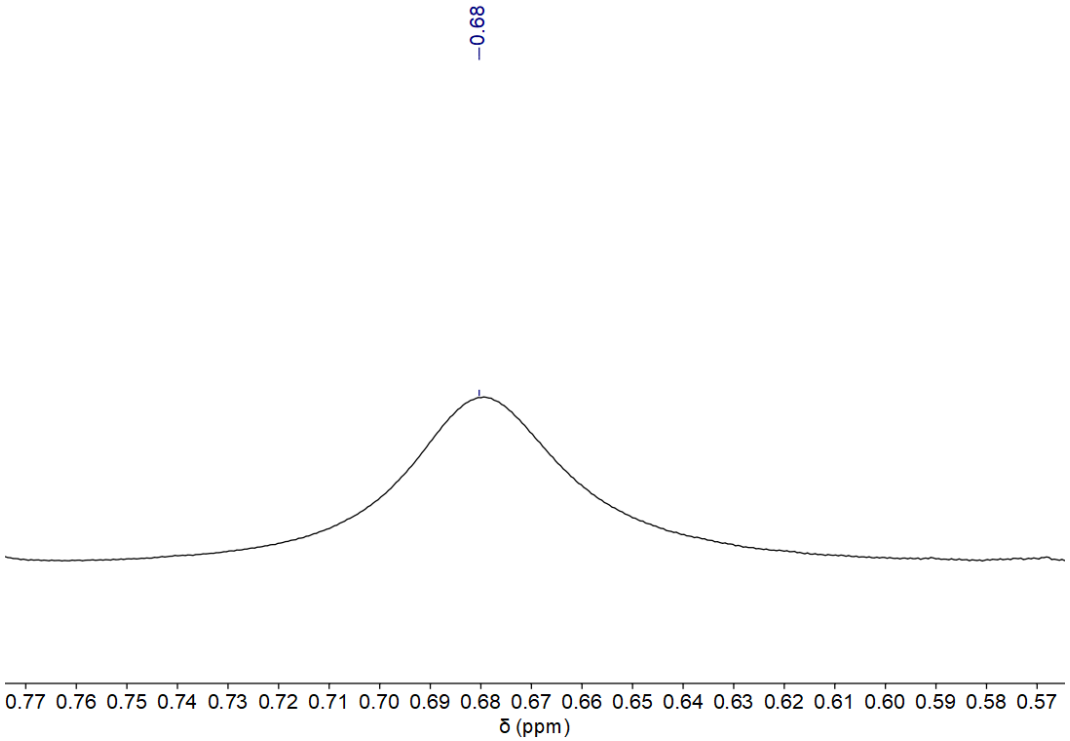

Figure S15. ^{1}H{^{11}B} NMR spectrum of **5**, with greatly enlarged boron range (25 °C, benzene-d_6, 300.19 MHz).

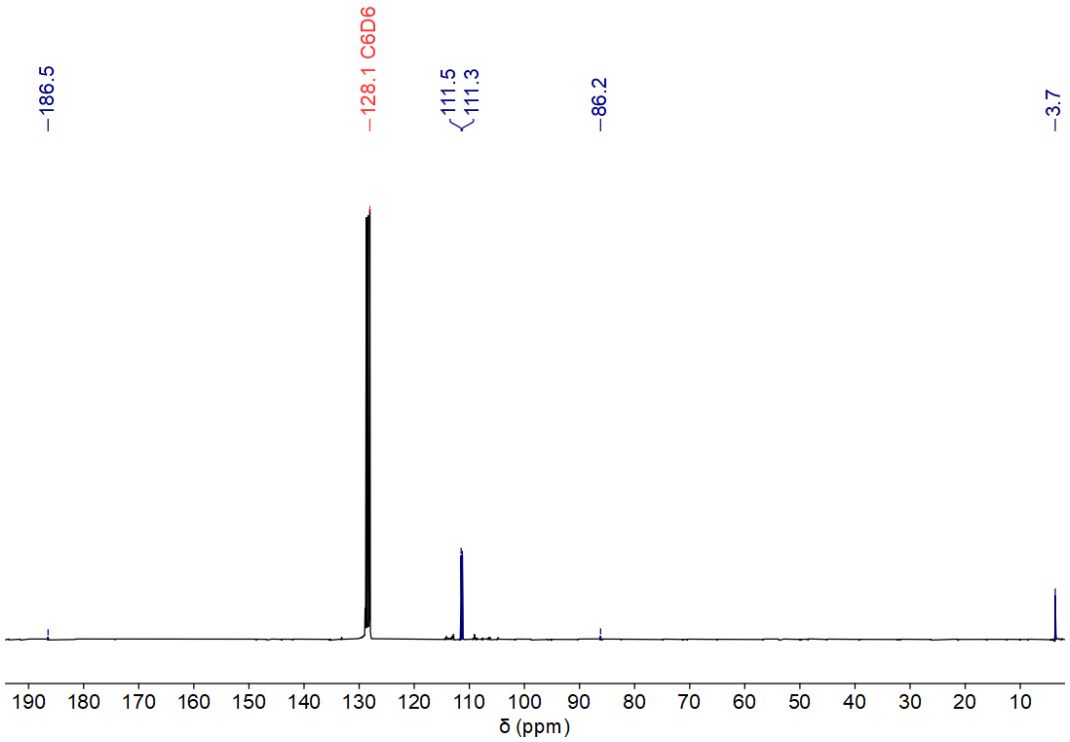

Figure S16. ^{13}C NMR spectrum of **5** (25 °C, benzene-d_6, 75.5 MHz).

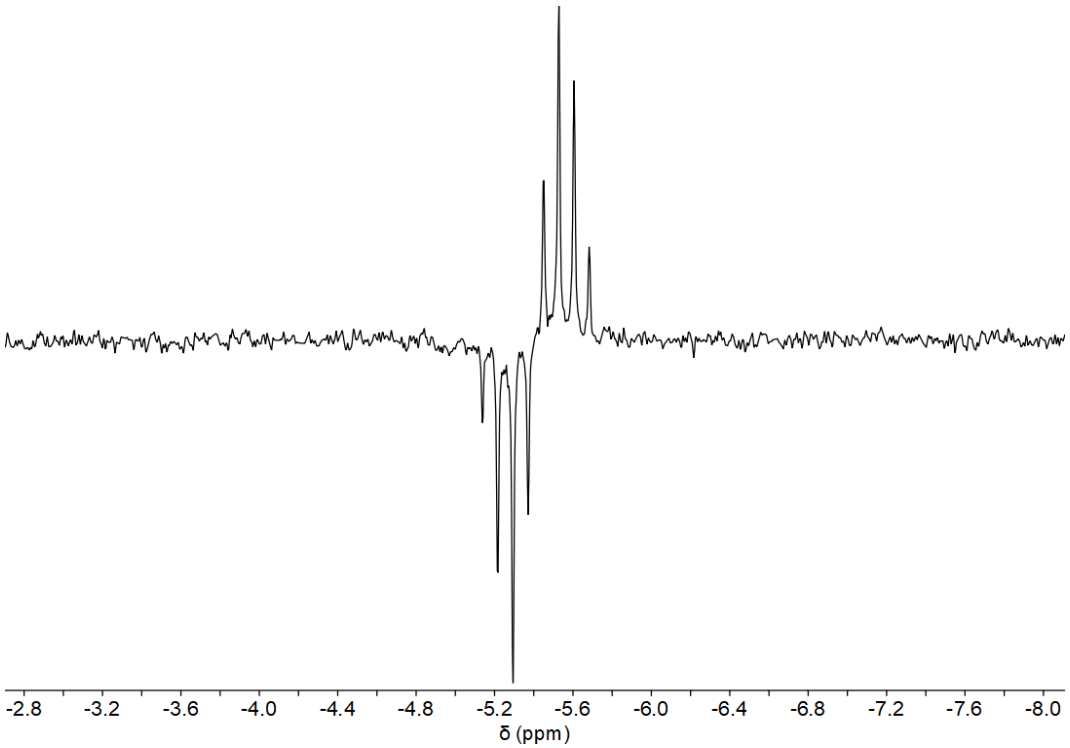

Figure S17. ^{29}Si INEPT NMR spectrum of **5** (25 °C, benzene-d_6, 59.6 MHz).

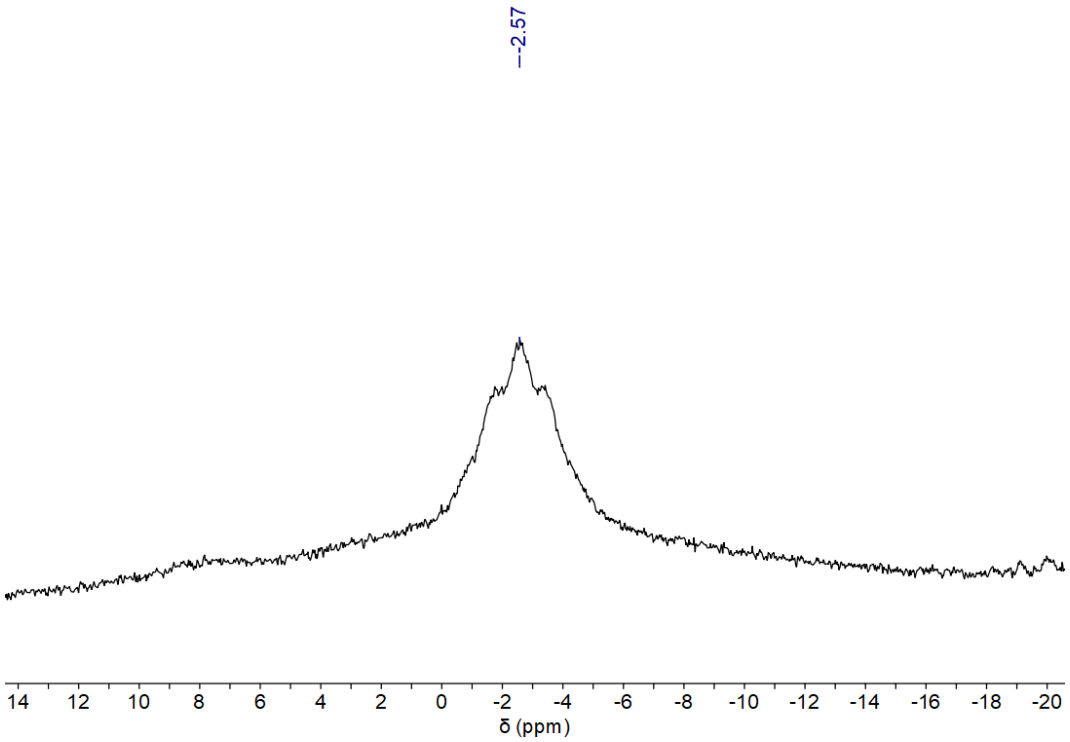

Figure S18. ^{11}B NMR spectrum of **5** (25 °C, benzene-d_6, 96.32 MHz).

3.4. NMR spectra of complex 6

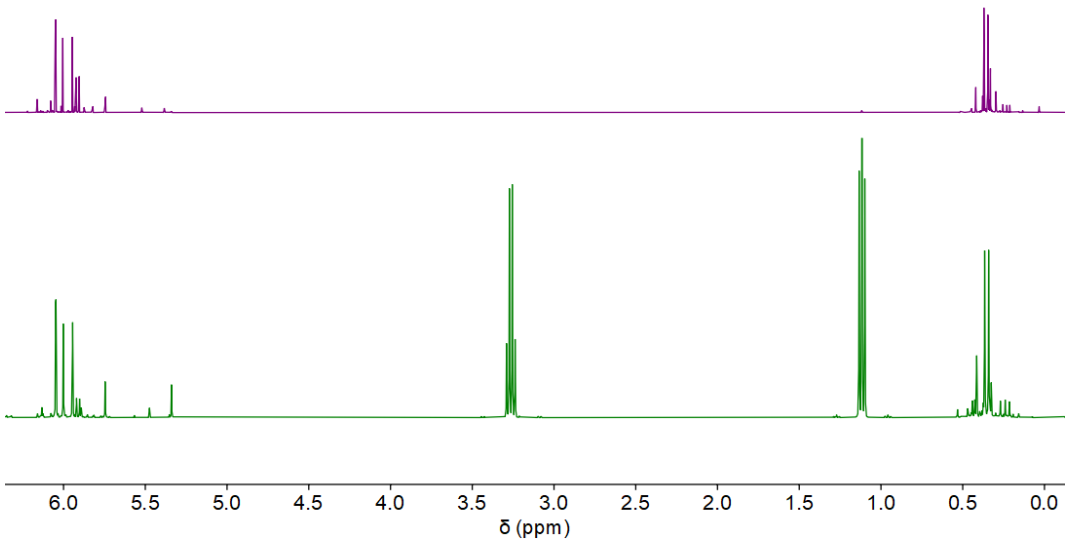

Figure S19. ^{1}H NMR spectra of **6**. Top: room temperature, benzene, 0.43 mmol **1**, 0.43 mmol MeLi (25 °C, benzene-d_6, 300.20 MHz). Bottom: room temperature, diethyl ether, 0.02 mmol **1**, 0.02 mmol MeLi as single crystals (25 °C, benzene-d_6, 400.13 MHz).

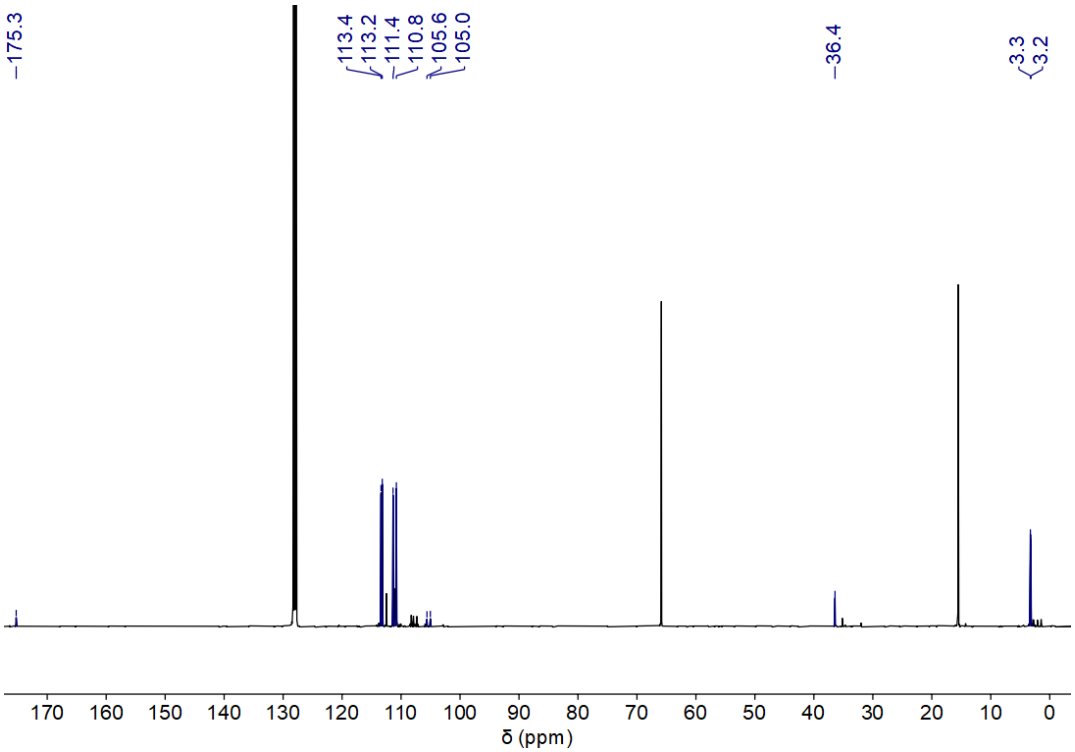

Figure S20. ^{13}C NMR spectrum of **6** (25 °C, benzene-d_6, 100.03 MHz).

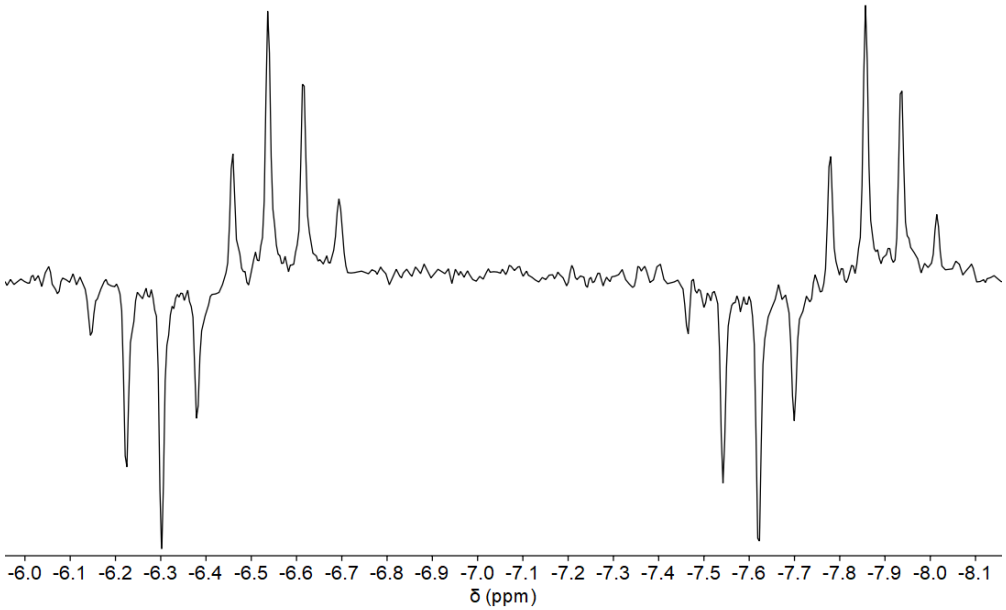

Figure S21. ^{29}Si INEPT NMR spectrum of **6** (25 °C, benzene-d_6, 79.5 MHz).

3.5. NMR spectra of complex 7

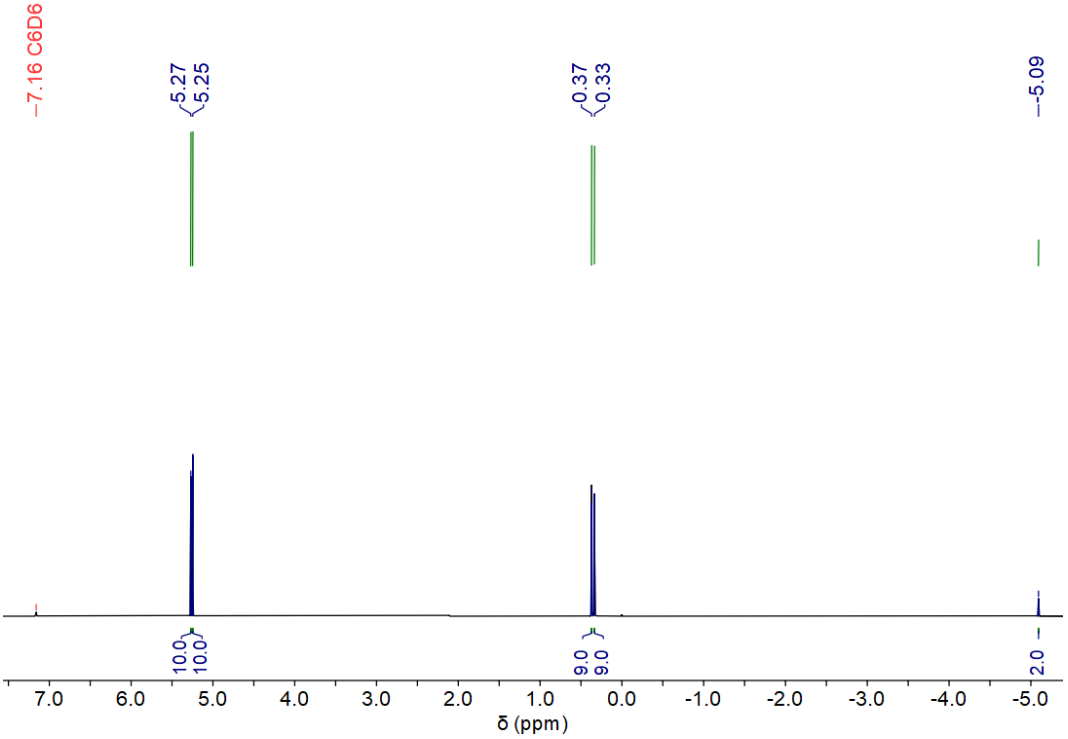

Figure S22. ^{1}H NMR spectrum of **7** (25 °C, benzene-d_6, 400.13 MHz).

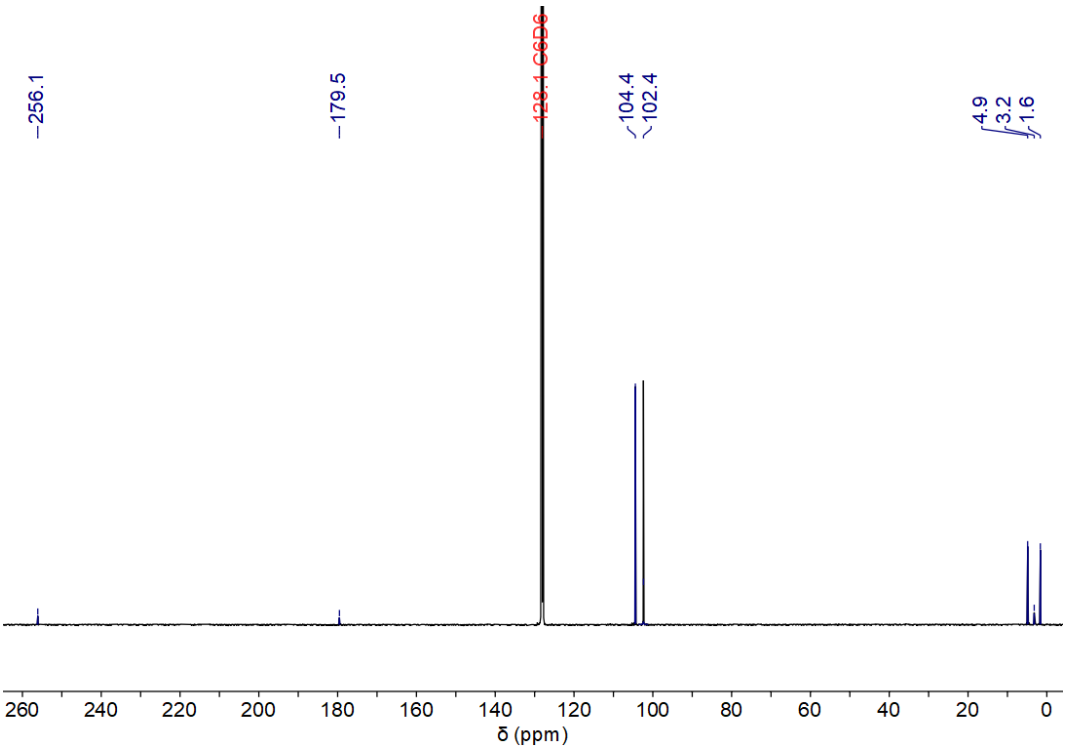

Figure S23. ^{13}C NMR spectrum of **7** (25 °C, benzene-d_6, 100.6 MHz).

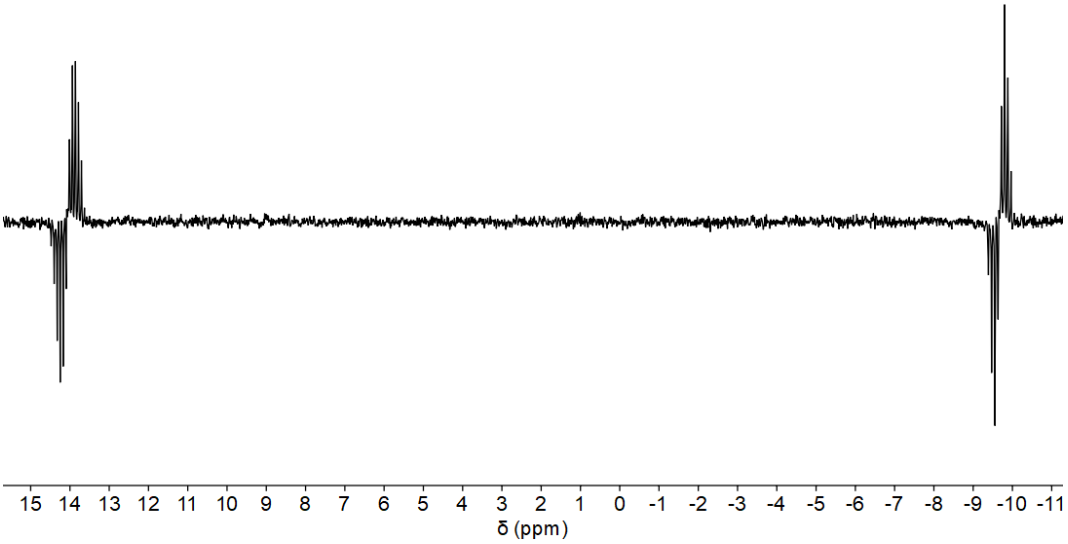

Figure S24. ^{29}Si INEPT NMR spectrum of **7** (25 °C, benzene-d_6, 79.5 MHz).

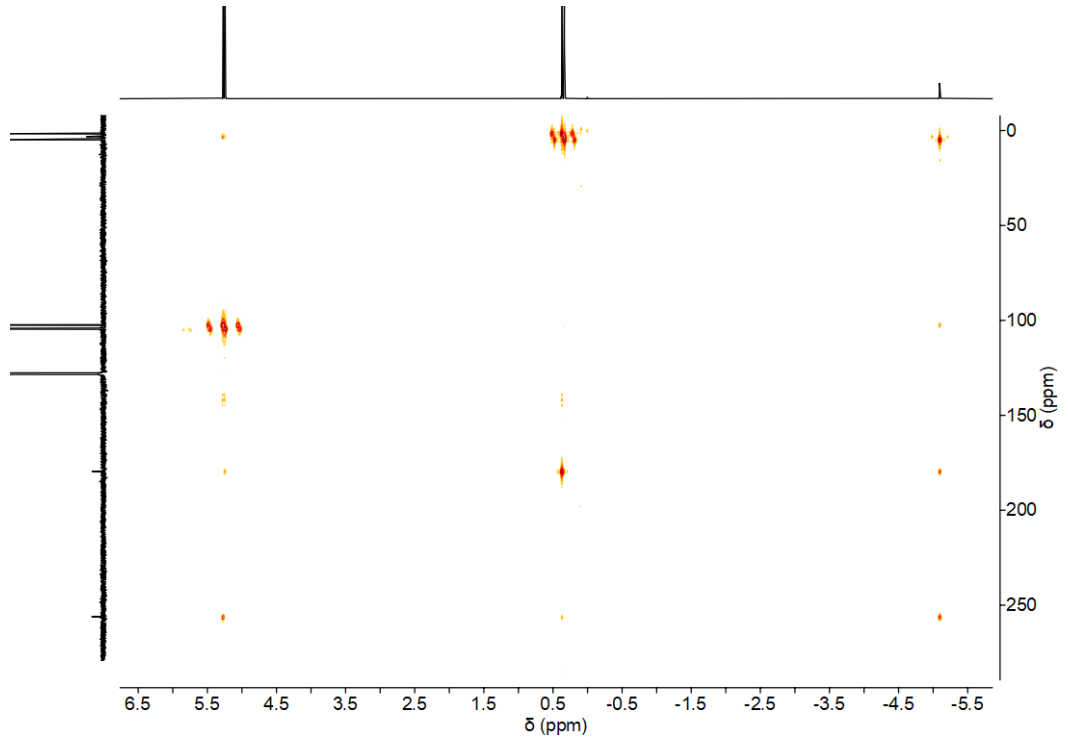

Figure S 25. ^{1}H ^{13}C HMBC NMR spectrum of **7** (25 °C, benzene-d_6, 400.13 MHz).

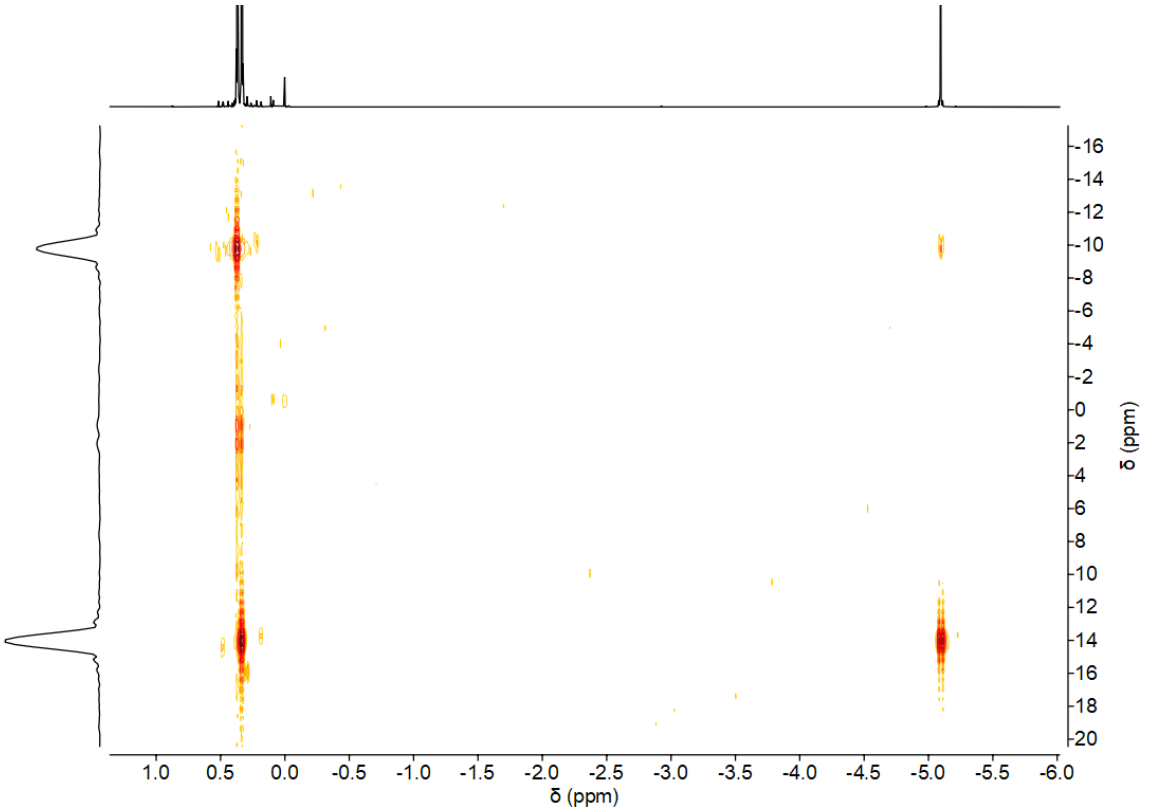

Figure S 26. ^{1}H ^{29}Si HMBC NMR spectrum of **7** (25 °C, benzene-d_6, 400.13 MHz).

3.6. NMR spectra of complex 8

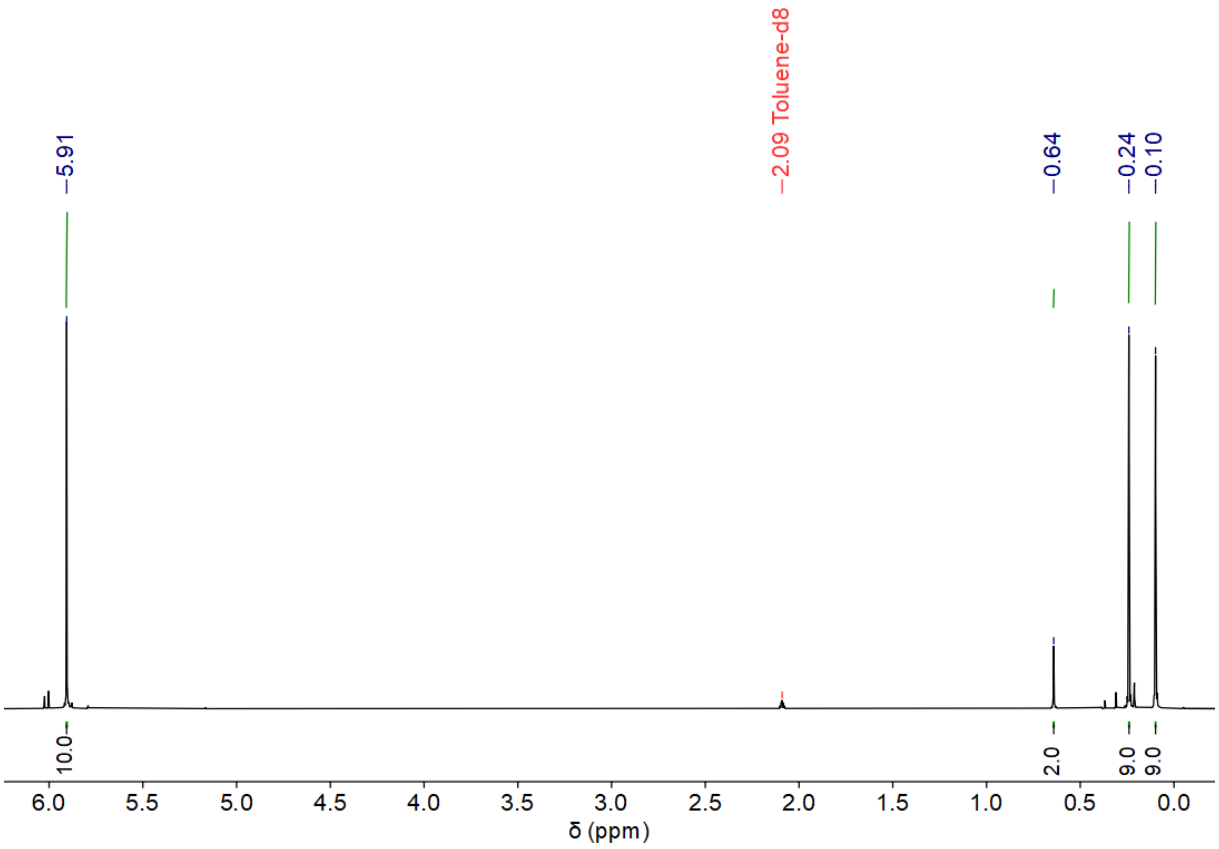

Figure S27. ^{1}H NMR spectrum of **8** (25 °C, toluene-d_8, 400.13 MHz).

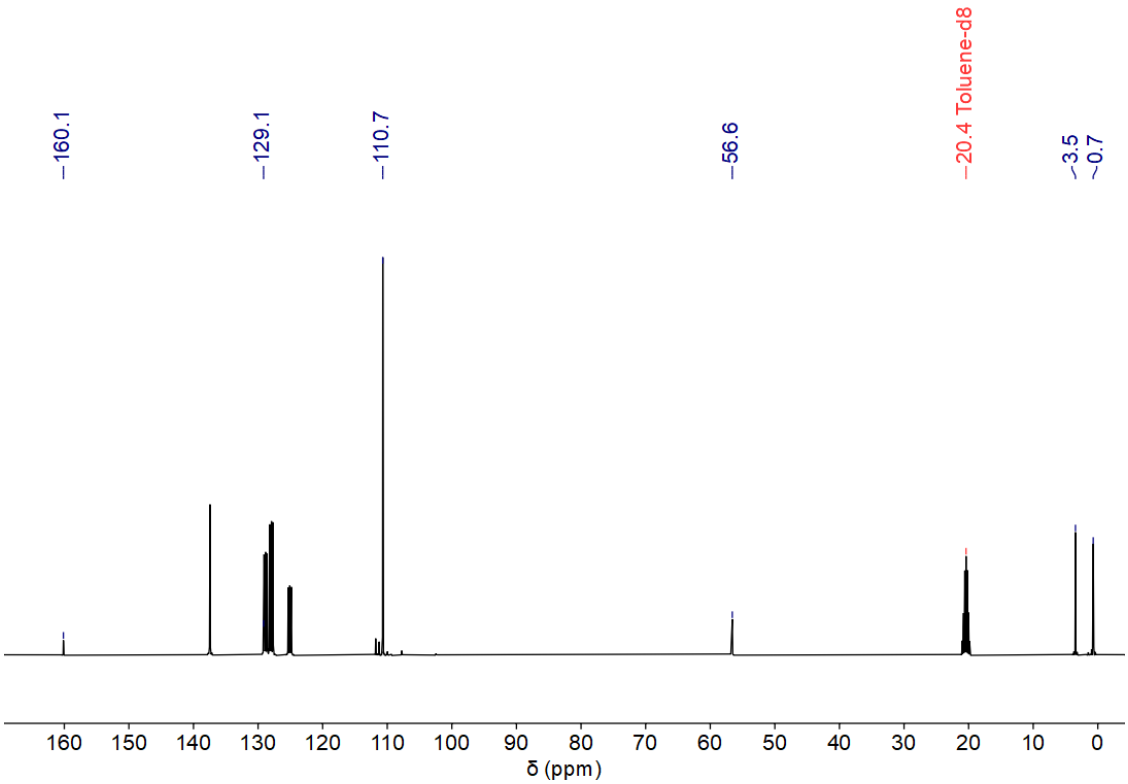

Figure S28. ^{13}C NMR spectrum of **8** (25 °C, toluene-d_8, 100.63 MHz).

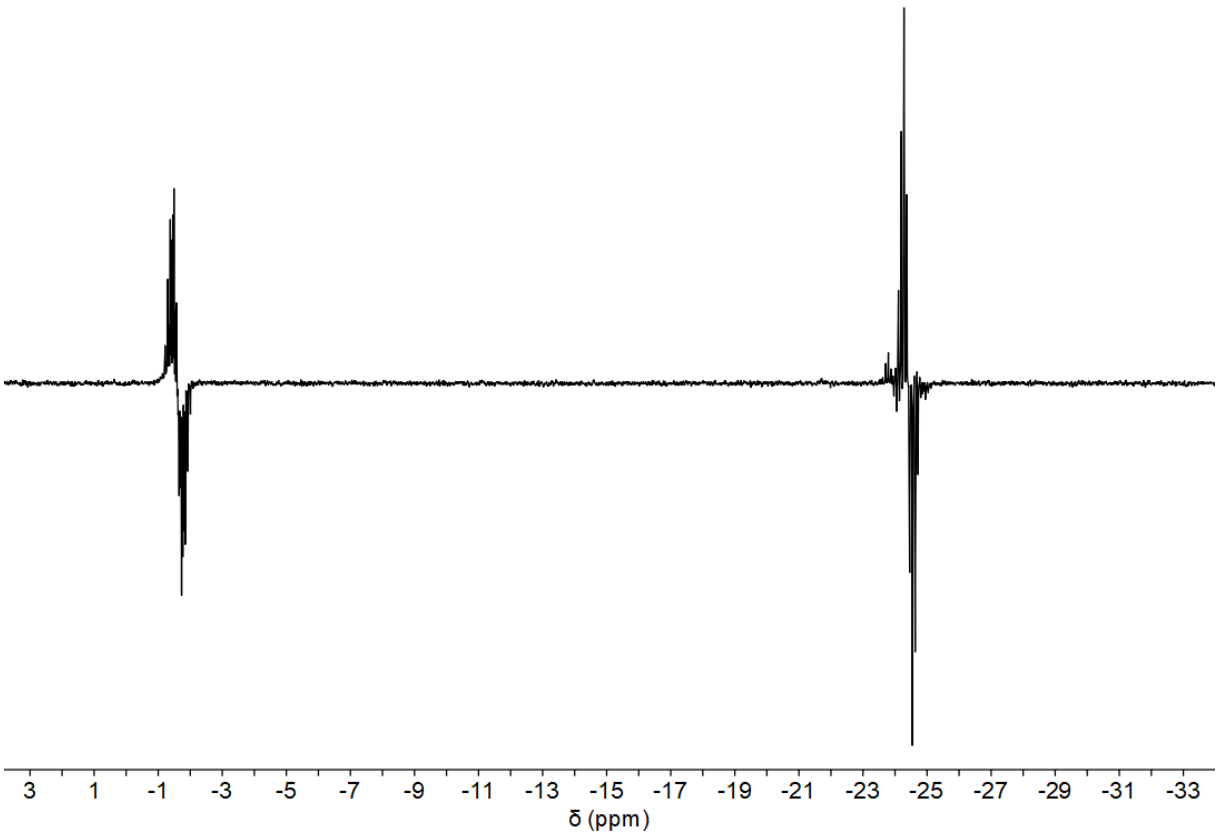

Figure S29. ^{29}Si INEPT NMR spectrum of **8** (25 °C, toluene-d_8, 59.63 MHz).

3.7. NMR spectra of complex 9 via route 1

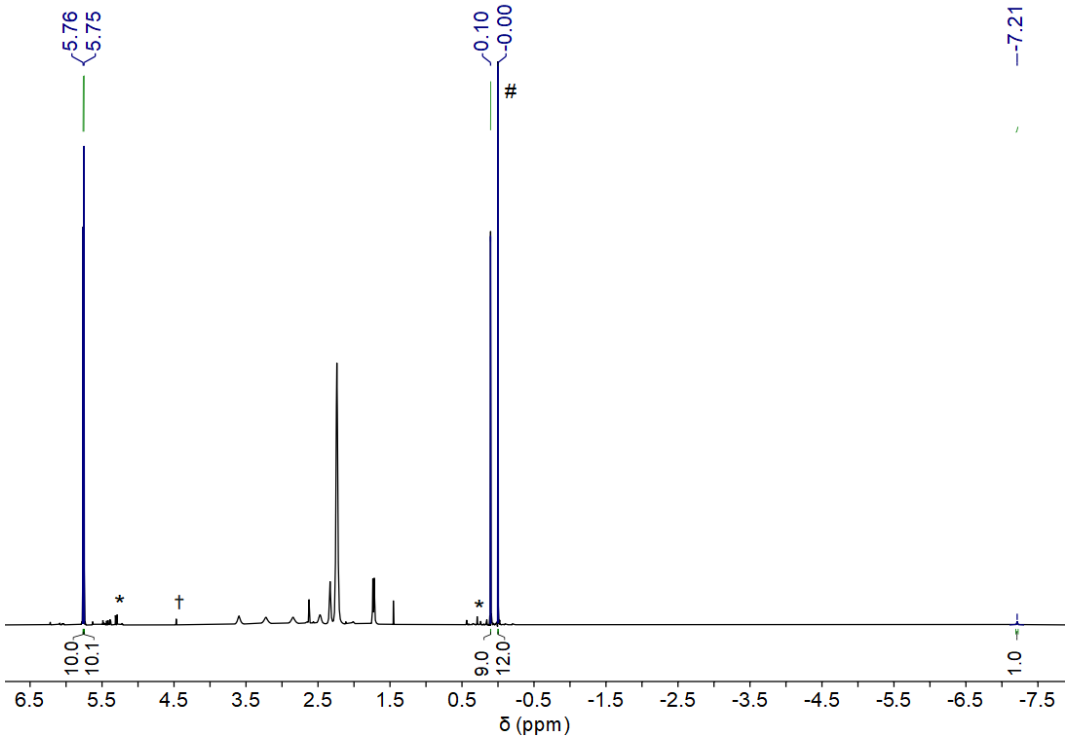

Figure S30. ^{1}H NMR spectrum of the reaction mixture obtained from route 1 (25 °C, benzene-d_6, 300.20 MHz). The region 1.40 – 3.50 ppm shows the products of dehydrocoupling of $H_3B{\cdot}NMe_2H$. # $SiMe_4$, * decomposition products, † H_2.

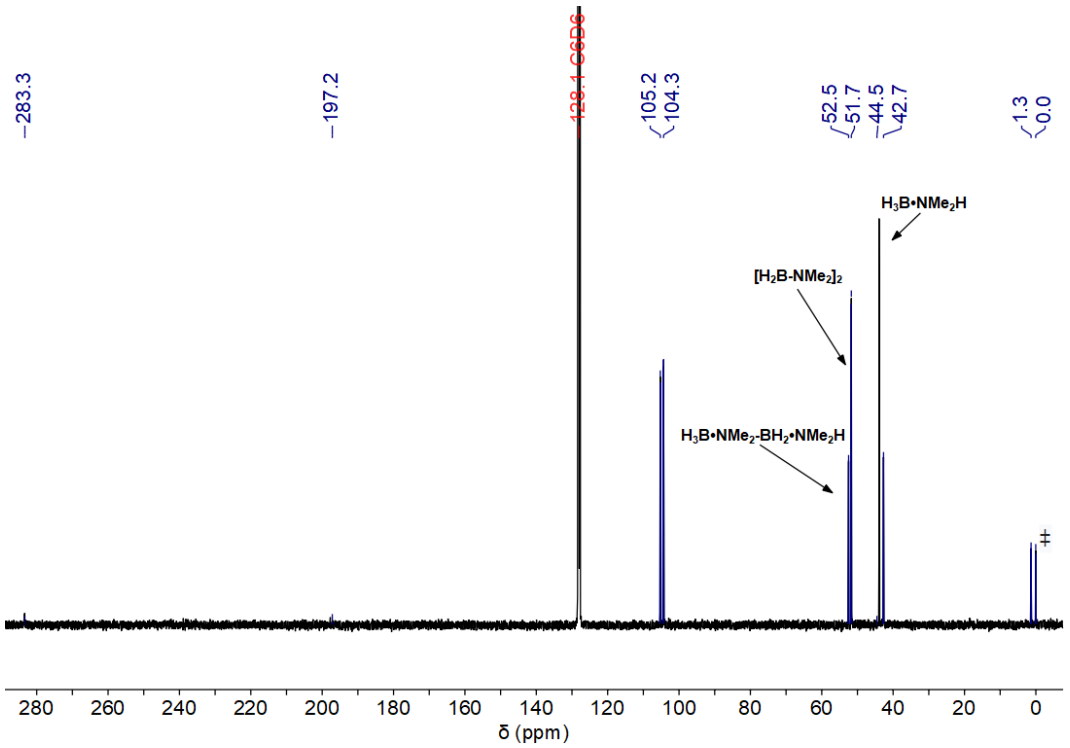

Figure S31. ^{13}C NMR spectrum of the reaction mixture obtained from route 1 (25 °C, benzene-d_6, 100.63 MHz). ‡ $SiMe_4$.

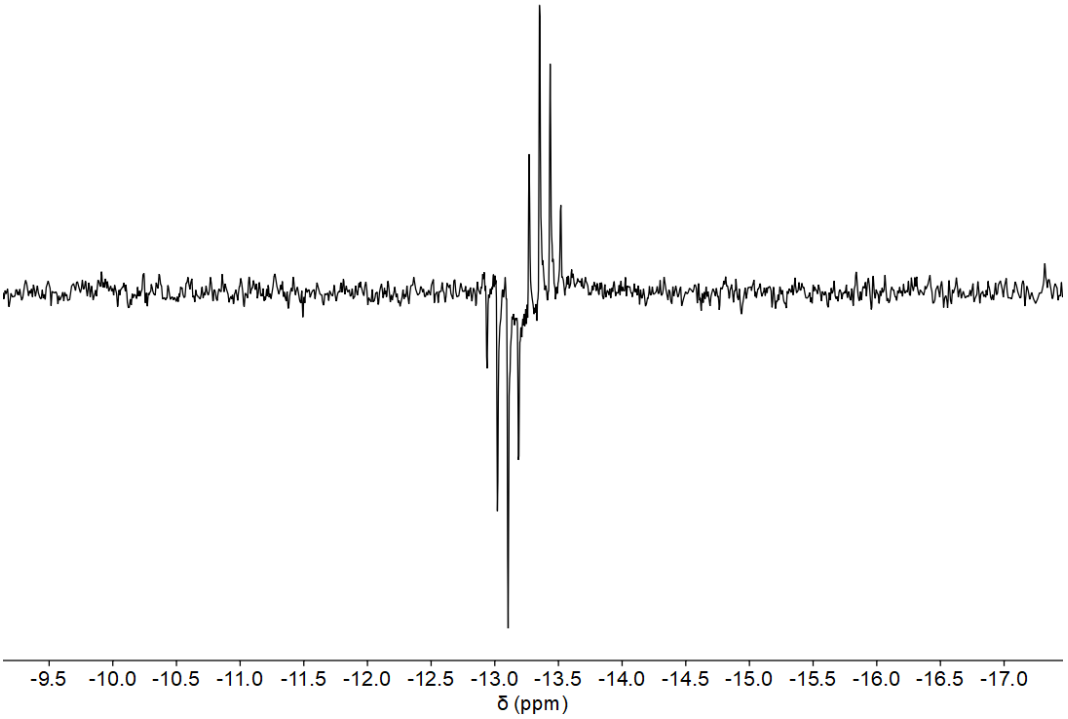

Figure S32. ^{29}Si INEPT NMR spectrum of **9** (25 °C, benzene-d_6, 79.49 MHz).

3.8. NMR spectra of complex 9 via route 2

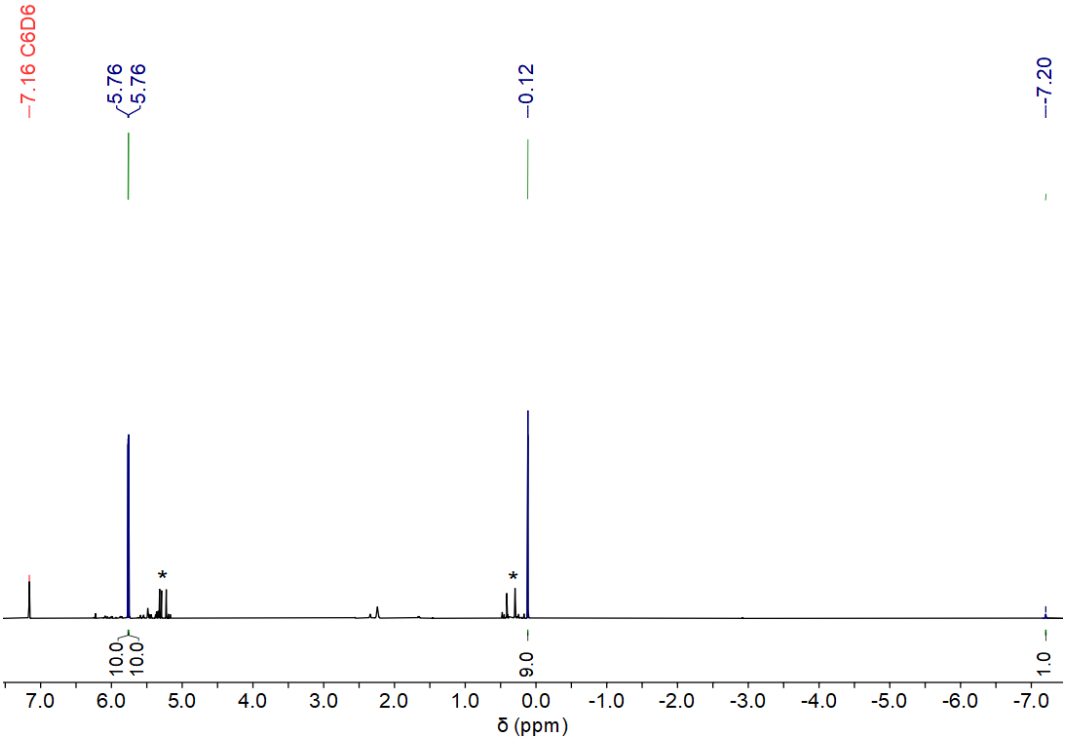

Figure S33. ^{1}H NMR spectrum of **9** (25 °C, benzene-d_6, 400.13 MHz). * decomposition products.

3.9. NMR spectra of complex 10

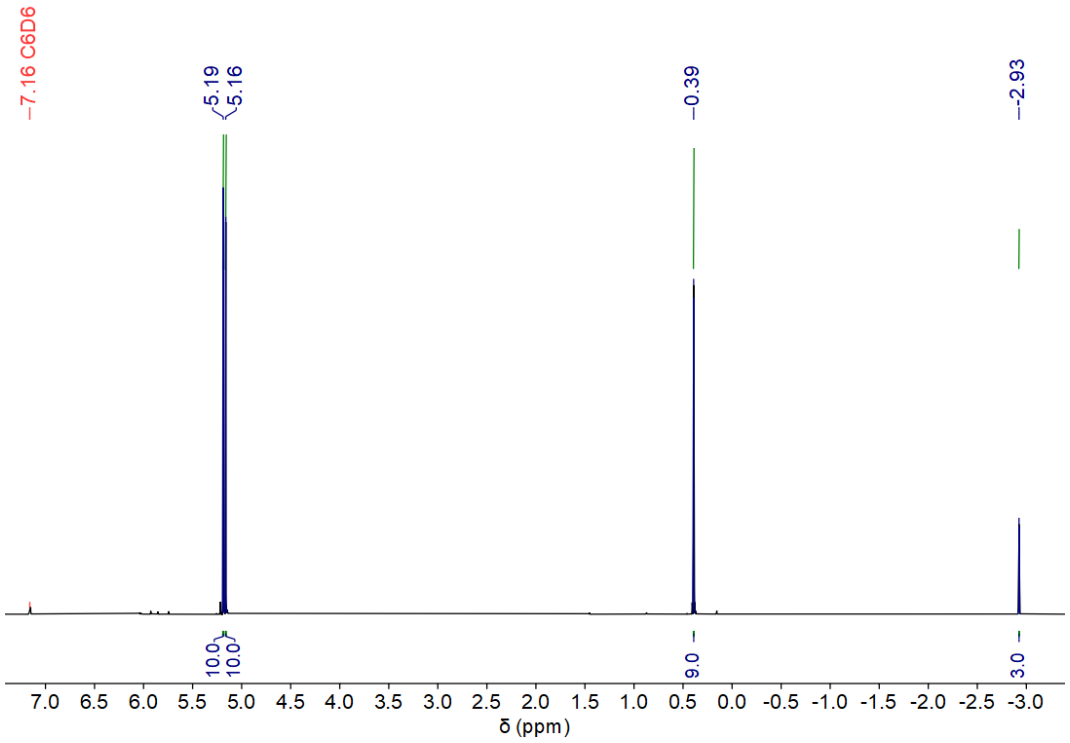

Figure S34. ^{1}H NMR spectrum of **10** (25 °C, benzene-d_6, 400.13 MHz).

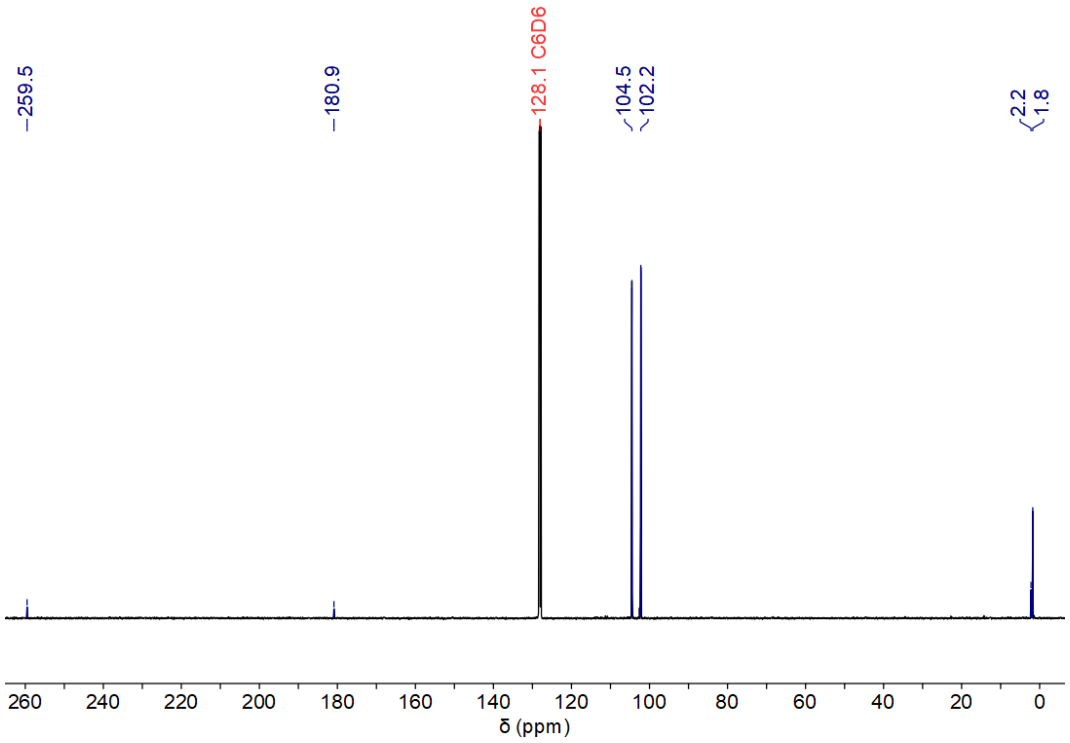

Figure S35. ^{13}C NMR spectrum of **10** (25 °C, benzene-d_6, 75.47 MHz).

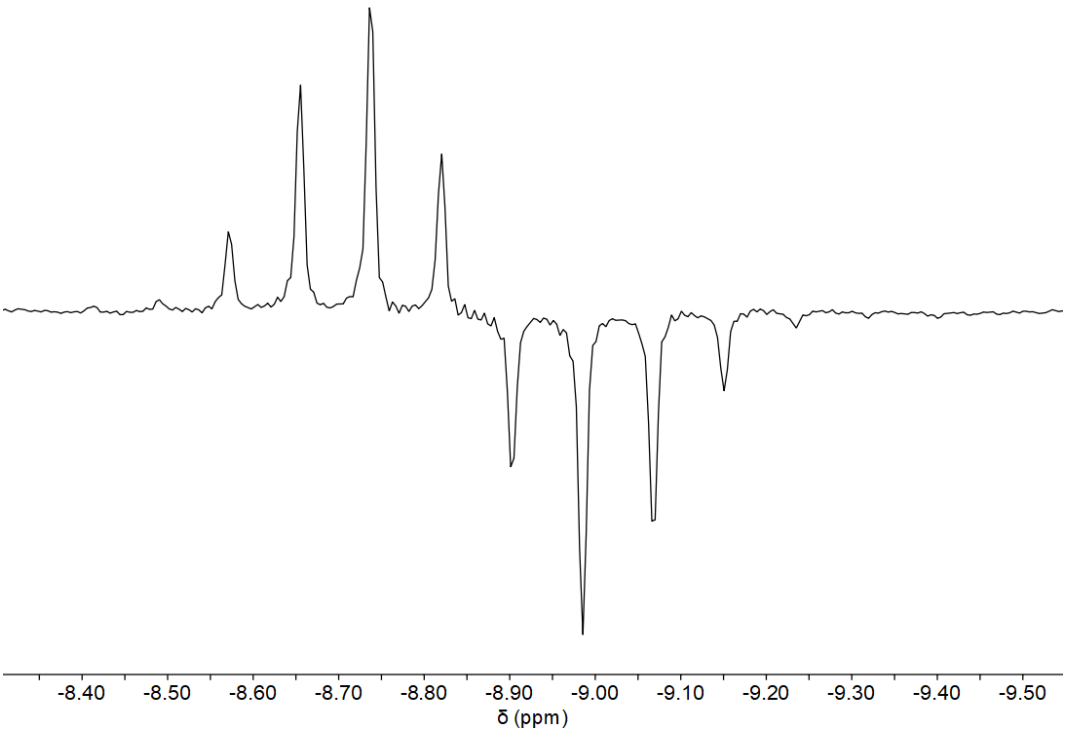

Figure S36. ^{29}Si INEPT NMR spectrum of **10** (25 °C, benzene-d_6, 59.63 MHz).

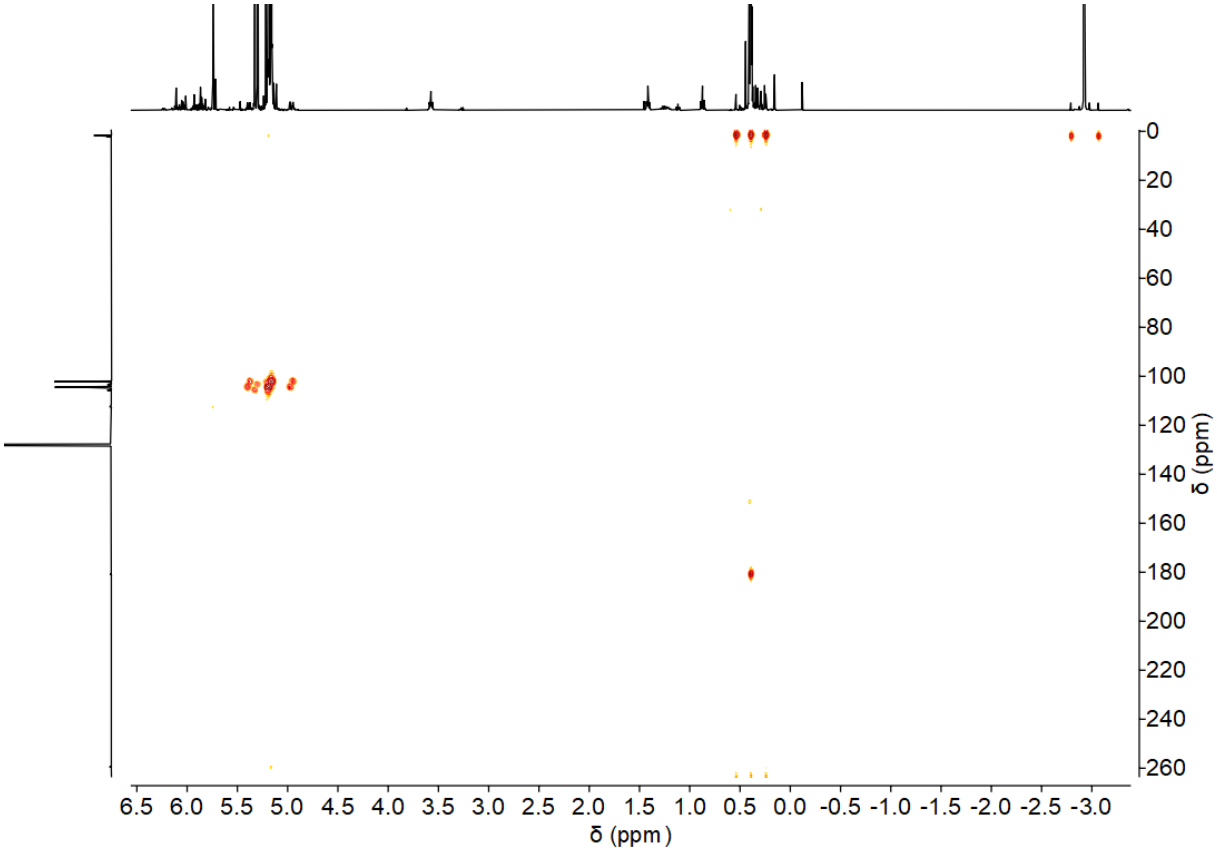

Figure S 37. ^{1}H ^{13}C HMBC NMR spectrum of **10** (25 °C, benzene-d_6, 400.13 MHz).

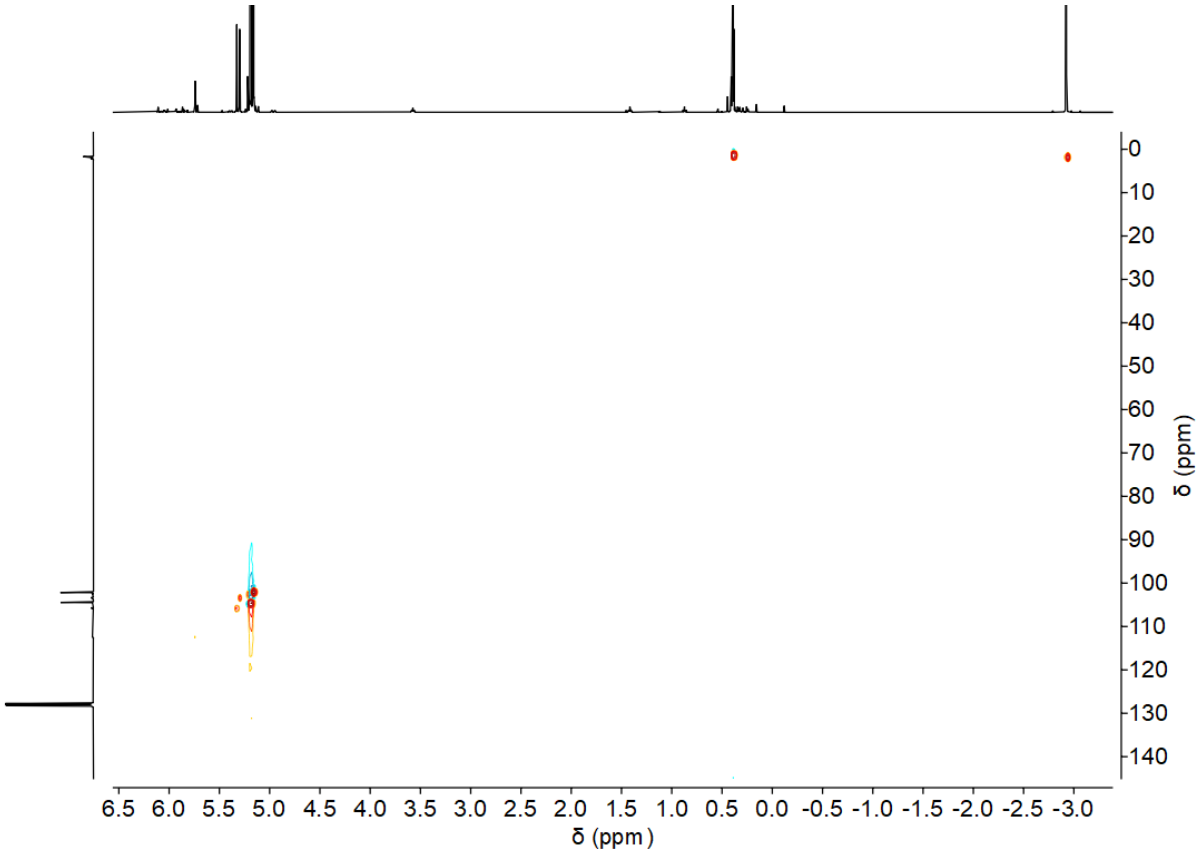

Figure S 38. ^{1}H ^{13}C HSQC NMR spectrum of **10** (25 °C, benzene-d_6, 400.13 MHz).

3.10. NMR spectra of complex 11

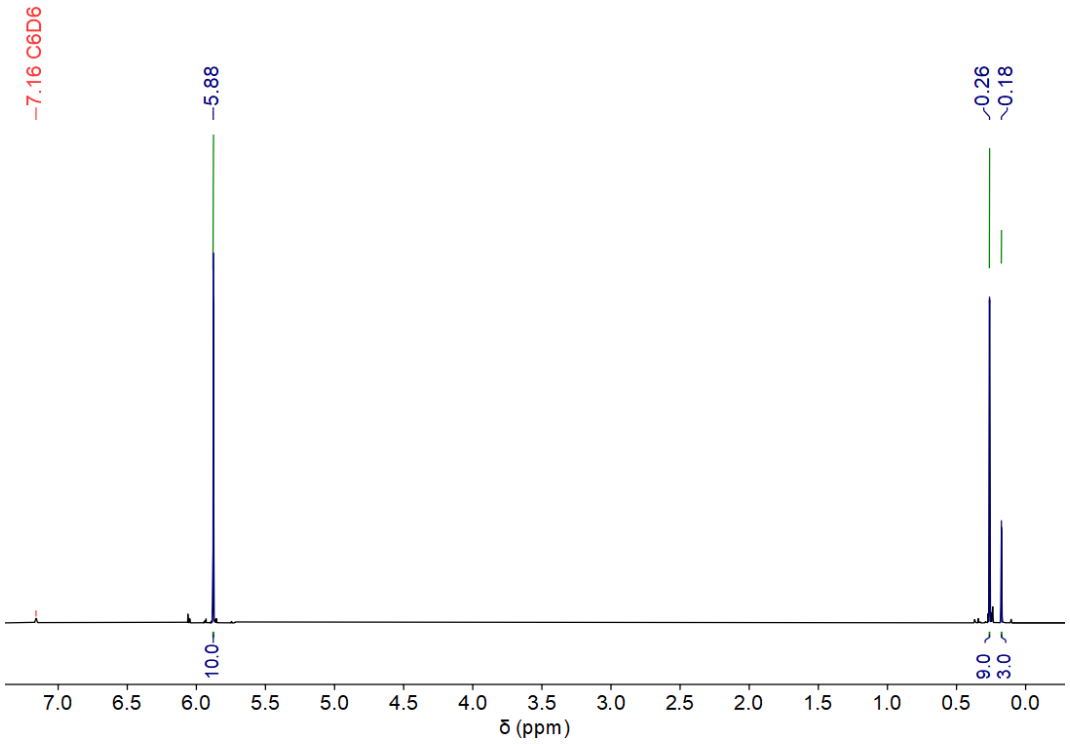

Figure S39. ^{1}H NMR spectrum of **11** (25 °C, benzene-d_6, 400.13 MHz).

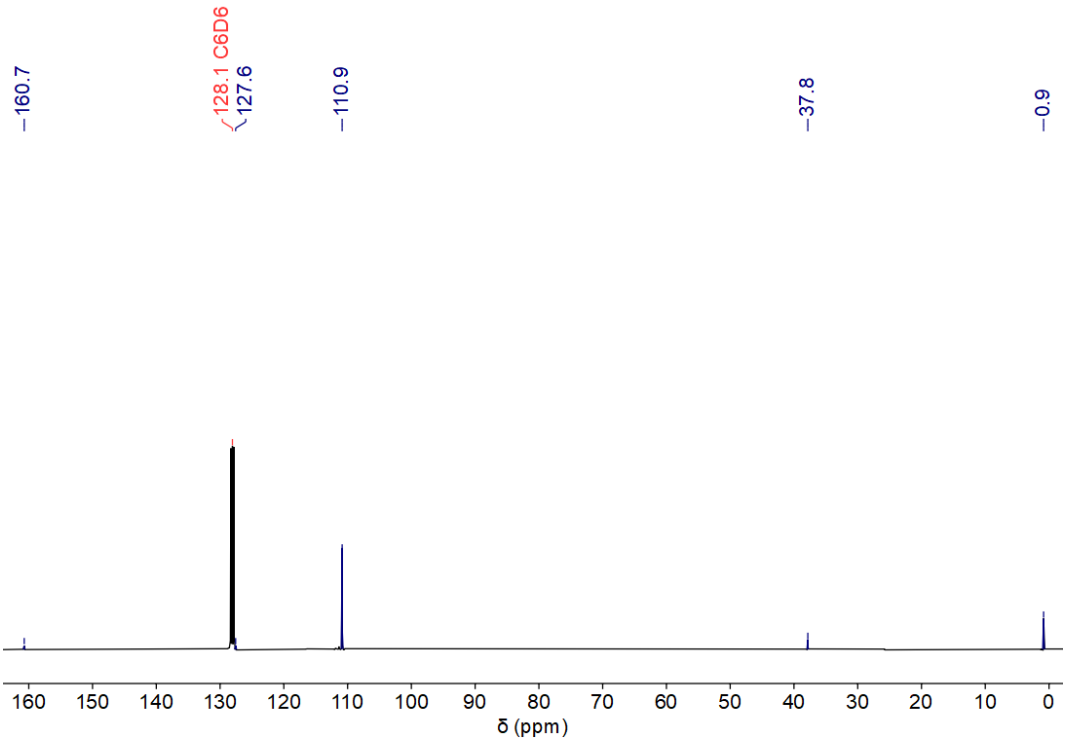

Figure S40. ^{13}C NMR spectrum of **11** (25 °C, benzene-d_6, 75.47 MHz).

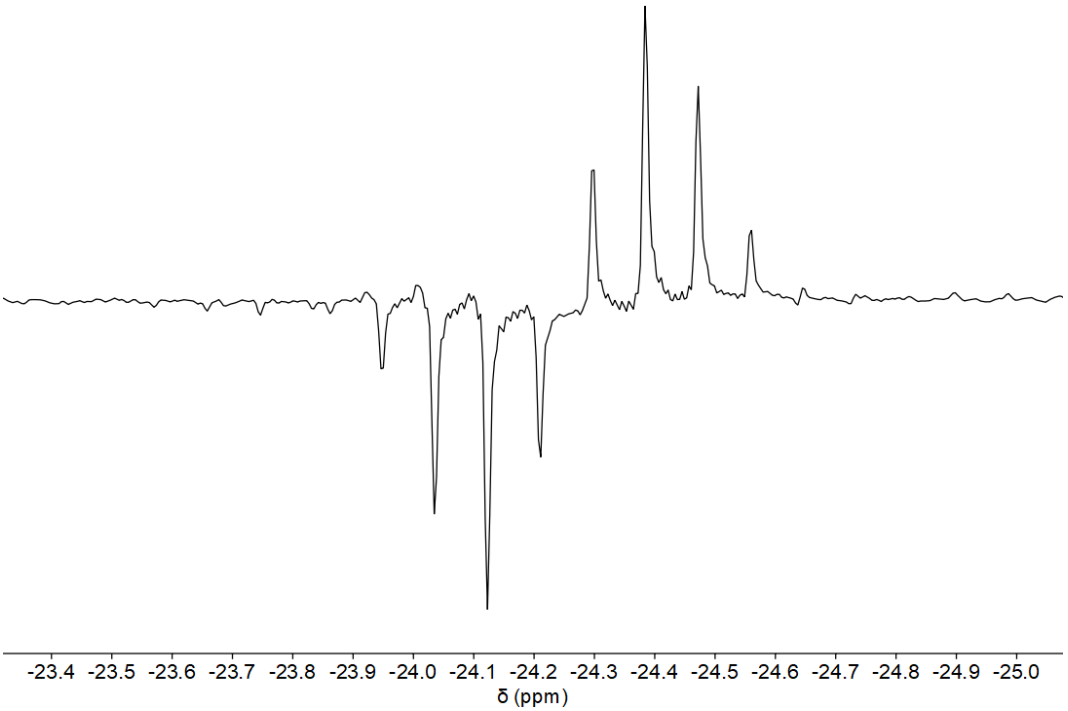

Figure S41. ^{29}Si INEPT NMR spectrum of **11** (25 °C, benzene-d_6, 59.63 MHz).

3.11. NMR spectra of complex $BH_2(\mu\text{-}Me_2N)(\mu\text{-}H)BH_2$

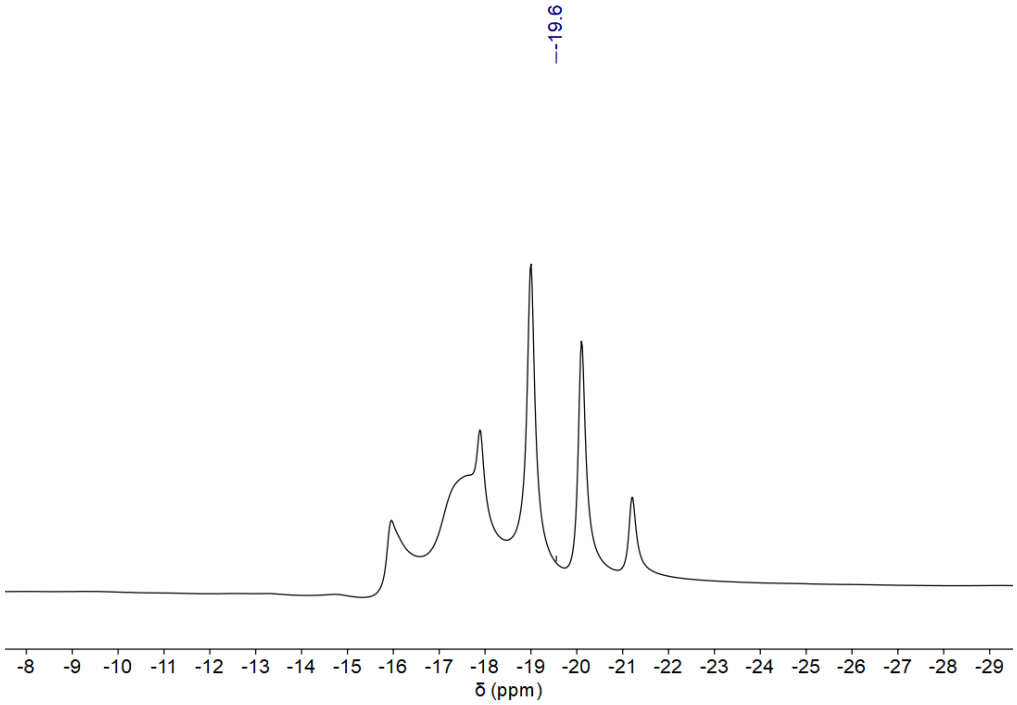

Figure S42. ^{11}B NMR spectrum of $BH_2(\mu\text{-}Me_2N)(\mu\text{-}H)BH_2$ (25 °C, toluene-d_8, 96.32 MHz).

3.12. NMR spectra of the reaction mixture from dehydrocoupling of $H_3B{\cdot}NMe_2H$ with complex 1/MeLi

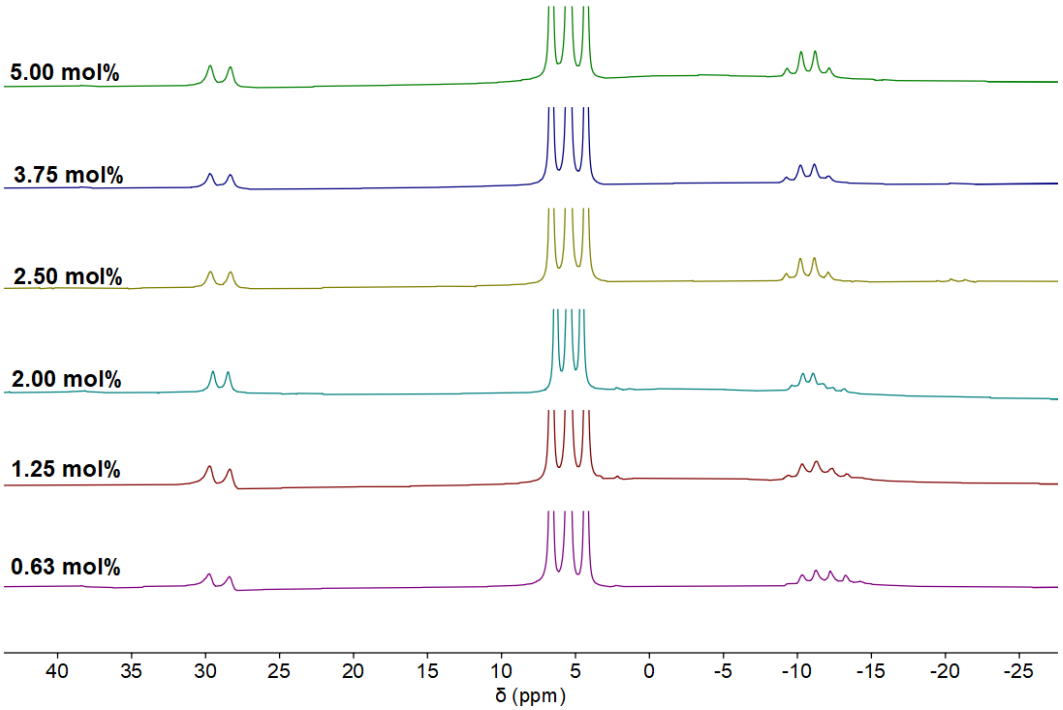

Figure S43. ^{11}B NMR spectra of dehydrocoupling of $H_3B{\cdot}NMe_2H$. Conditions: room temperature, toluene, (25 °C, toluene-d_8, 300.20 MHz).

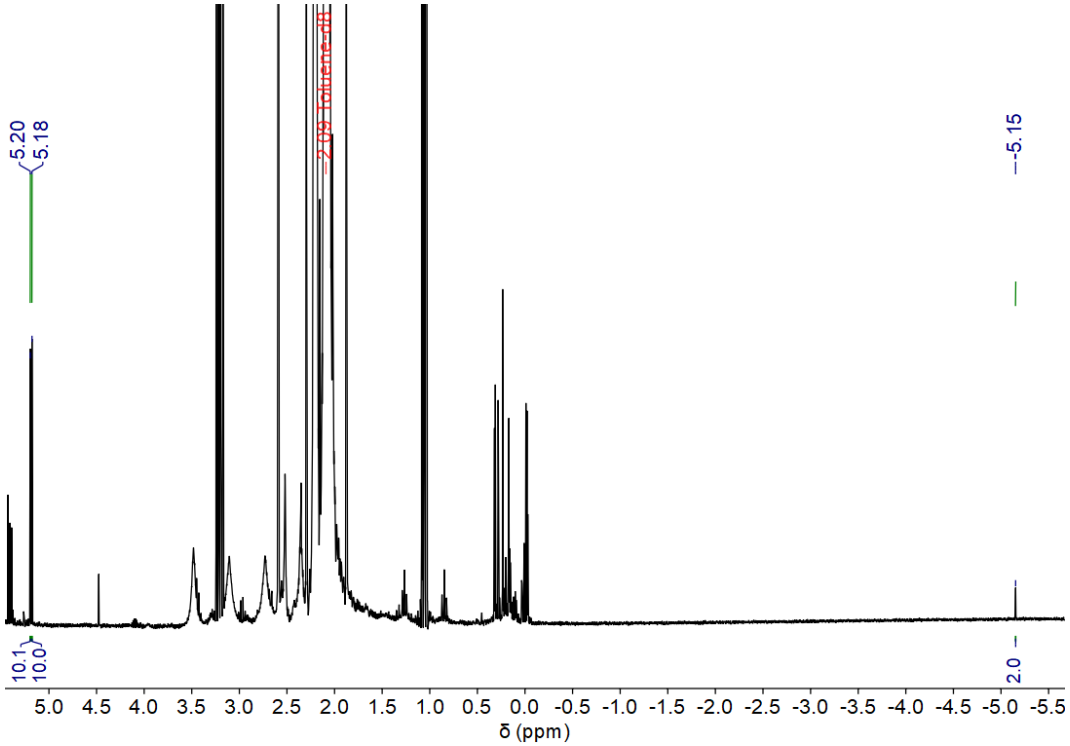

Figure S44. ^{1}H NMR spectrum of dehydrocoupling of $H_3B{\cdot}NMe_2H$. Conditions: room temperature, toluene, 2.5 mol% **1**, 5.2 mol% MeLi (25 °C, toluene-d_8, 300.20 MHz).

3.13. NMR spectra of time-resolved dehydrocoupling experiments

All experiments were performed in an open system connected to an oil bubbler. NMR samples were taken at given times directly from Schlenk flasks containing V_0 = 4 mL of the reaction solutions in toluene-d_8.

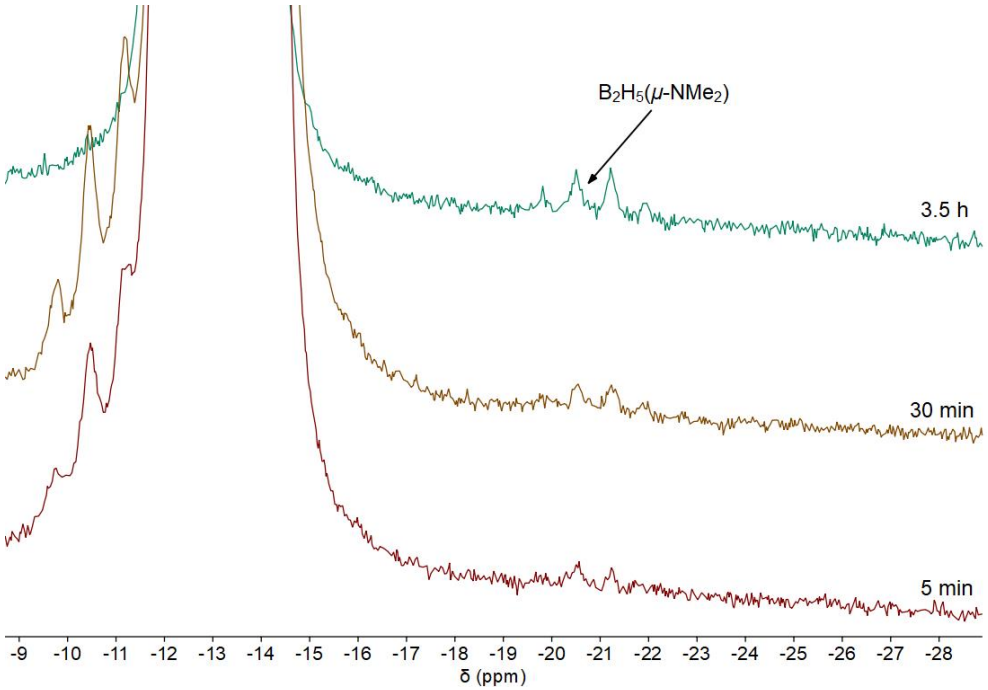

Figure S45. Time resolved ^{11}B NMR spectra of a dehydrocoupling experiment. Conditions: room temperature, toluene, 2.5 mol% **1**, 5.2 mol% MeLi (25 °C, toluene-d_8, 96.32 MHz).

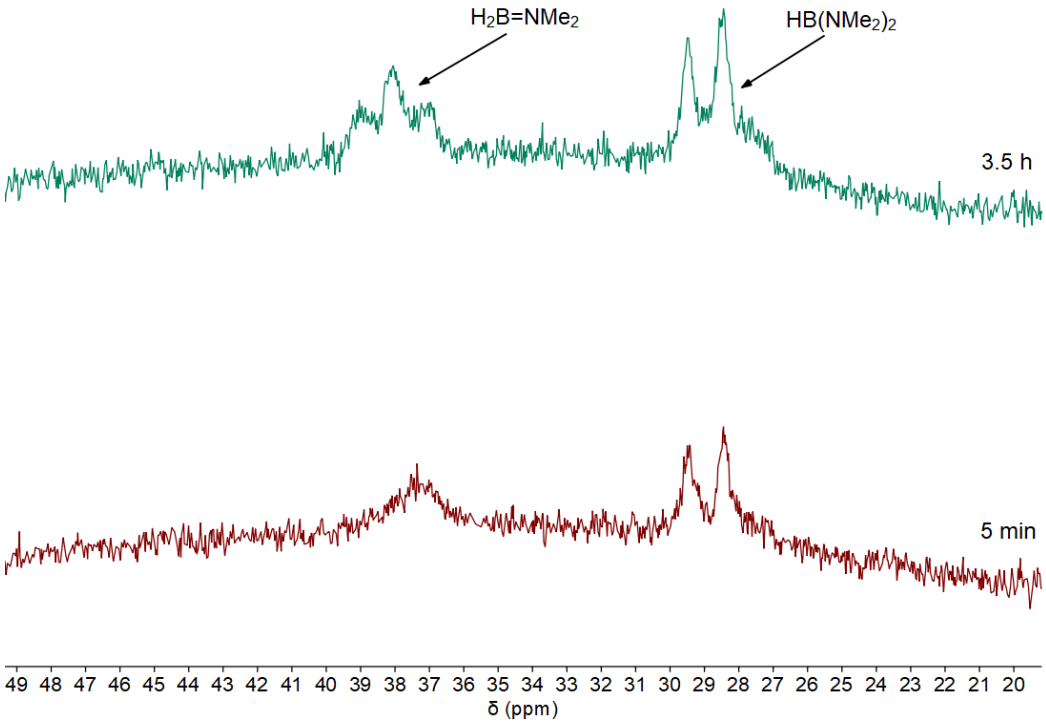

Figure S46. Time resolved ^{11}B NMR spectra of a dehydrocoupling experiment. Conditions: room temperature, toluene, 2.5 mol% **1**, 5.2 mol% MeLi (25 °C, toluene-d_8, 96.32 MHz).

3.14. NMR spectra of MeLi activation of complex 1

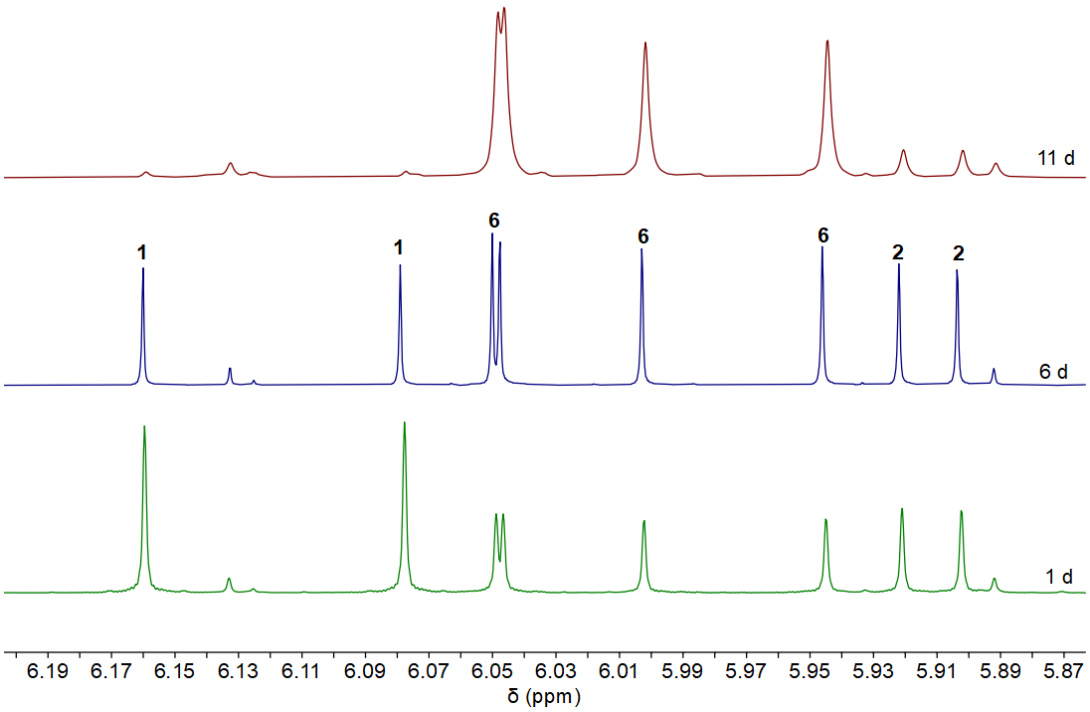

Figure S47. Time resolved ^{1}H NMR spectra of the reaction of **1** with MeLi. Conditions: room temperature, benzene, 0.02 mmol **1**, 0.02 mmol MeLi (25 °C, benzene-d_6, 300.20 MHz).

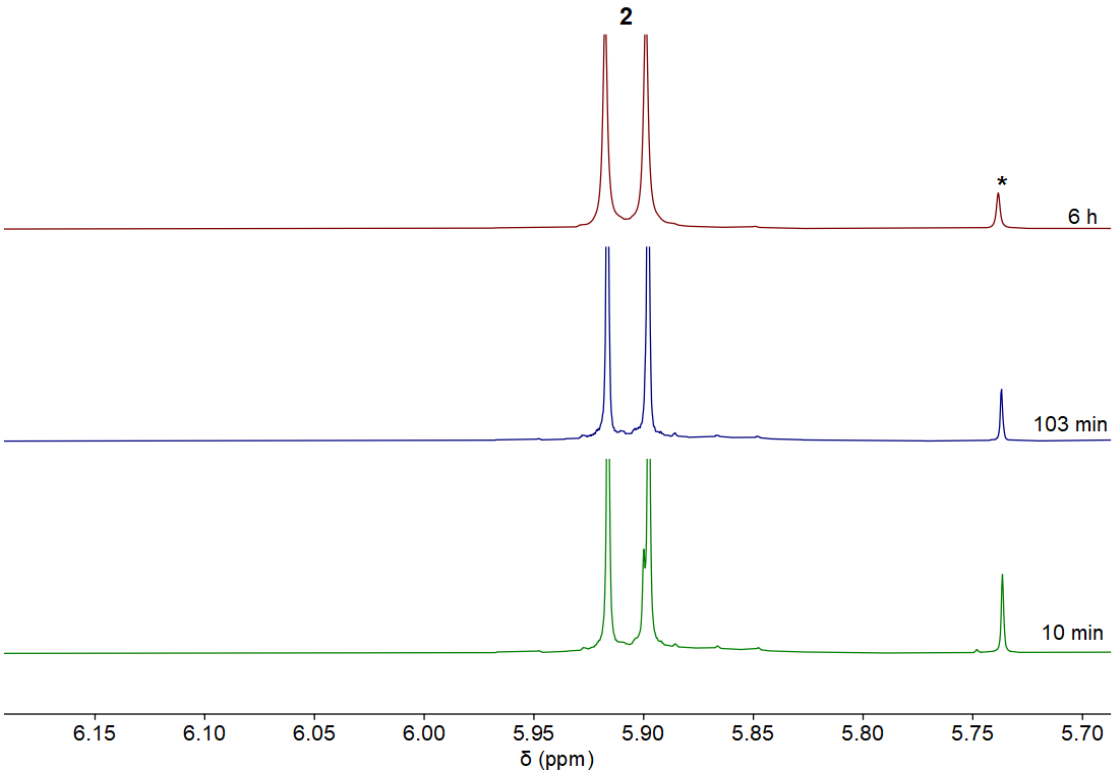

Figure S48. Time resolved ^{1}H NMR spectra of the reaction of **1** with MeLi. Conditions: room temperature, benzene, 0.04 mmol **1**, 0.09 mmol MeLi (25 °C, benzene-d_6, 400.13 MHz). * corresponds to unknown species.

3.15. NMR spectra of catalytic dehydrocoupling of $H_3B{\cdot}NMe_2H$ with complex 1/MeLi and NMe_2H doping

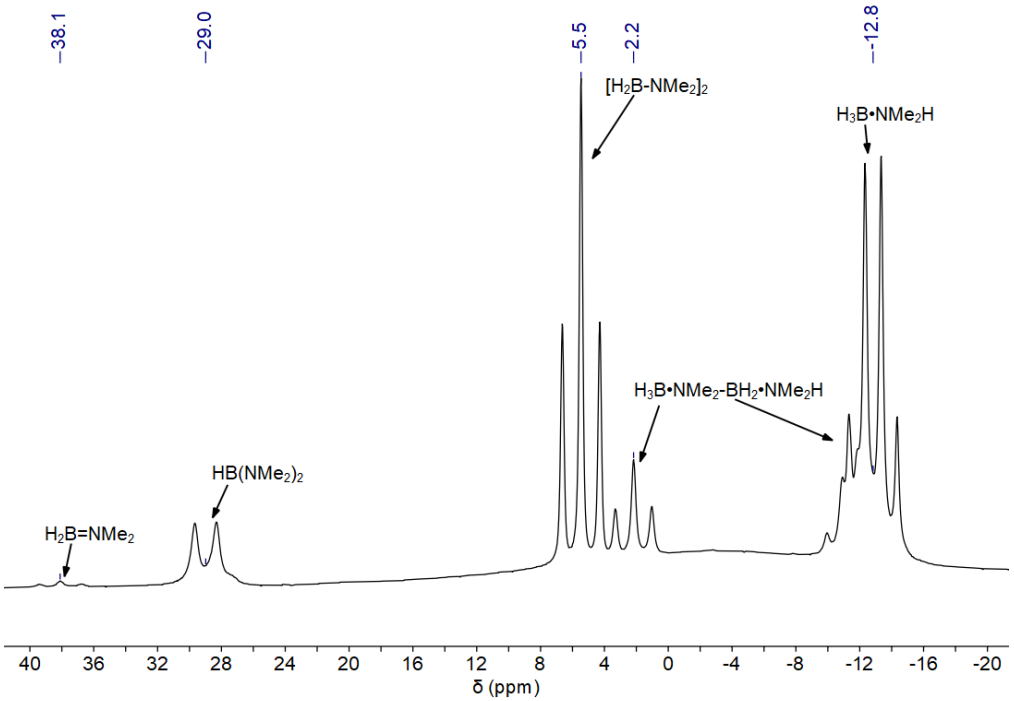

Figure S49. ^{11}B NMR spectrum of dehydrocoupling of $H_3B{\cdot}NMe_2H$. Conditions: room temperature, toluene, 2.5 mol% **2**, 5.2 mol% MeLi, 5.00 mol % NMe_2H (25 °C, toluene-d_8, 96.32 MHz).

3.16. NMR spectra of catalytic dehydrocoupling of $H_3B{\cdot}NMe_2H$ with complex 1/MeLi and $BH_3{\cdot}THF$ doping

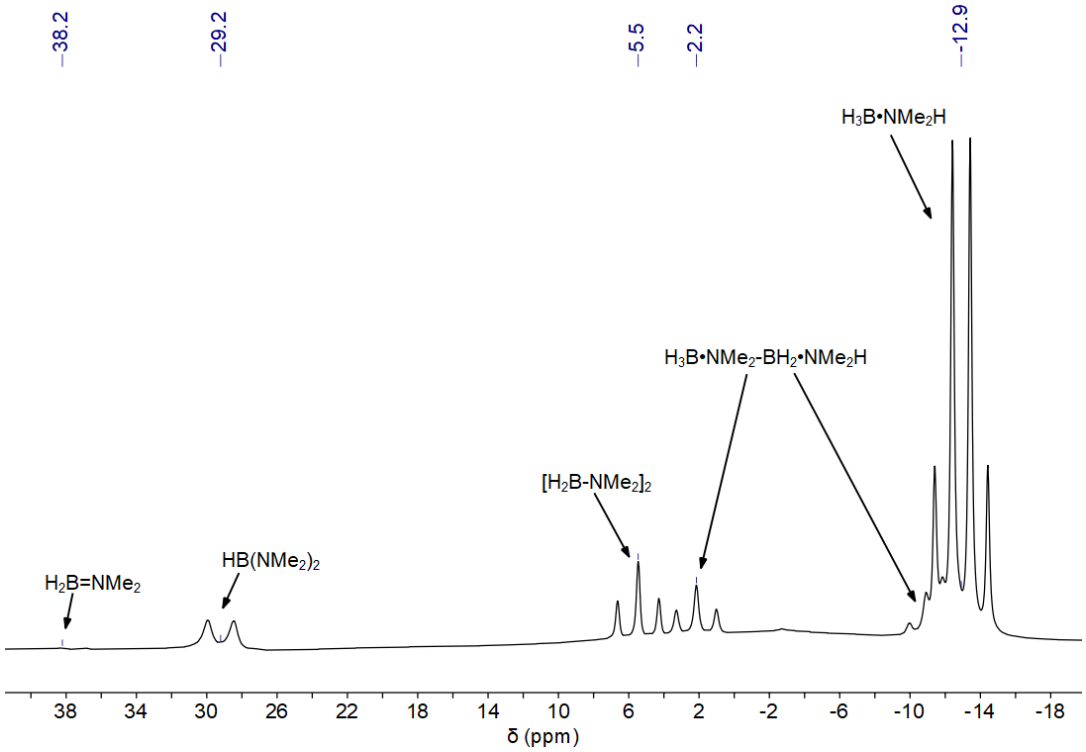

Figure S50. ^{11}B NMR spectrum of dehydrocoupling of $H_3B{\cdot}NMe_2H$. Conditions: room temperature, toluene, 2.5 mol% **2**, 5.2 mol% MeLi, 5.00 mol % $BH_3{\cdot}THF$ (25 °C, toluene-d_8, 96.32 MHz).

3.17. NMR spectra of catalytic dehydrocoupling of $H_3B{\cdot}NMe_2H$ with complex 2

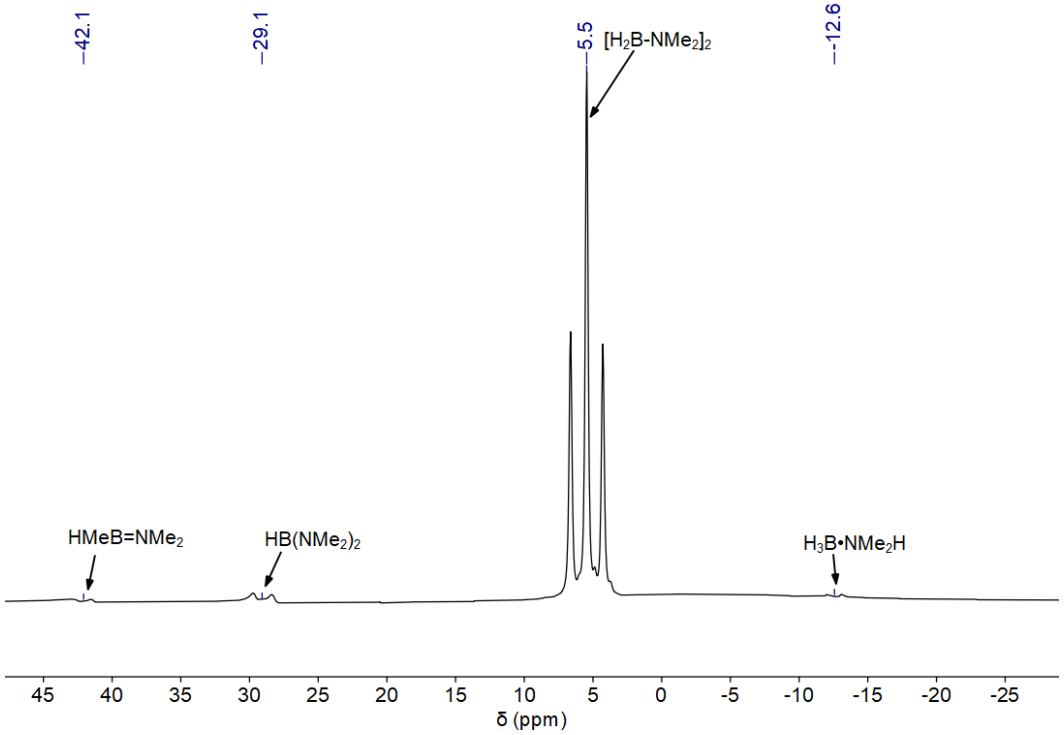

Figure S51. ^{11}B NMR spectrum of dehydrocoupling of $H_3B{\cdot}NMe_2H$. Conditions: room temperature, toluene, 2.5 mol% **2**, 5.2 mol% MeLi (25 °C, toluene-d_8, 96.32 MHz).

3.18. NMR spectra of catalytic dehydrocoupling of $H_3B{\cdot}NMe_2H$ with complex 4

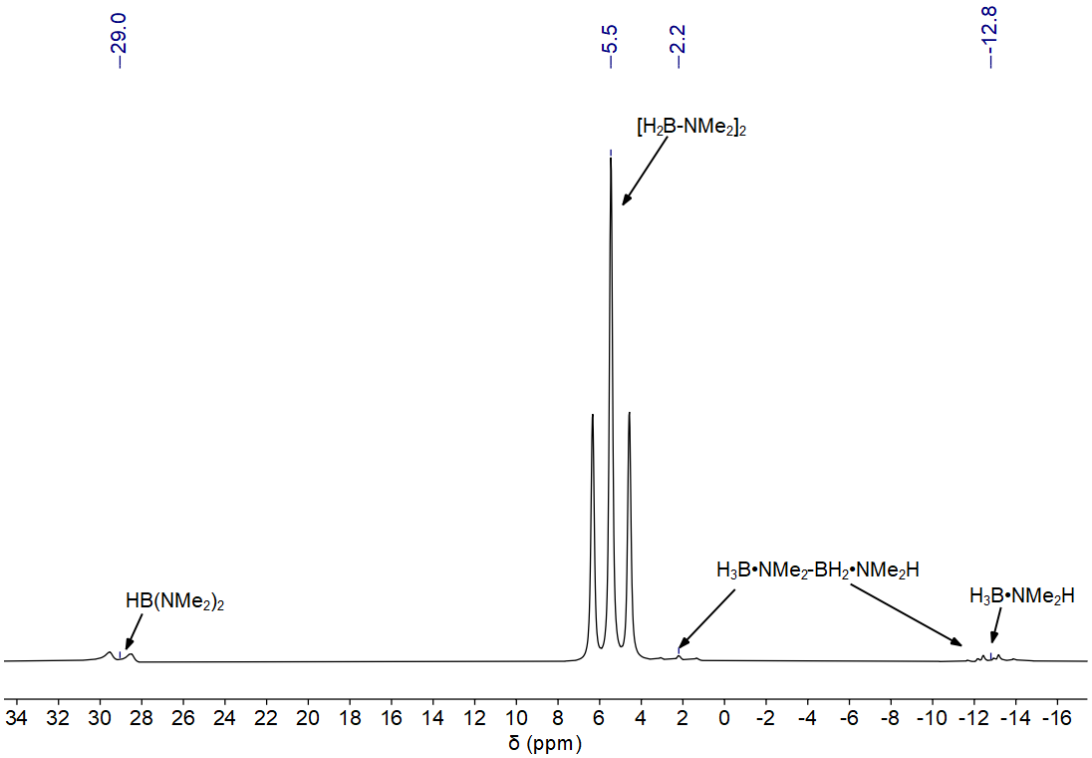

Figure S52. ^{11}B NMR spectrum of dehydrocoupling of $H_3B{\cdot}NMe_2H$. Conditions: room temperature, toluene, 2.5 mol% **4** (25 °C, toluene-d_8, 96.32 MHz).

3.19. NMR spectra of catalytic dehydrocoupling of $H_3B{\cdot}NMe_2H$ with complex 5

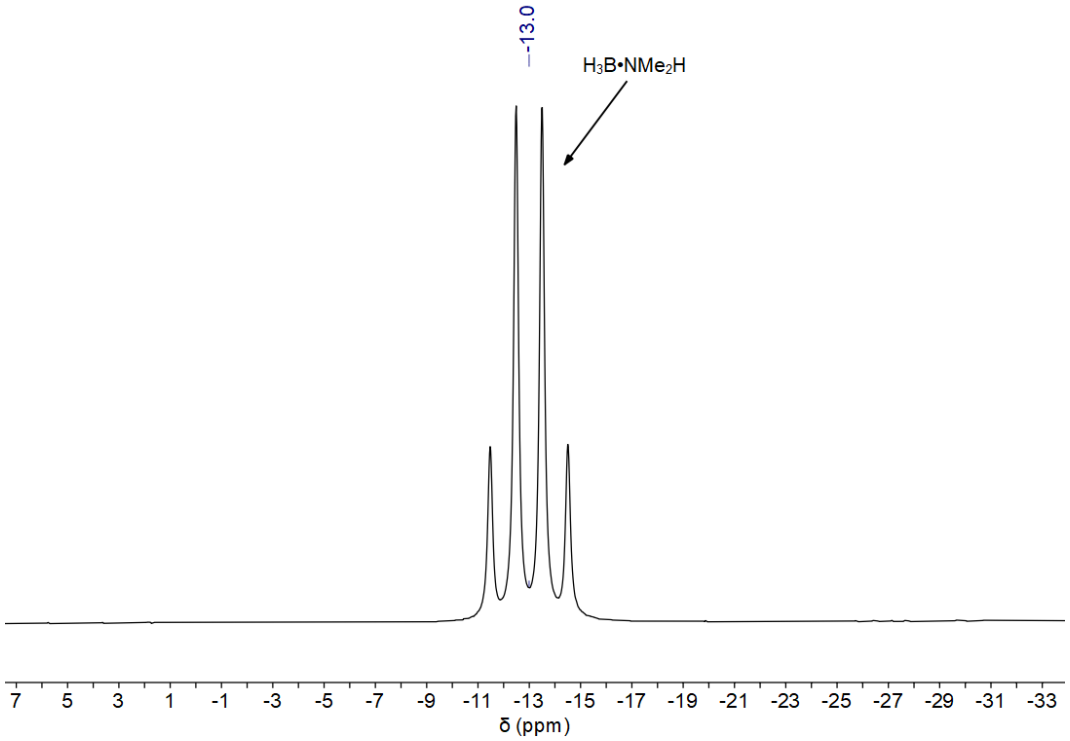

Figure S53. ^{11}B NMR spectrum of dehydrocoupling of $H_3B{\cdot}NMe_2H$. Conditions: room temperature, toluene, 2.5 mol% **5** (25 °C, toluene-d_8, 96.32 MHz).

3.20. NMR spectra of catalytic dehydrocoupling of $H_3B{\cdot}NMe_2H$ with complex 7

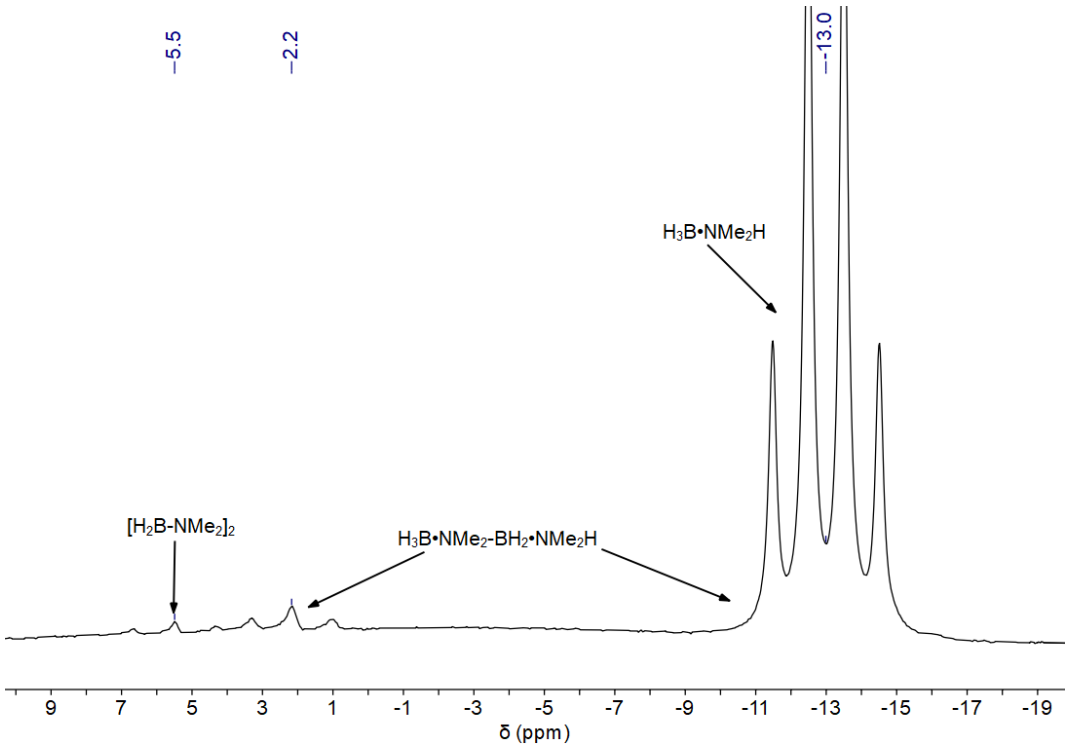

Figure S54. ^{11}B NMR spectrum of dehydrocoupling of $H_3B{\cdot}NMe_2H$. Conditions: room temperature, toluene, 2.5 mol% **7** (25 °C, toluene-d_8, 96.32 MHz).

3.21. NMR spectra of catalytic dehydrocoupling of $H_3B{\cdot}NMe_2H$ with complex 9

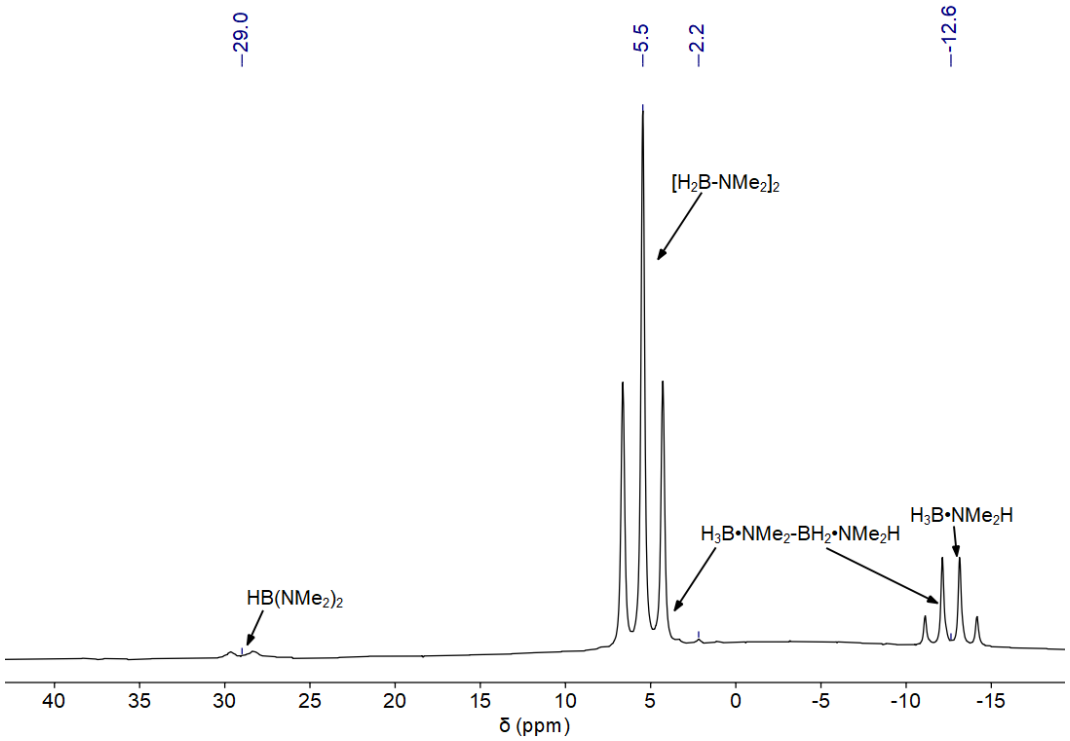

Figure S55. ^{11}B NMR spectrum of dehydrocoupling of $H_3B{\cdot}NMe_2H$. Conditions: room temperature, toluene, 2.5 mol% **9** (25 °C, toluene-d_8, 96.32 MHz).

3.22. NMR spectra of catalytic dehydrocoupling of $H_3B{\cdot}NMe_2H$ with complex 10

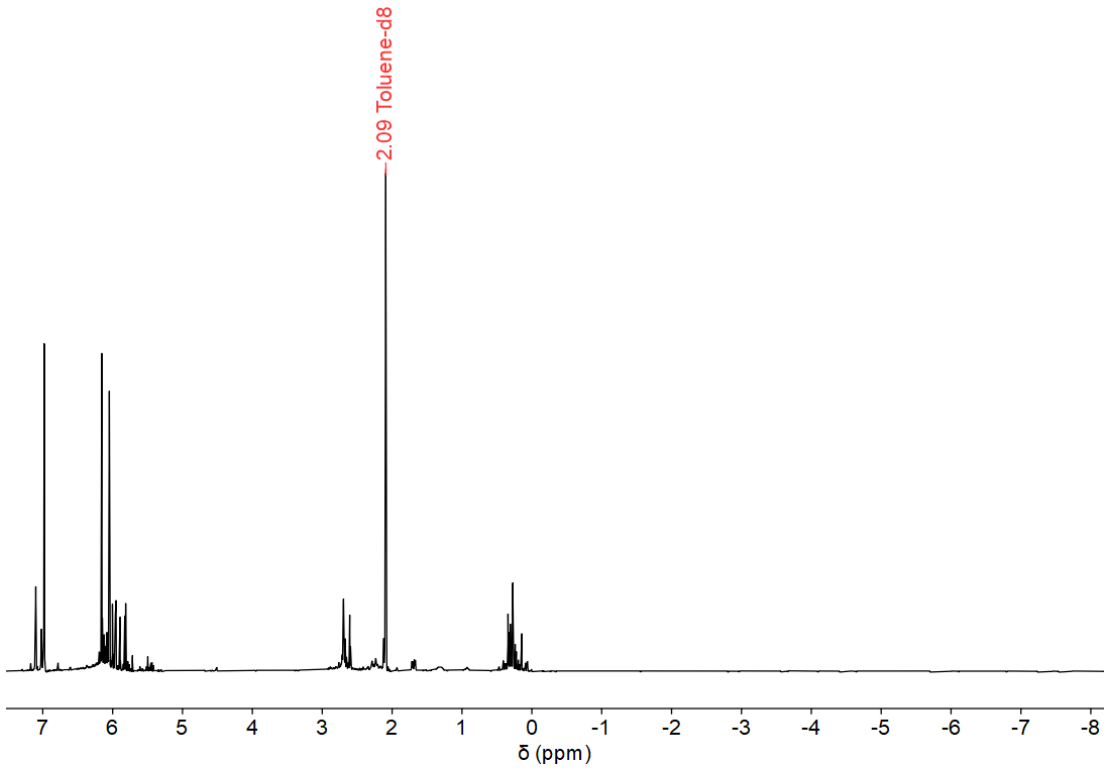

Figure S56. ^1H NMR spectra of dehydrocoupling of $H_3B{\cdot}NMe_2H$. Conditions: room temperature, toluene, 2.5 mol% **10** (25 °C, toluene-d_8, 400.13 MHz).

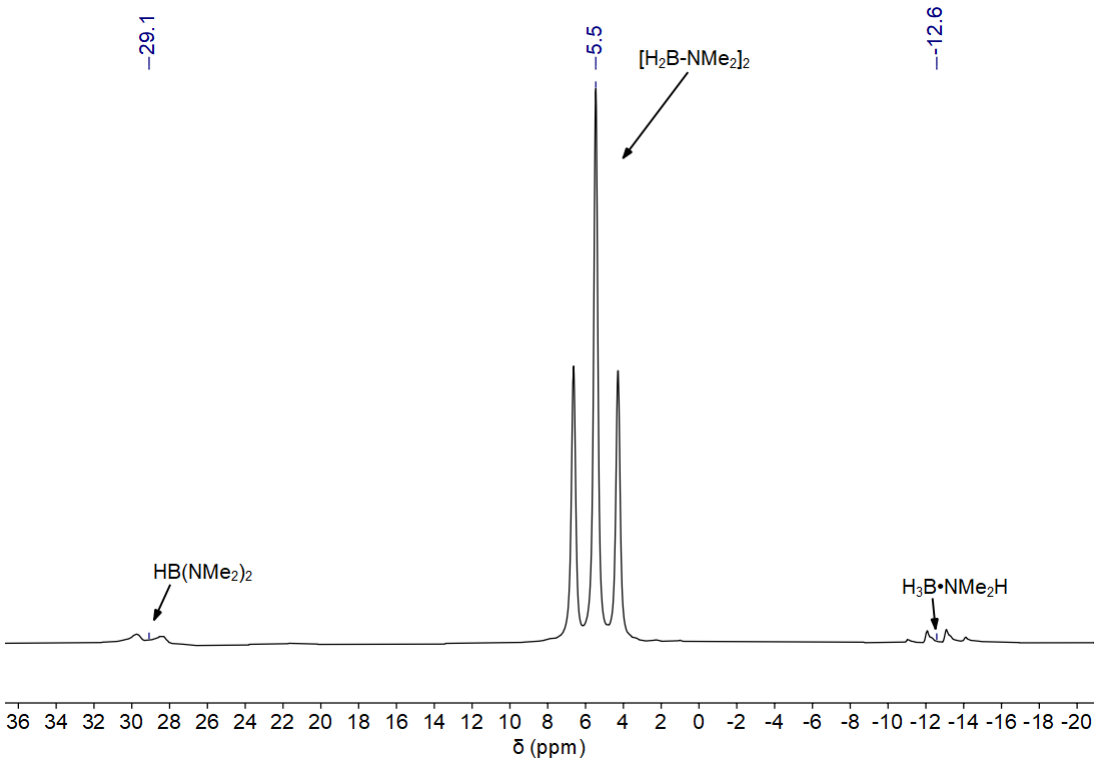

Figure S57. ^{11}B NMR spectrum of dehydrocoupling of $H_3B{\cdot}NMe_2H$. Conditions: room temperature, toluene, 2.5 mol% **10** (25 °C, toluene-d_8, 96.32 MHz).

3.23. NMR spectra of catalytic dehydrocoupling of deuterated amine boranes

3.23.1. NMR spectra after dehydrocoupling of $H_3B{\cdot}NMe_2D$

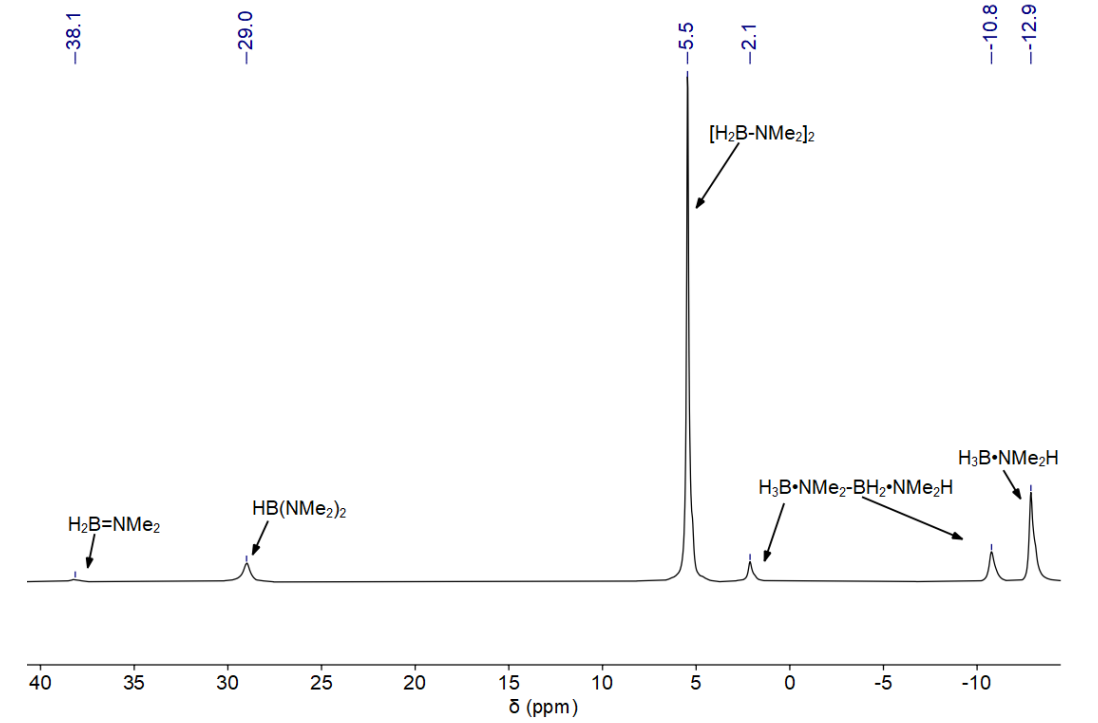

Figure S58. ^{11}B{^{1}H} spectrum of dehydrocoupling of $H_3B{\cdot}NMe_2D$. Conditions: room temperature, toluene, 2.5 mol% **1**, 5.2 mol% MeLi (25 °C, toluene-d_8, 96.32 MHz).

3.23.2. NMR spectra after dehydrocoupling of $D_3B{\cdot}NMe_2H$

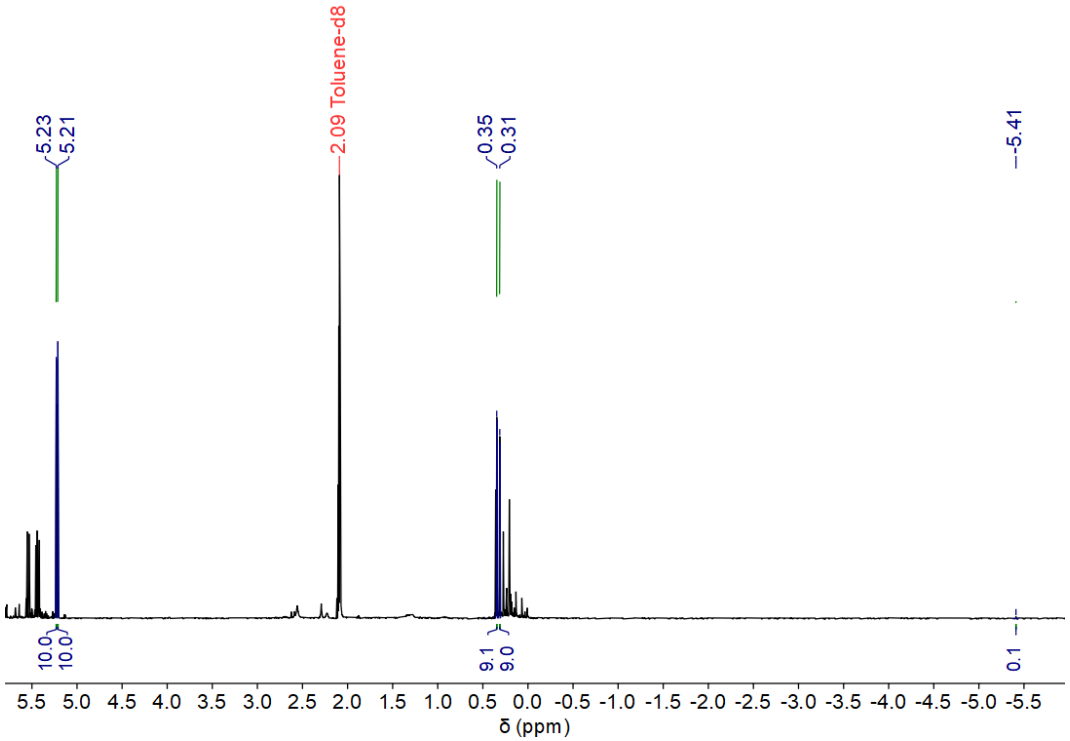

Figure S59. ^1H NMR spectrum of dehydrocoupling of $D_3B{\cdot}NMe_2H$. Conditions: room temperature, toluene, 2.5 mol% **1**, 5.2 mol% MeLi. The CH_2 resonance of protonated **7** at -5.41 ppm is absent, indicating the presence of a CD_2 group by exclusive transfer of B-D to the Zr complex **7** (25 °C, toluene-d_8, 300.20 MHz).

3.23.3. NMR spectra after dehydrocoupling of $D_3B{\cdot}NMe_2D$

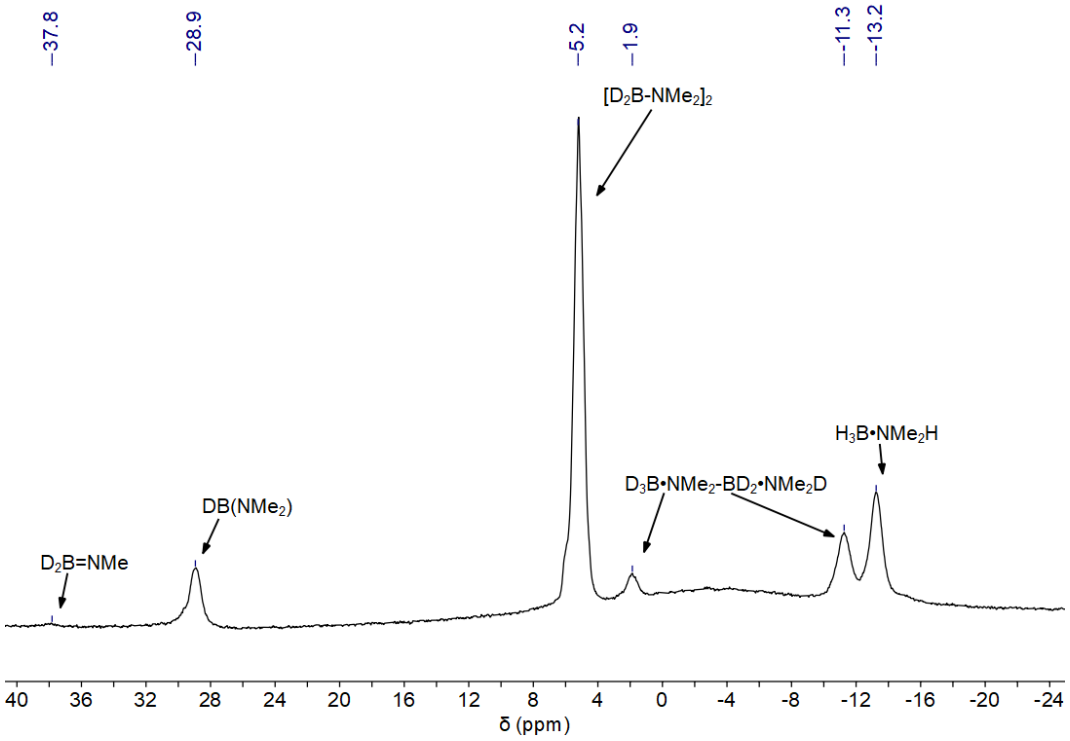

Figure S60. ^{11}B spectrum of dehydrocoupling of $D_3B{\cdot}NMe_2D$. Conditions: room temperature, toluene, 2.5 mol% **1**, 5.2 mol% MeLi (25 °C, toluene-d_8, 96.32 MHz).

3.24. NMR spectra of dehydrocoupling of $H_3B{\cdot}NMe_2H$, activation with $Li[NMe_2{\cdot}BH_3]$

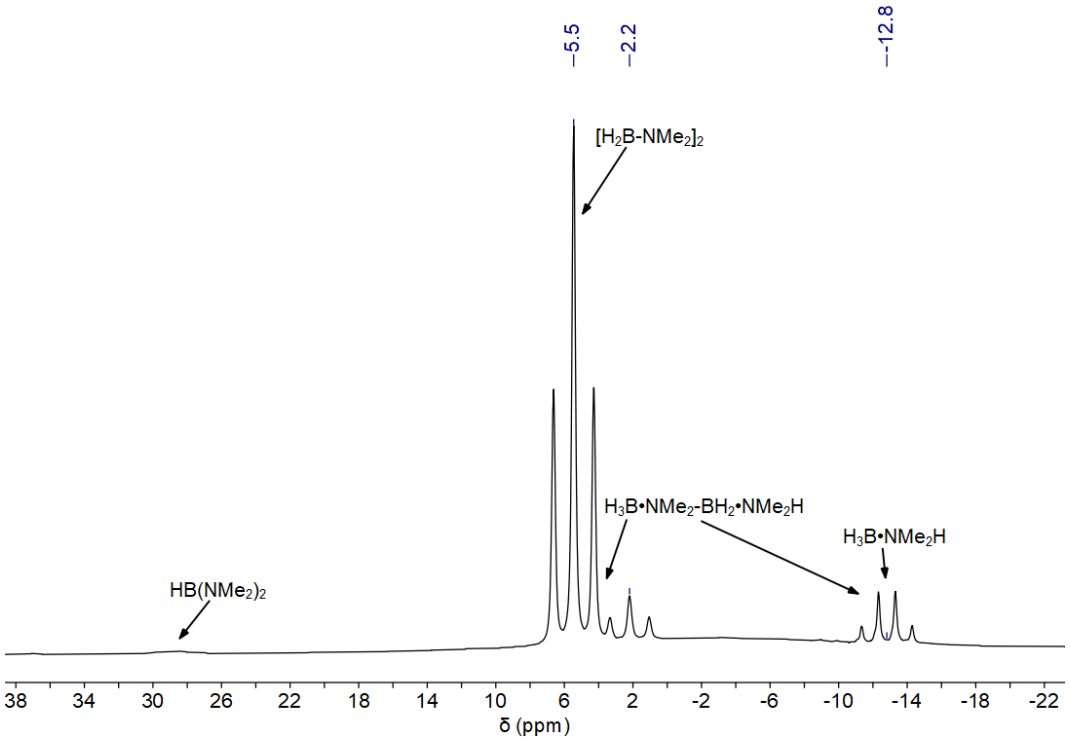

Figure S61. ^{11}B NMR spectrum of catalytic dehydrocoupling of $H_3B{\cdot}NMe_2H$. Conditions: room temperature, toluene, 2.5 mol% **1**, 5.0 mol% $Li[NMe_2{\cdot}BH_3]$ (25 °C, toluene-d_8, 96.32 MHz).

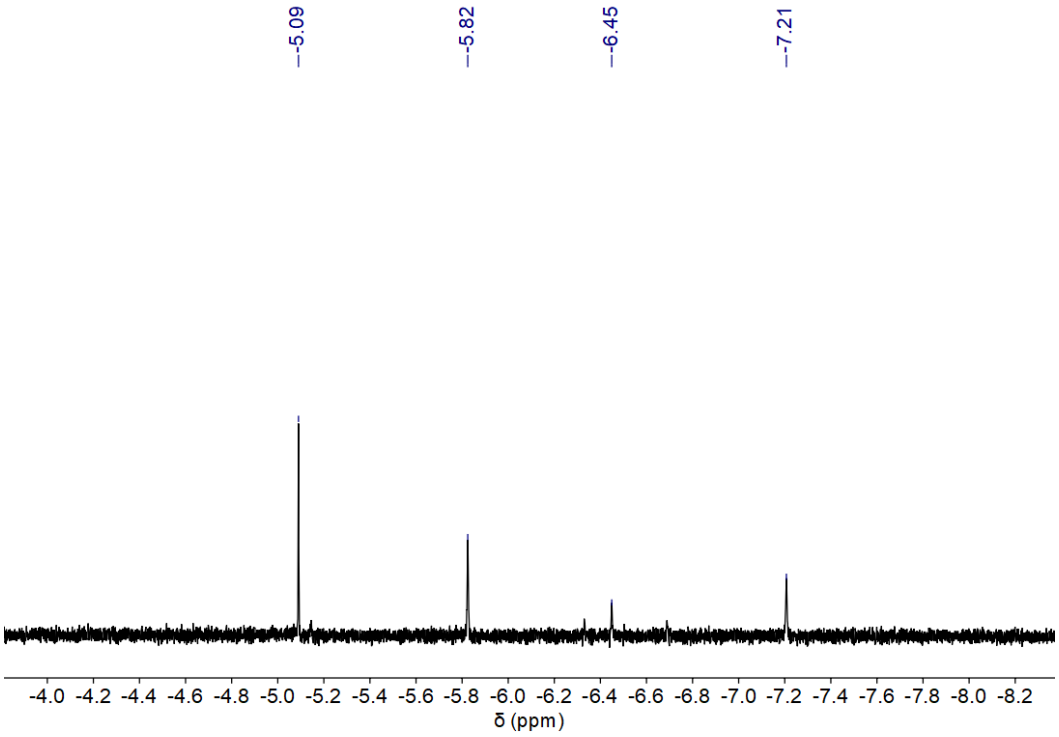

Figure S62. ^{1}H NMR spectrum of the high field region of a stoichiometric reaction of **1** with $Li[NMe_2{\cdot}BH_3]$. Conditions: room temperature, benzene, 0.07 mmol **1**, 0.14 mmol $Li[NMe_2{\cdot}BH_3]$ (25 °C, benzene-d_6, 300.13 MHz).

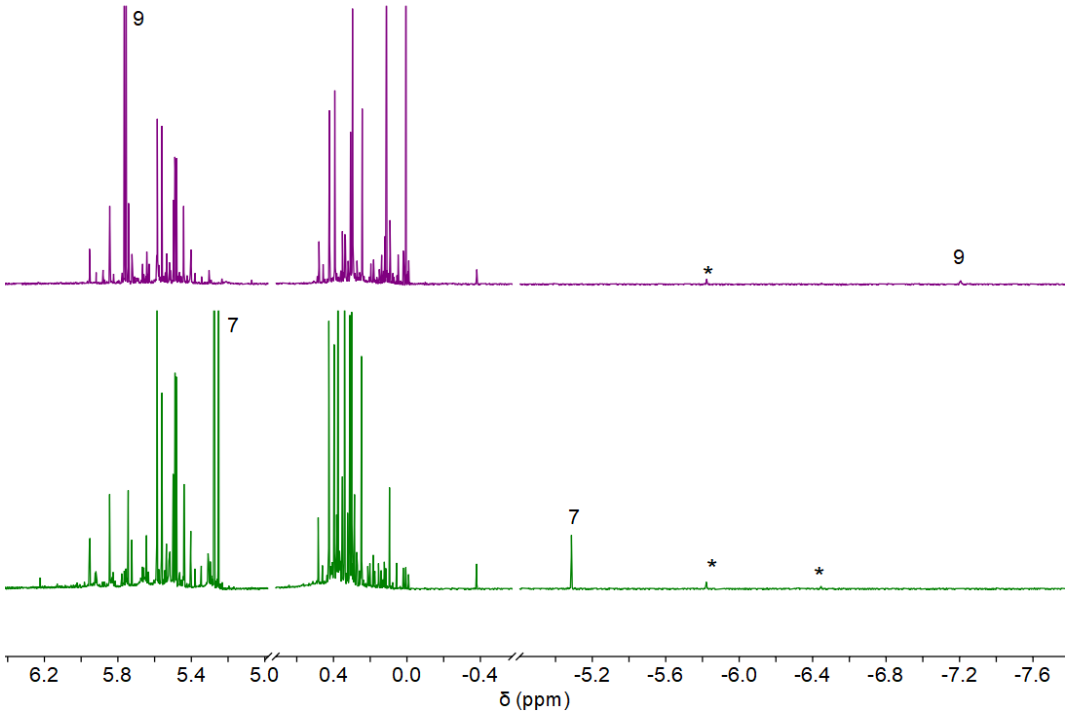

Figure S63. ^{1}H NMR spectra of stoichiometric reaction of $H_3B{\cdot}NMe_2H$ with **1**. Conditions: room temperature, benzene, 1.33 mmol $H_3B{\cdot}NMe_2H$ (green: 0.07 mmol **1**, 0.14 mmol $Li[NMe_2{\cdot}BH_3]$ with vacuo, purple: 0.07 mmol **1**, 0.14 mmol $Li[NMe_2{\cdot}BH_3]$ without vacuo) (25 °C, benzene-d_6, 300.20 MHz). * corresponds to unknown species.

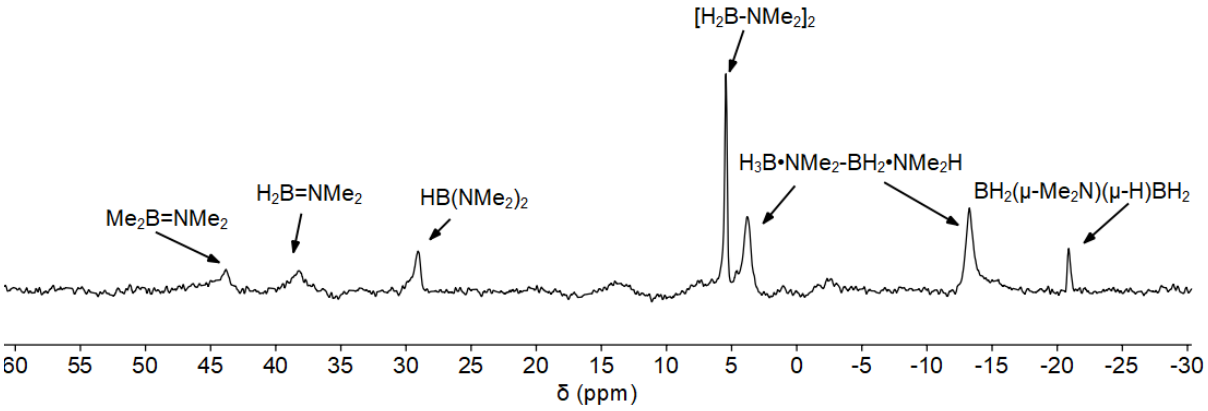

Figure S64. ^{11}B NMR spectrum stoichiometric reaction of $H_3B{\cdot}NMe_2H$ with **1**. Conditions: room temperature, toluene, 0.07 mmol **1**, 0.14 mmol $Li[NMe_2{\cdot}BH_3]$ (25 °C, benzene-d_6, 96.32 MHz).

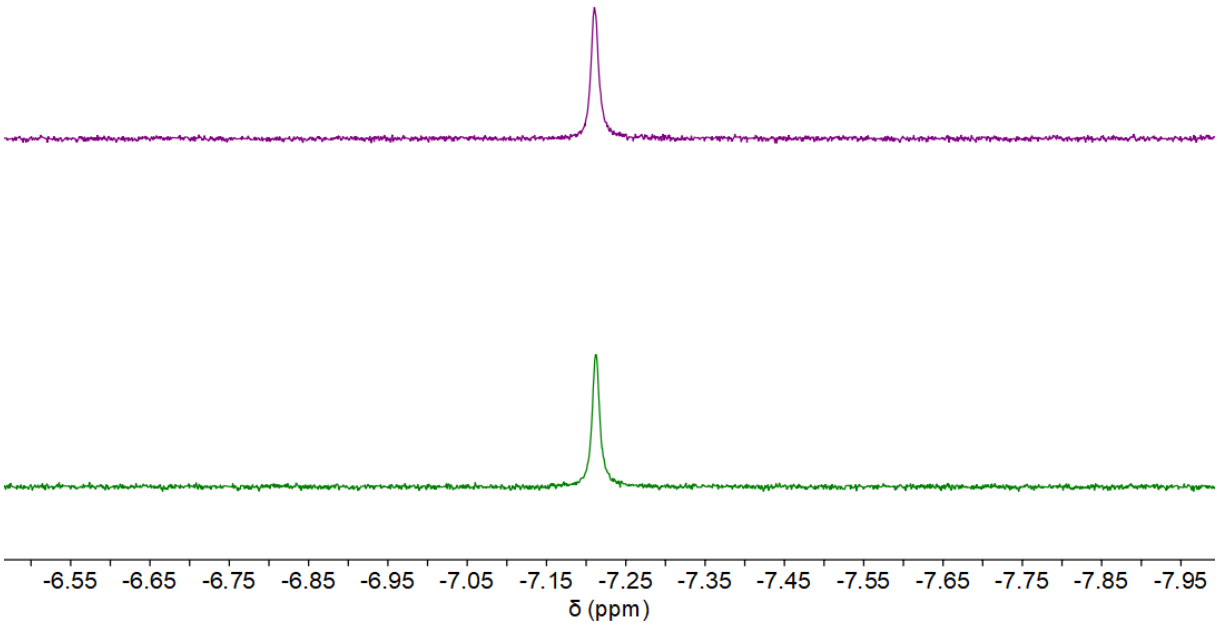

Figure S65. Comparison of $^{1}H\{^{11}B\}$ (purple) and ^{1}H NMR spectra (green) of stoichiometric reaction of $H_3B{\cdot}NMe_2H$ with **1**. Conditions: room temperature, toluene, 0.07 mmol **1**, 0.56 mmol $Li[NMe_2{\cdot}BH_3]$ (25 °C, benzene-d_6, 300.20 MHz).

3.25. NMR spectra of stoichiometric experiments

3.25.1. Comparison of the stoichiometric reaction of 4 with $BH_3{\cdot}THF$

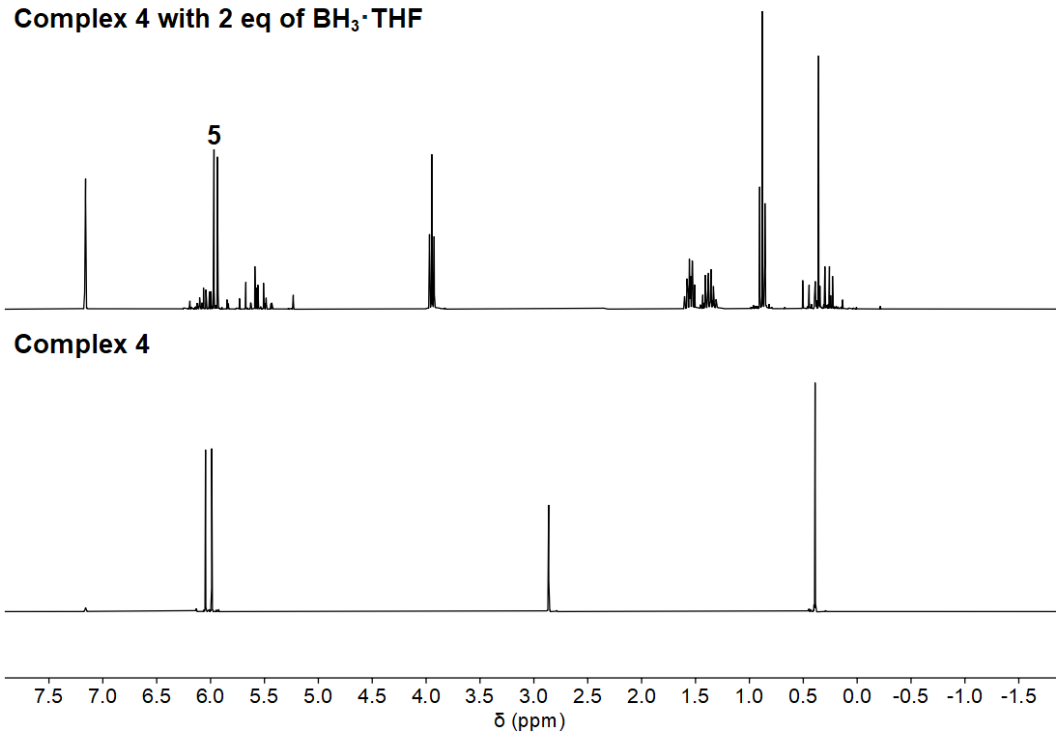

Figure S66. ^{1}H NMR spectrum of stoichiometric reaction of **4** with $BH_3{\cdot}THF$ (25 °C, benzene-d_6, 300.13 MHz).

3.25.2. NMR spectrum of the stoichiometric reaction of $H_3B{\cdot}NMeH_2$ with 1/MeLi

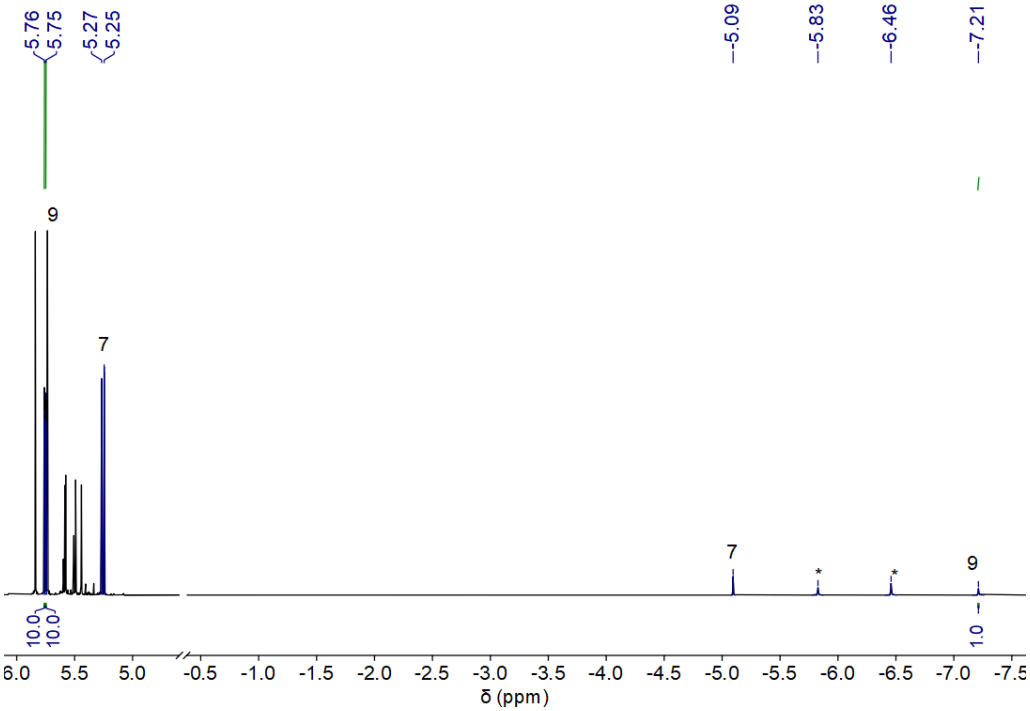

Figure S67. ^{1}H NMR spectrum of stoichiometric reaction of $H_3B{\cdot}NMeH_2$ with **1**/MeLi. Conditions: room temperature, benzene, 0.02 mmol **1**, 0.05 mmol MeLi (25 °C, benzene-d_6, 300.20 MHz). The region between 0.5 and 5.0 ppm which shows the products of dehydrocoupling of $H_3B{\cdot}NMeH_2$ has been omitted. * corresponds to unknown species.

3.25.3. NMR spectrum of the stoichiometric reaction of $H_3B{\cdot}NMe_2H$ with 1/MeLi

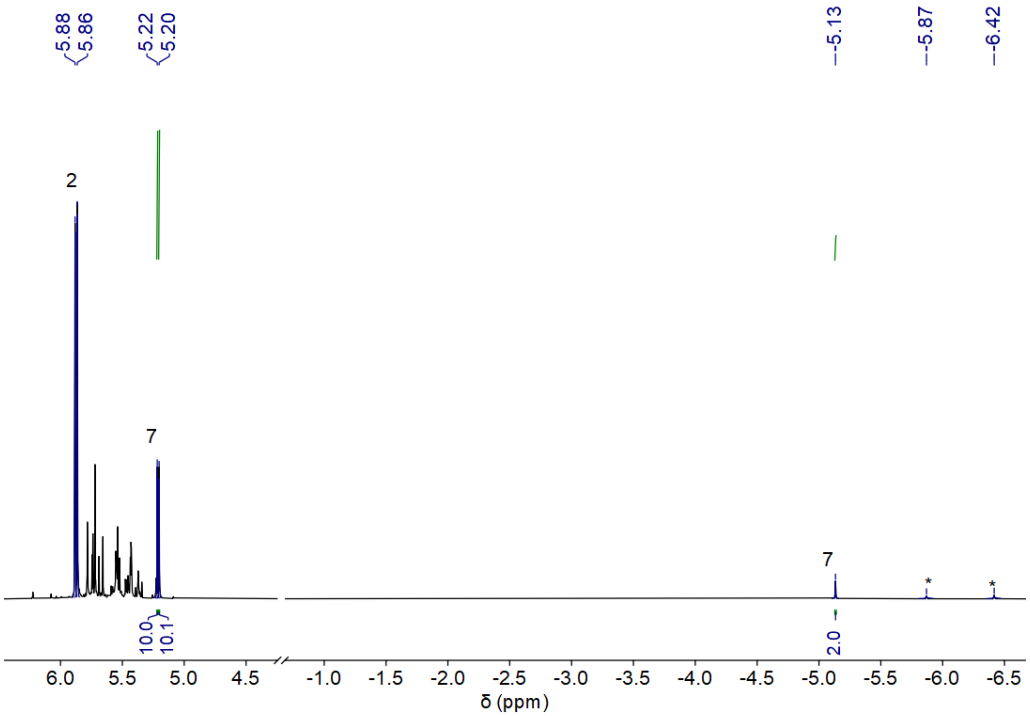

Figure S68. ^{1}H NMR spectrum of stoichiometric reaction of $H_3B{\cdot}NMe_2H$ with **1**/MeLi. Conditions: room temperature, toluene, 0.04 mmol **1**, 0.07 mmol MeLi (25 °C, toluene-d_8, 300.20 MHz). The region between -1.0 and 4.5 ppm which shows the products of dehydrocoupling of $H_3B{\cdot}NMeH_2$ has been omitted.

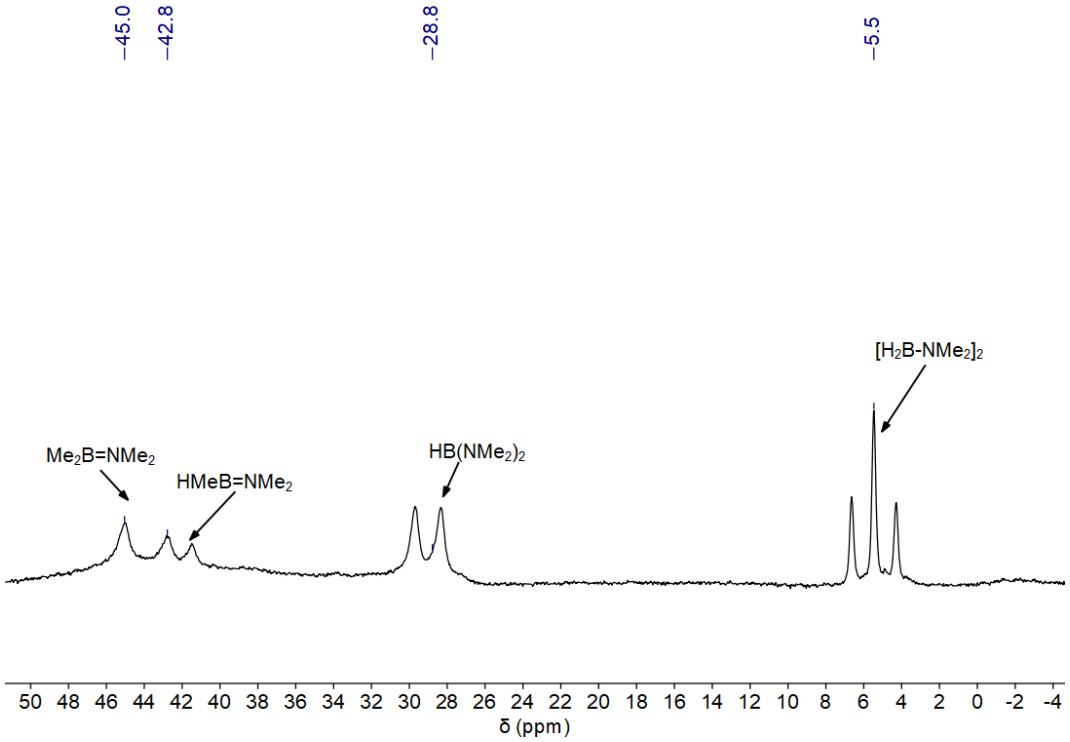

Figure S69. ^{11}B NMR spectrum of stoichiometric reaction of $H_3B{\cdot}NMe_2H$ with **1**/MeLi. Conditions: room temperature, toluene, 0.04 mmol **1**, 0.07 mmol MeLi. (25 °C, toluene-d_8, 96.32 MHz).

3.25.4. NMR spectrum of stoichiometric reaction of $D_3B{\cdot}NMe_2H$ with 1/MeLi

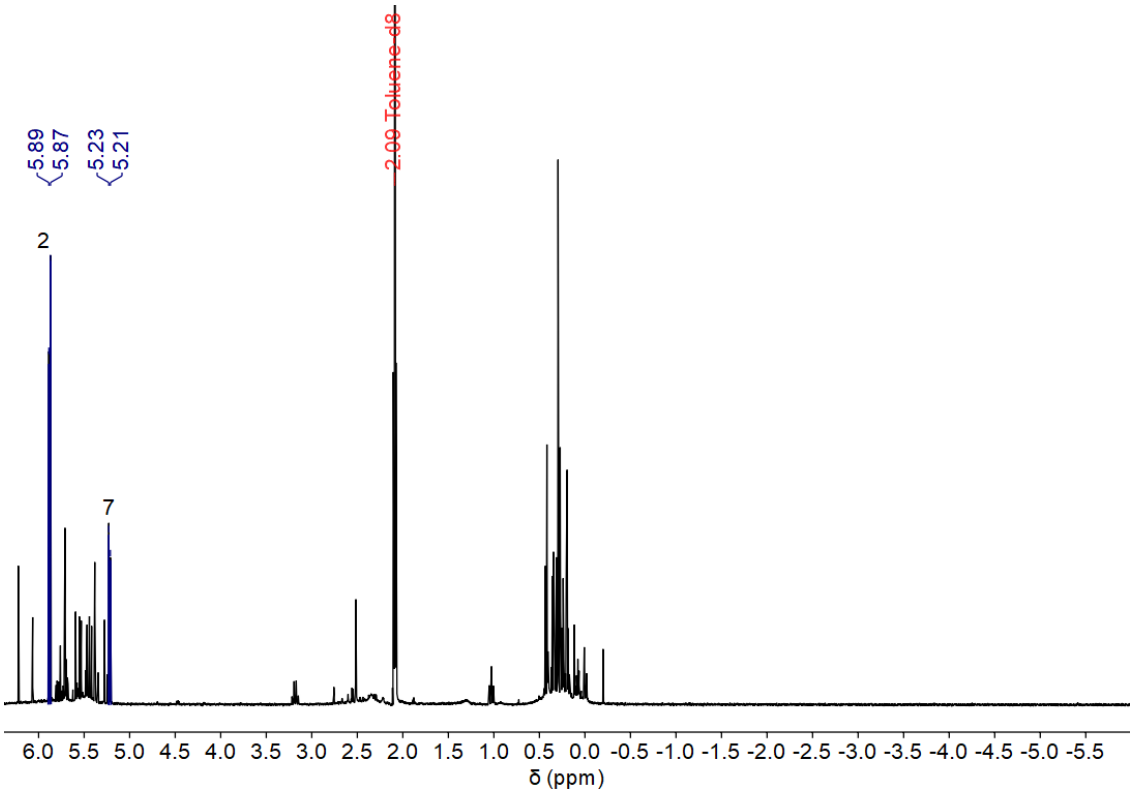

Figure S70. ^{1}H NMR spectrum of stoichiometric reaction of $D_3B{\cdot}NMe_2H$ with **1**/MeLi. Conditions: room temperature, toluene, 0.06 mmol **1**, 0.14 mmol MeLi (25 °C, toluene-d_8, 300.20 MHz).

3.25.5. NMR spectrum of stoichiometric reaction of $H_3B{\cdot}NMe_2D$ with 1/MeLi

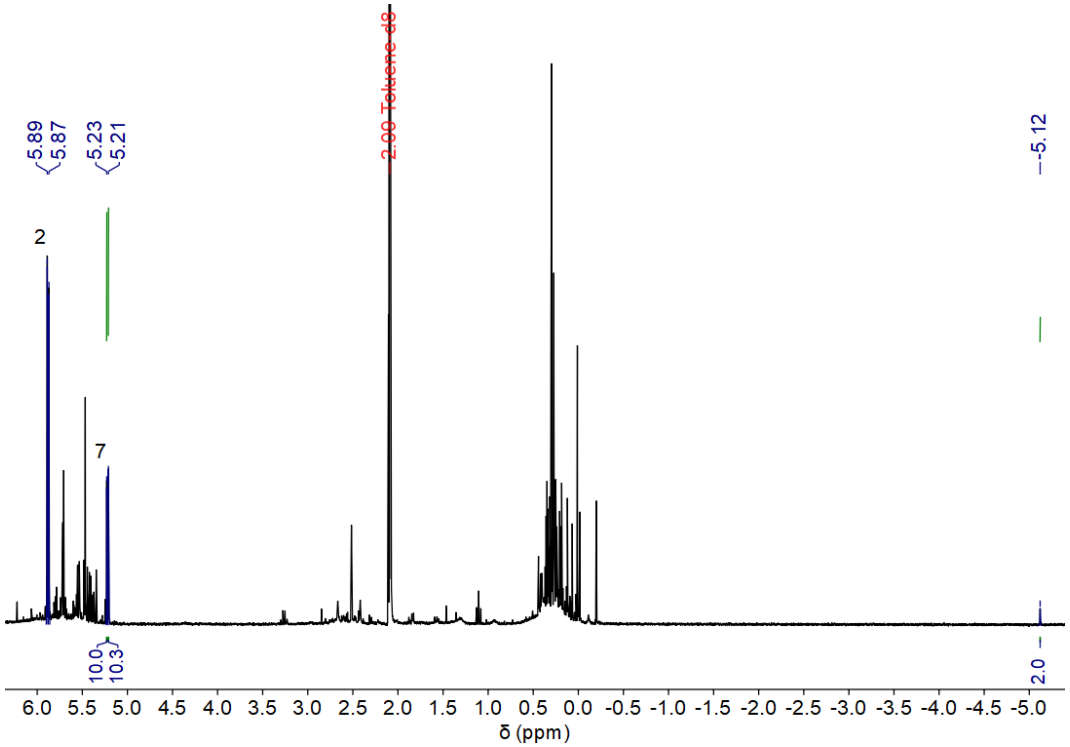

Figure S71. ^{1}H NMR spectrum of stoichiometric reaction of $H_3B{\cdot}NMe_2D$ with **1**/MeLi. Conditions: room temperature, toluene, 0.06 mmol **1**, 0.14 mmol MeLi (25 °C, toluene-d_8, 300.20 MHz).

3.25.6. NMR spectrum of stoichiometric reaction of $H_3B{\cdot}NMe_2H$ with complex 2

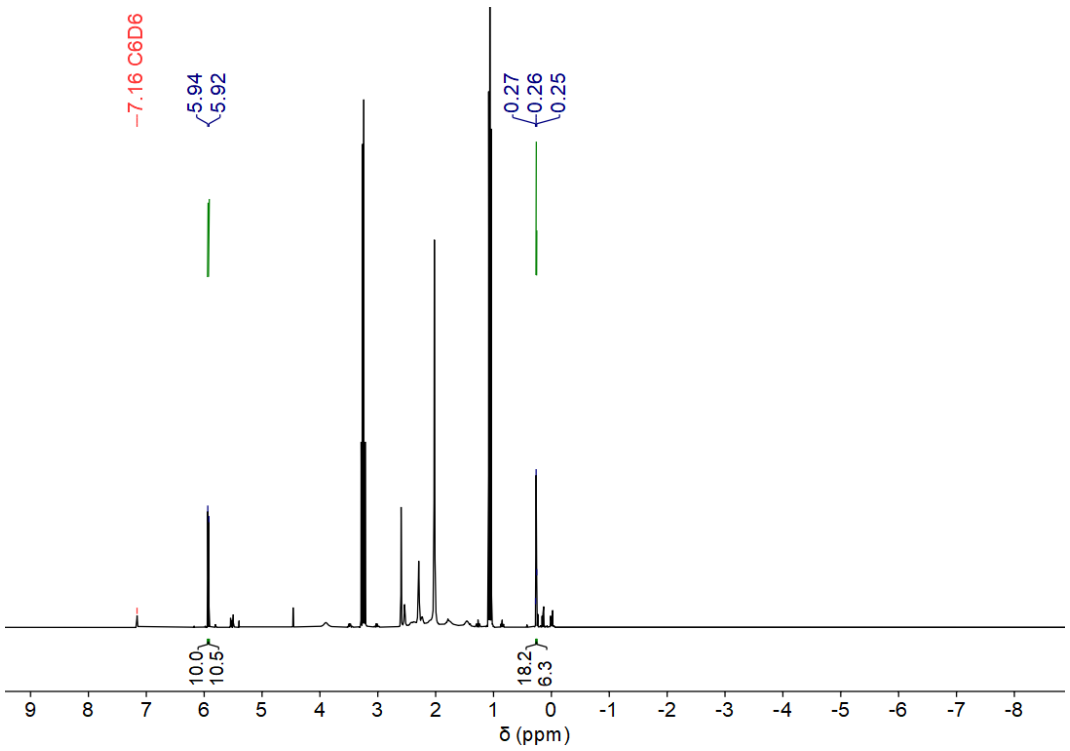

Figure S72. ^{1}H NMR spectra of stoichiometric reaction of $H_3B{\cdot}NMe_2H$ with complex **2**. Conditions: room temperature, benzene, 0.03 mmol **2**, 0.06 mmol $H_3B{\cdot}NMe_2H$ (25 °C, benzene-d_6, 400.13 MHz).

3.25.7. NMR spectrum of stoichiometric reaction of $H_3B{\cdot}NMe_2H$ with complex 4

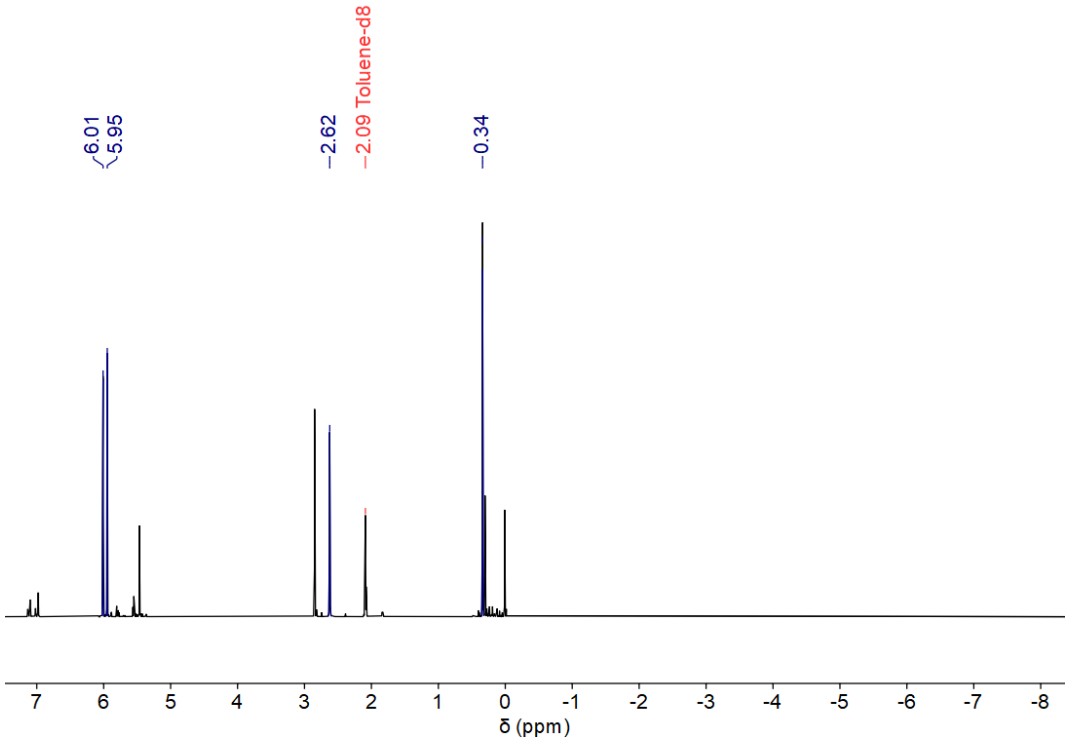

Figure S73. ^{1}H NMR spectrum of stoichiometric reaction of $H_3B{\cdot}NMe_2H$ with complex **4**. Conditions: room temperature, toluene, 0.06 mmol **4**, 0.14 mmol MeLi (25 °C, toluene-d_8, 300.20 MHz).

3.25.8. NMR spectra of stoichiometric reaction of $Li[NMe_2{\cdot}BH_3]$ with complex 6

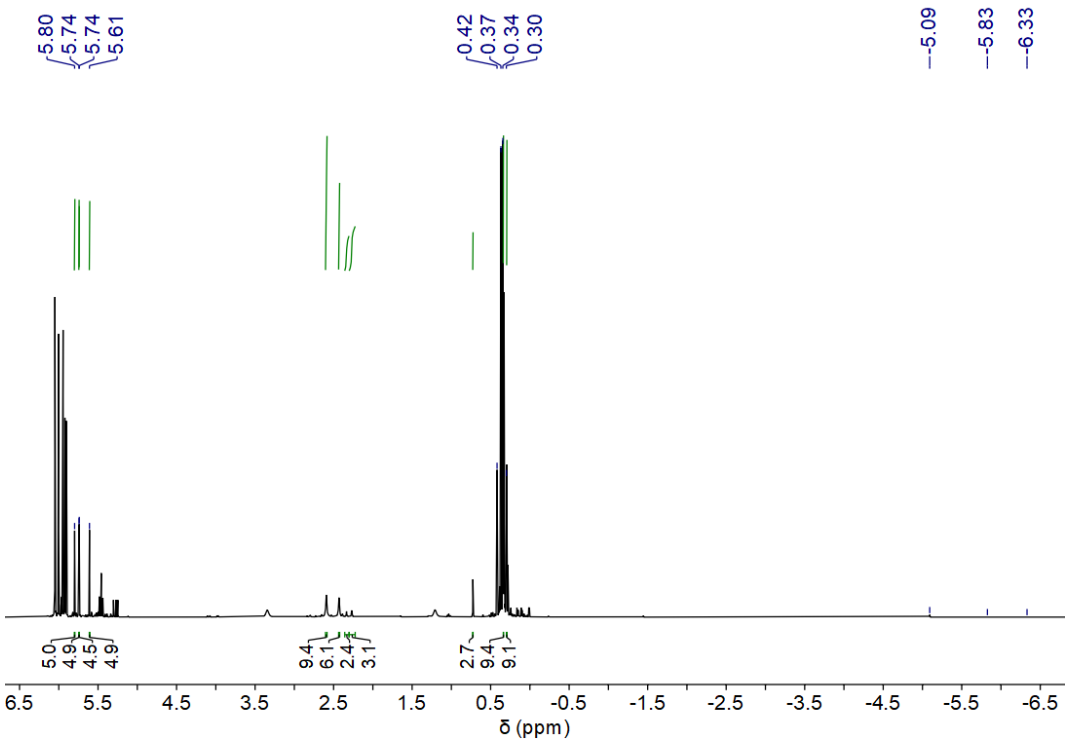

Figure S74. ^{1}H NMR spectra of stoichiometric reaction of $Li[NMe_2BH_3]$ with complex **6**. Conditions: room temperature, benzene, 0.02 mmol **6**, 0.02 mmol $Li[NMe_2BH_3]$ (25 °C, benzene-d_6, 400.13 MHz).

3.25.9. NMR spectra of the stoichiometric reaction of $D_3B{\cdot}NMe_2H$ with complex 10

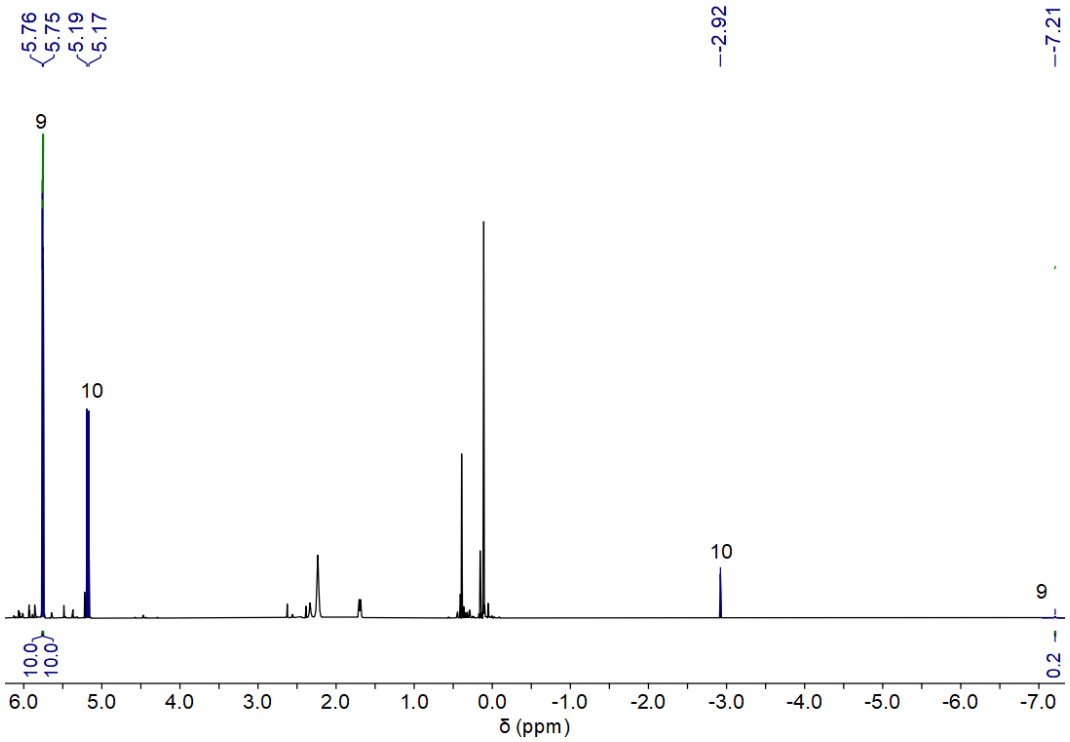

Figure S75. ^1H NMR spectrum of stoichiometric reaction of $D_3B{\cdot}NMe_2H$ with complex **10**. Conditions: room temperature, benzene, 0.04 mmol **1**. (25 °C, benzene-d_6, 300.20 MHz).

4. Details of UV/Vis spectroscopy

4.1. General information

UV-Vis studies were carried out using a Varian CARY 4000 spectrometer. To ensure the necessary anaerobic conditions for the oxygen and water sensitive zirconocene catalyst system the measurements were performed in a thermostatically controlled Schlenk vessel with a dip optrode (10 mm slit width) and fiber optics input and output.[1] Directly before each experiment the baseline was measured. The spectra were smoothed by Origin 2019b.

UV-Vis analysis of **6** and **9** was performed using an *analytikjena specord s* 600 diode array photometer. The samples were dissolved in Toluene in a 1 cm quartz cuvette with a Schlenk-Valve. If necessary, the samples were diluted using Schlenk techniques.

4.2. Experimental details

4.2.1. Complex 1

In a glovebox complex **1** (6.90 mg, 0.01 mmol) was transferred into a three-neck reaction vessel and dissolved in 31.7 mL of toluene and the measurement was started. The measurements were carried out at 25 °C.

4.2.2. Dilution of MeLi

MeLi (120 μL, 0.19 mmol) was added to 16.0 mL of toluene and was titrated with toluene in 5.0 mL steps. The measurements were carried out at 40 °C.

4.2.3. Complex 1 with MeLi

MeLi (12.5 μL, 0.02 mmol) was subsequently added to the reaction vessel containing **1** in 31.7 mL of toluene and the was measurement started. The measurements were carried out at 25 °C.

4.2.4. Catalytic dehydrocoupling of $H_3B{\cdot}NMe_2H$

In a glovebox complex **1** (6.90 mg, 0.01 mmol) and $H_3B{\cdot}NMe_2H$ (47 mg, 0.80 mmol) were transferred into a three-neck reaction vessel. All components were dissolved in 20.1 mL of toluene. MeLi (12.5 μL, 0.02 mmol) was added to the solution and the measurement was started. The measurements were carried out at 25 °C.

4.3. UV/Vis spectra

4.3.1. Complex 1

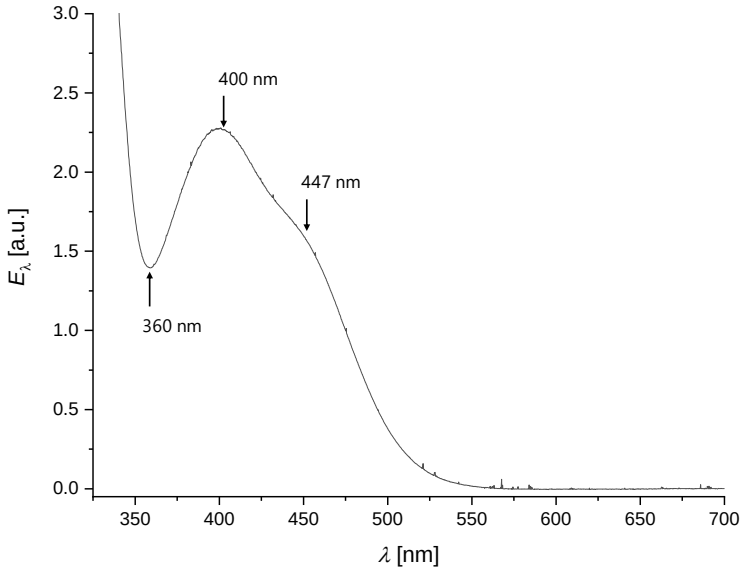

Figure S76. UV-Vis spectra of **1** (0.01 mmol in 31.7 mL of toluene).

4.3.2. Complex 2

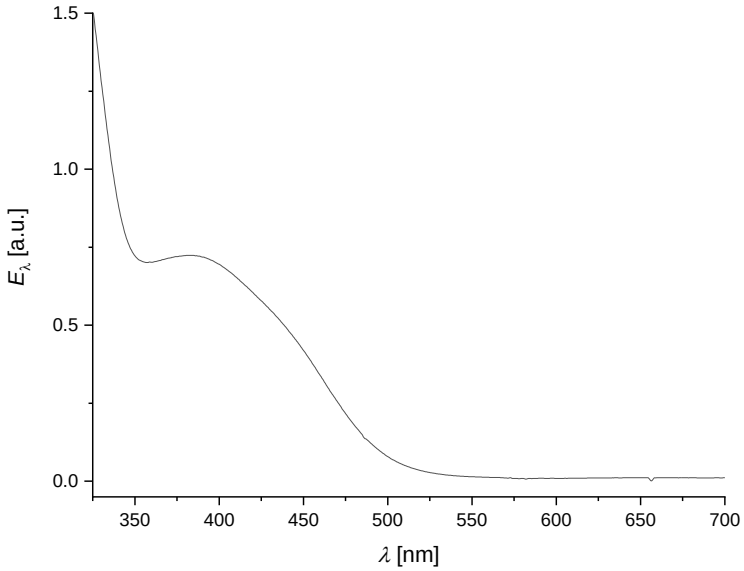

Figure S77. UV-Vis spectra of **2** (0.008 mmol in 6 mL of toluene).

4.3.3. Complex 6

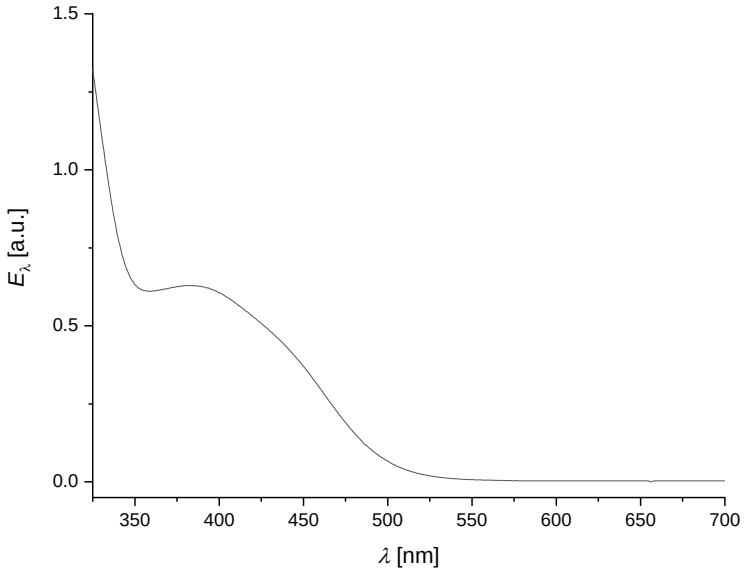

Figure S78. UV-Vis spectra of **6** (0.008 mmol in 6 mL of toluene).

4.3.4. Complex 9

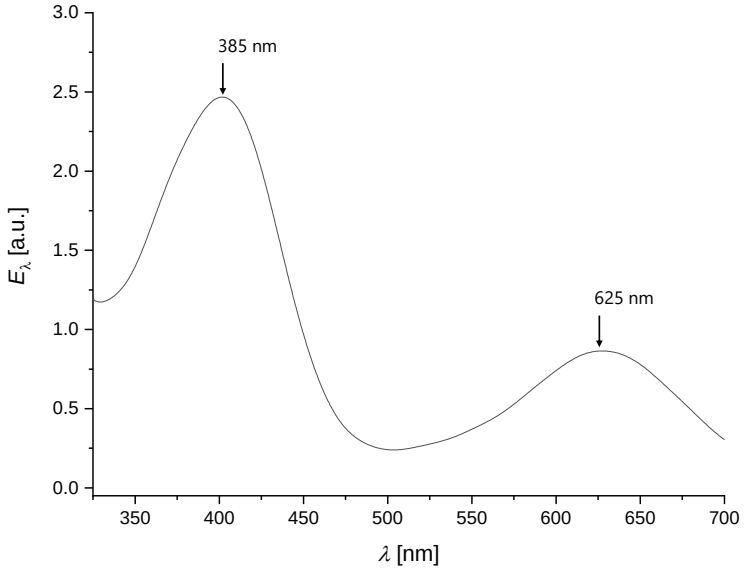

Figure S79. UV-Vis spectra of **9** (0.005 mmol in 4 mL of toluene).

4.3.5. Dilution of MeLi

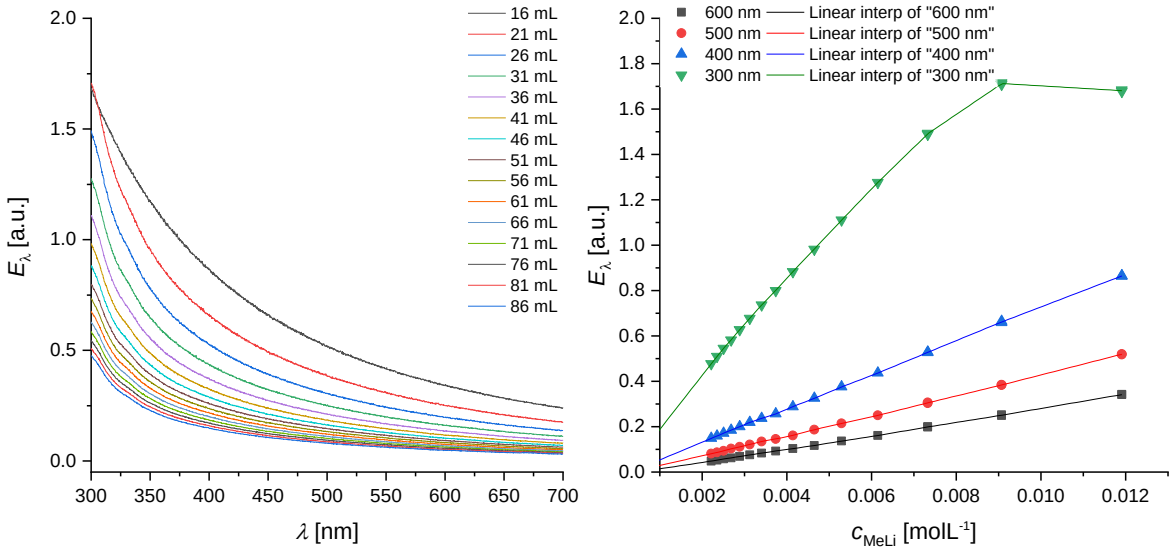

Figure S80. UV-Vis spectra of the dilution of MeLi (120 µL, 0.19056 mmol) in toluene at 40 °C (left). Plot of the extinction against c_{MeLi} (right).

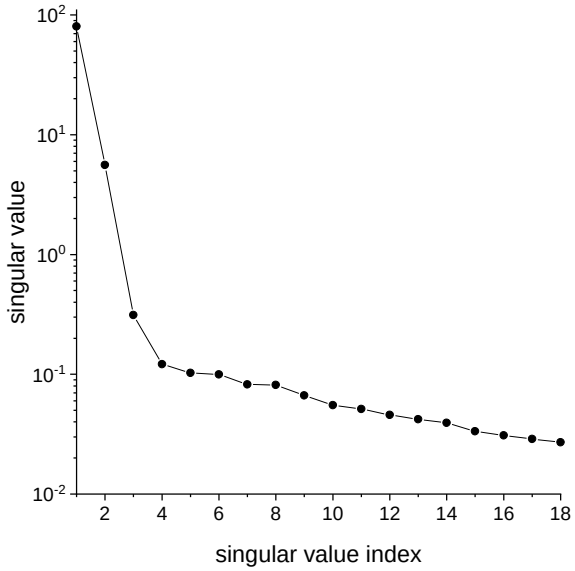

Figure S81. Singular Value Decomposition of the dilution of MeLi in toluene.

4.3.6. Complex 1 with MeLi

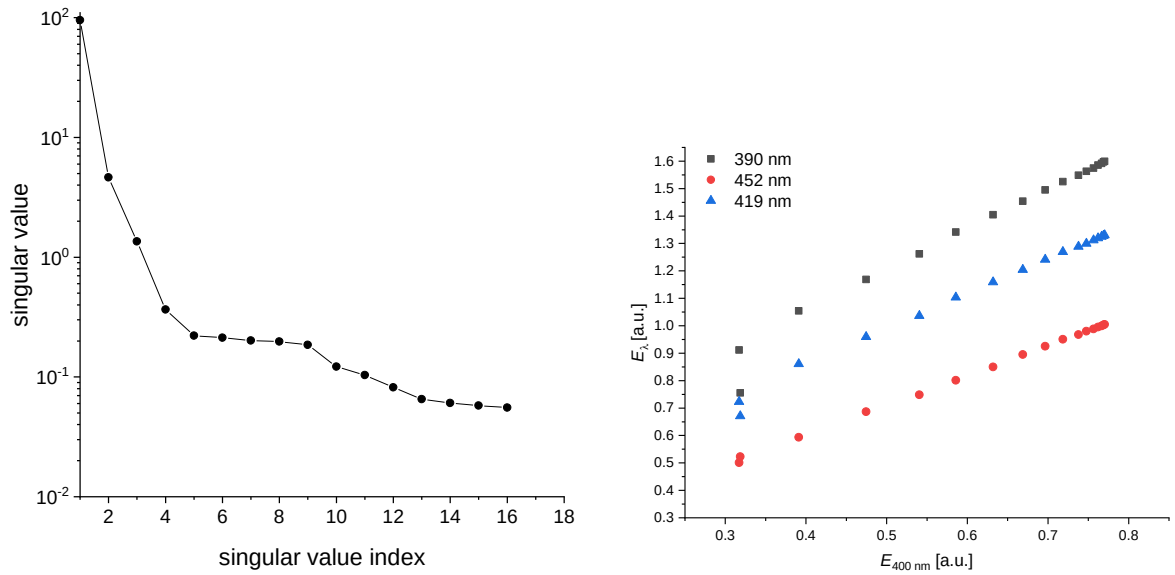

Figure S82. Singular Value Decomposition of the **1** activation with MeLi in toluene (left). Extinction diagram of the activation of **1** with MeLi (right).

4.3.7. UV/Vis spectra of dehydrocoupling of $H_3B{\cdot}NMe_2H$ with 1/MeLi

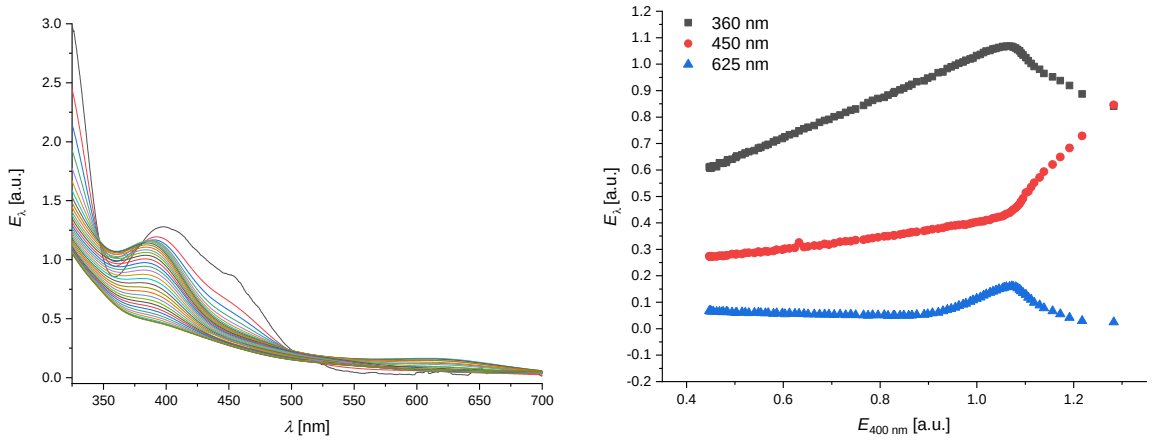

Figure S83. Spectra of UV-Vis monitoring of a catalytic dehydrocoupling of $H_3B{\cdot}NMe_2H$ with 2.5 mol% **1** and 5.2 mol% MeLi in 16 mL of toluene at 25 °C, cycle time 90 min (left). Extinction diagram of the catalytic reaction (right).

5. Details of vibrational spectroscopy

In this chapter the experimental IR and Raman spectra are presented. Additionally, the overlays of the calculated and experimental infrared spectra are displayed. The used level of theory is given at each specific spectrum.

5.1. Experimental and calculated vibrational spectra

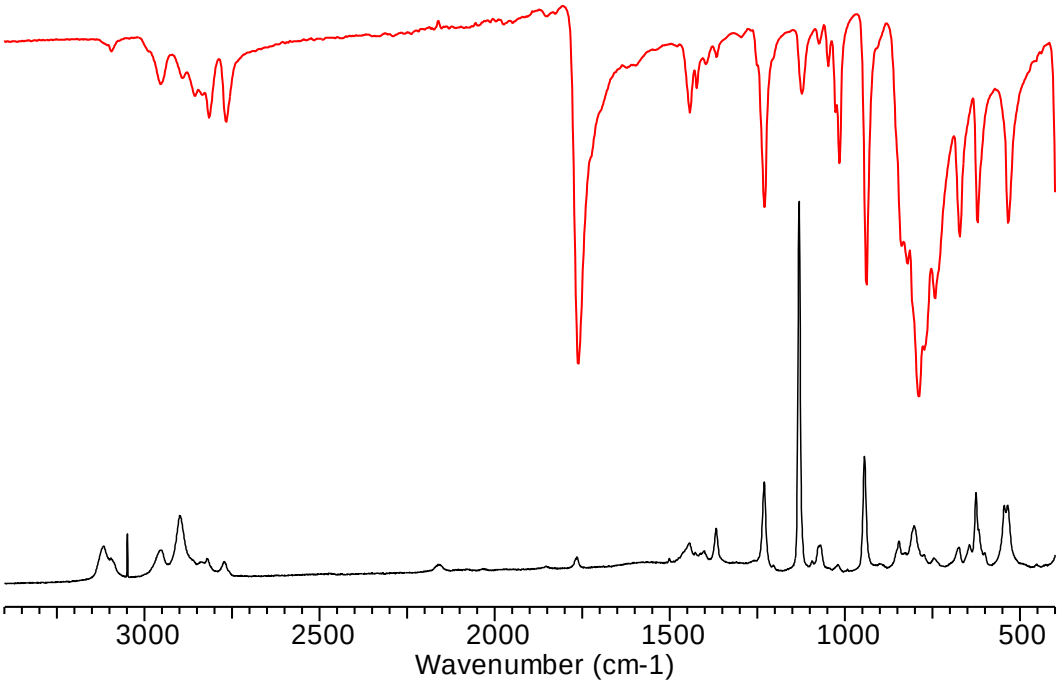

Figure S84. IR (red) and Raman (black) spectrum of complex **4**.

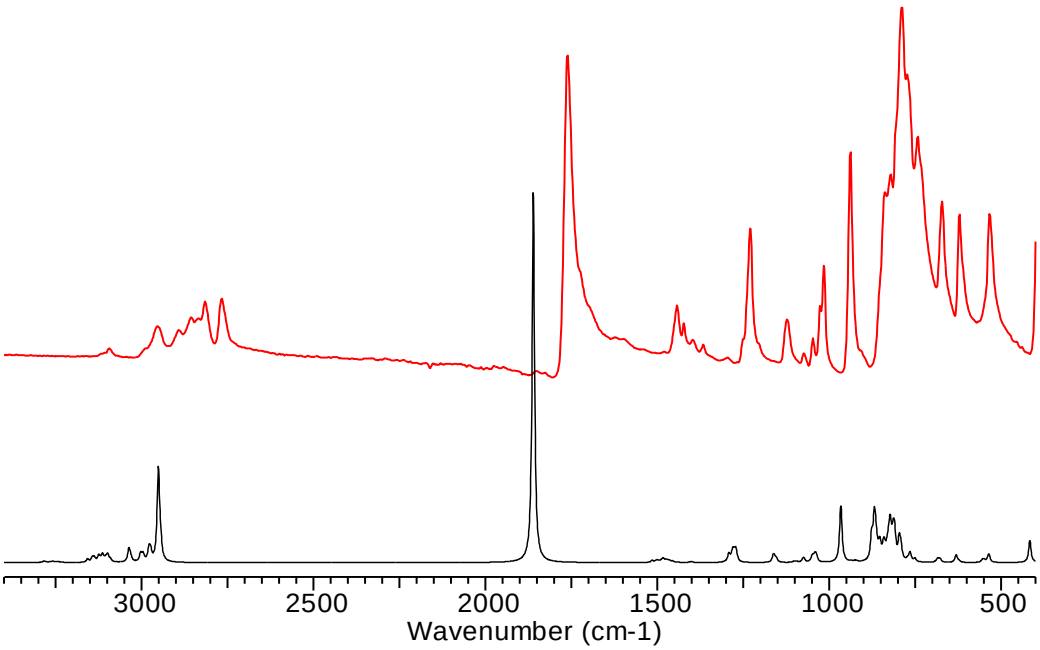

Figure S85. Calculated (black, B3LYP/GD3BJ/def2tzvp) and experimental (red) IR spectrum of **4**.

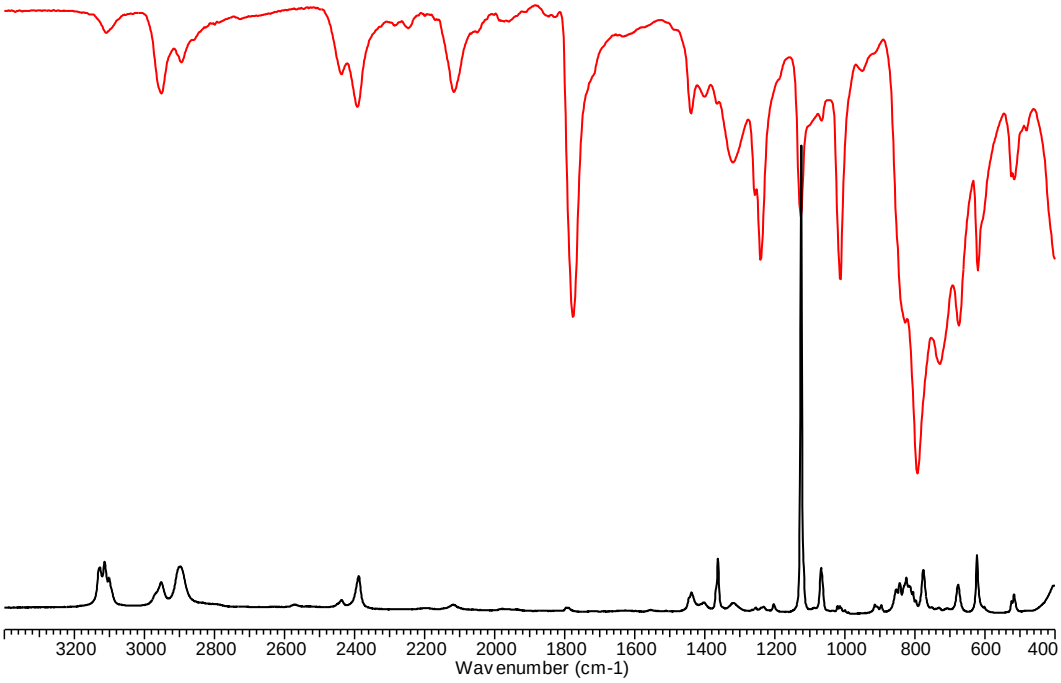

Figure S86. IR (red) and Raman (black) spectrum of complex **5**.

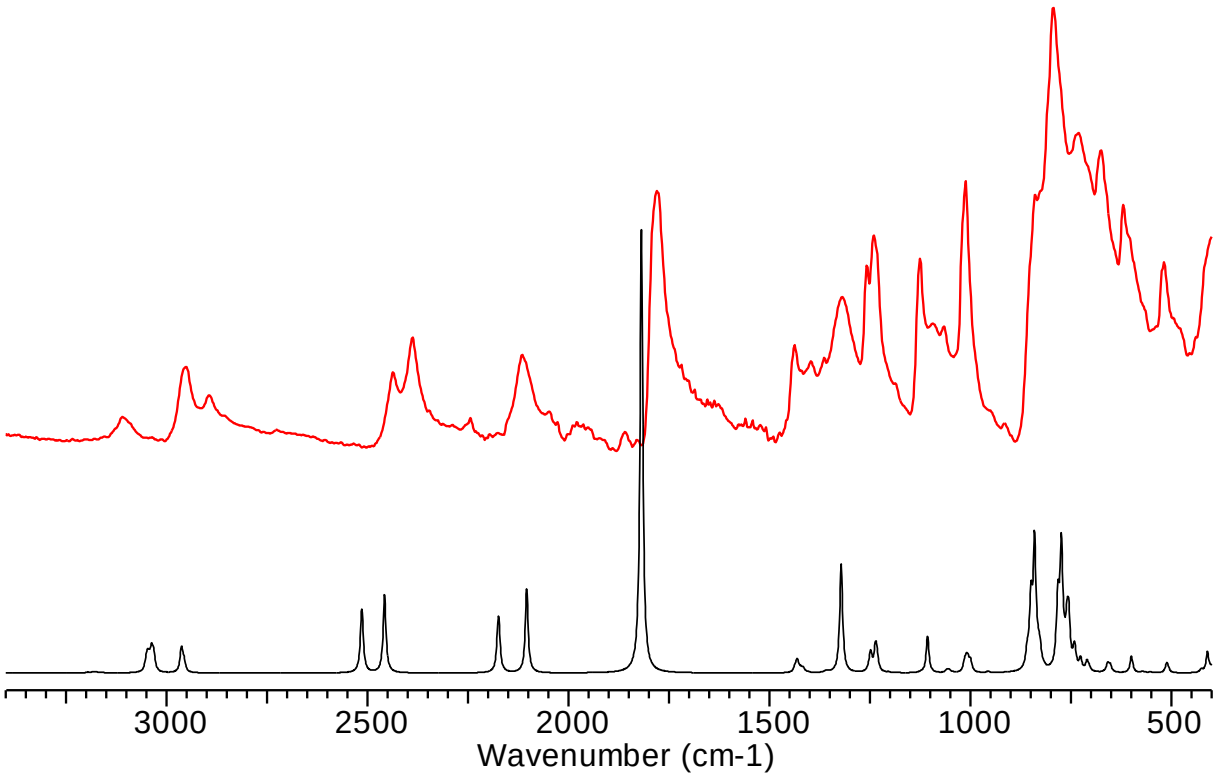

Figure S87. Calculated (black, BP86/TZVP/LANL2DZ) and experimental (red) IR spectrum of **5**.

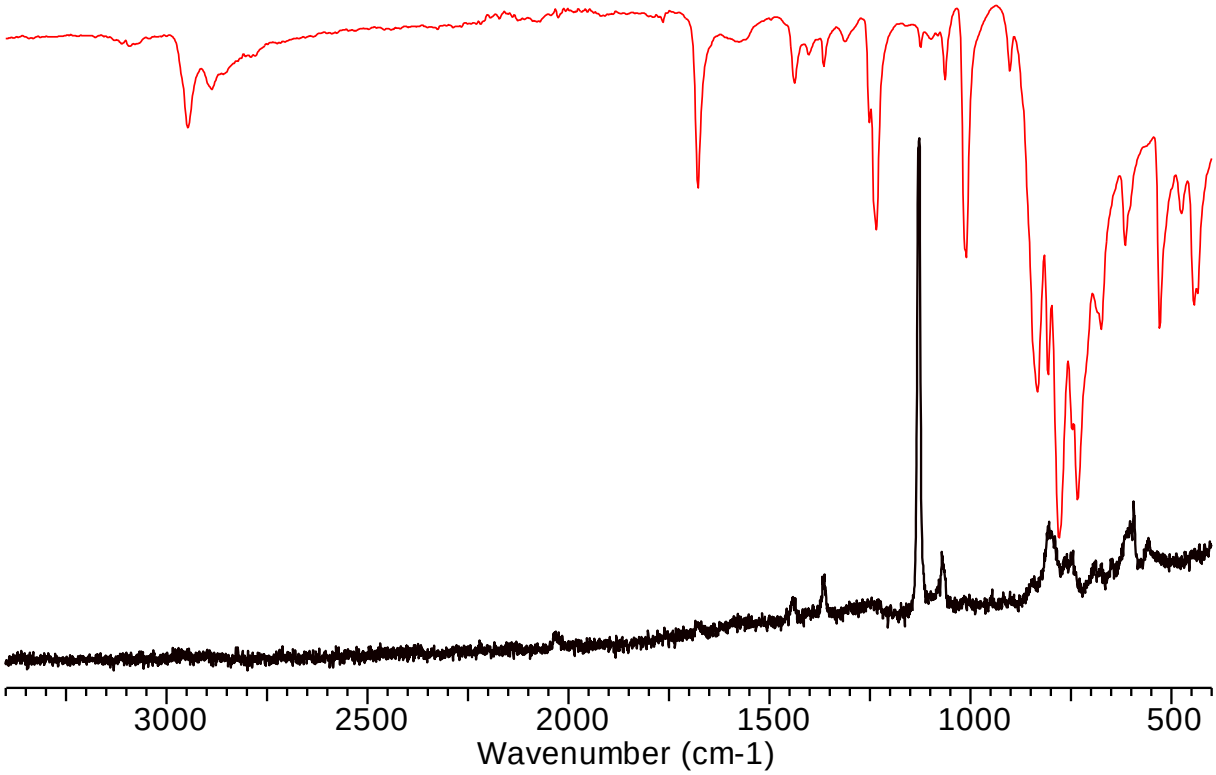

Figure S88. IR (red) and Raman (black) spectrum of complex **7**.

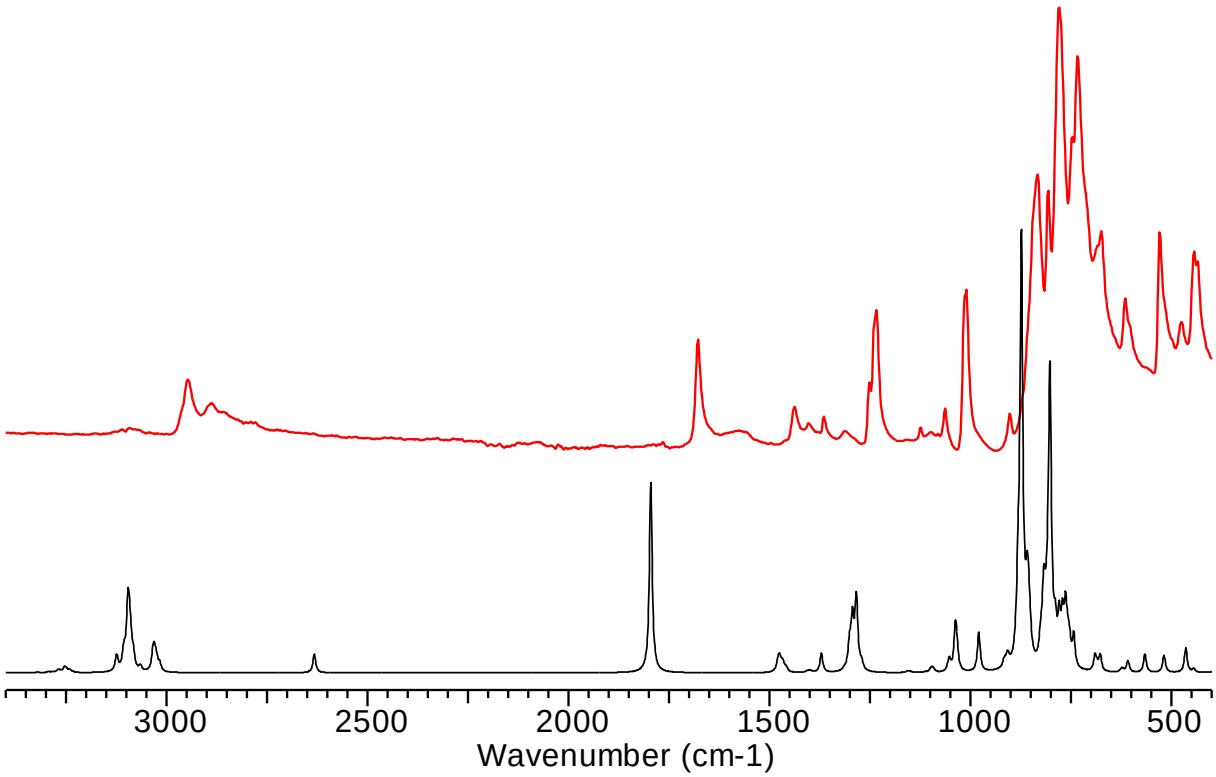

Figure S89. Calculated (black, B3LYP/GD3BJ/def2tzvp) and experimental (red) IR spectrum of **7**.

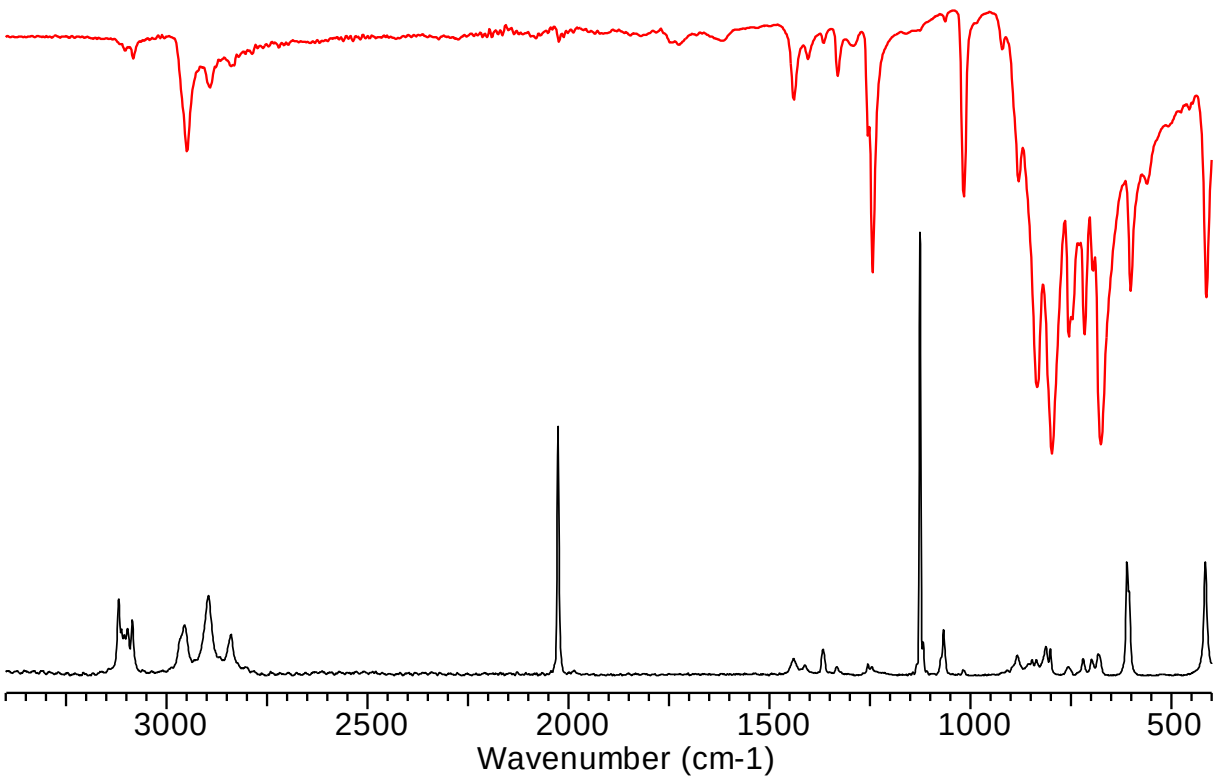

Figure S90. IR (red) and Raman (black) spectrum of complex **8**.

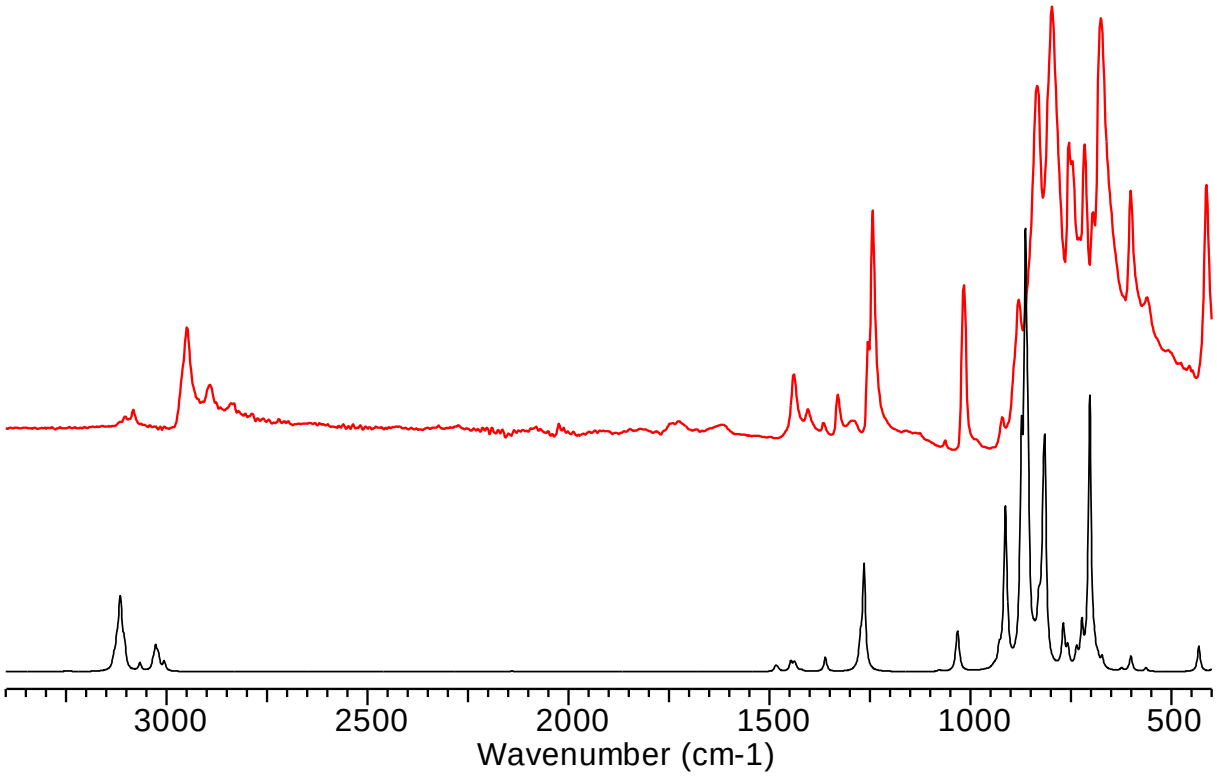

Figure S91. Calculated (black, B3LYP/GD3BJ/def2svp) and experimental (red) IR spectrum of **8**.

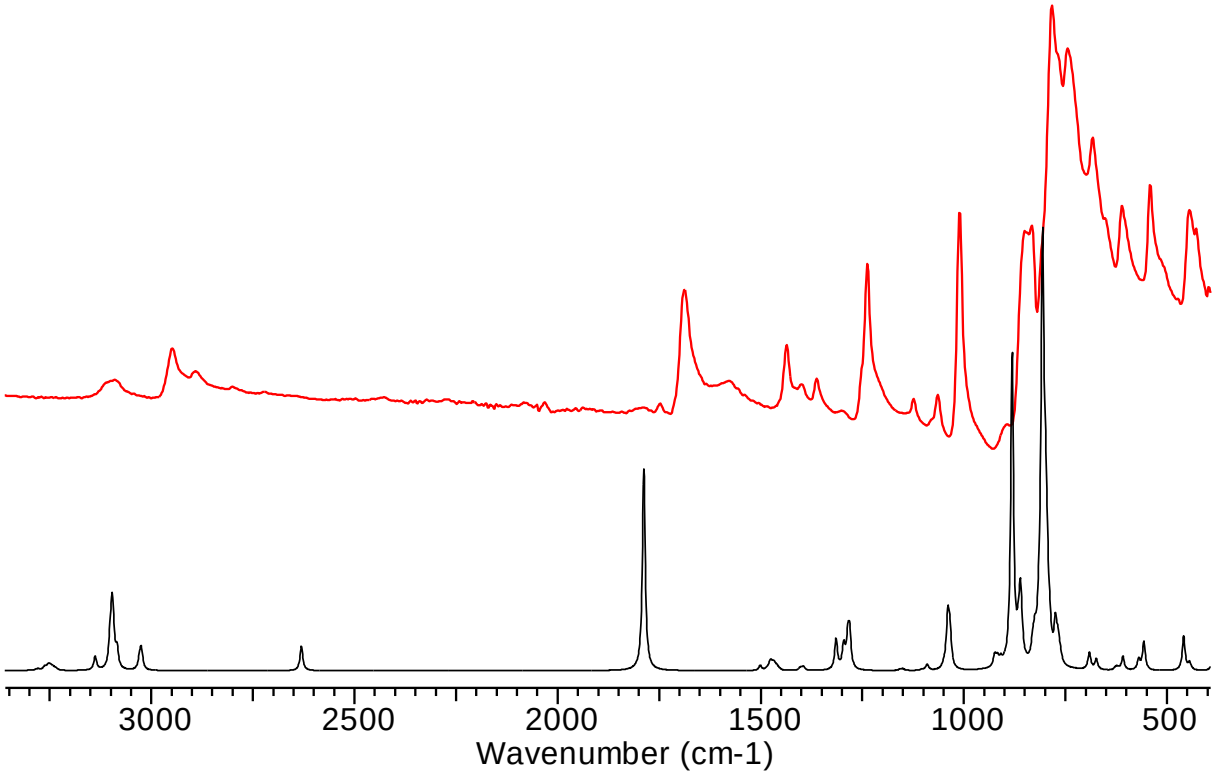

Figure S92. Calculated (black, B3LYP/GD3BJ/def2tzvp) and experimental (red) IR spectrum of **10**.

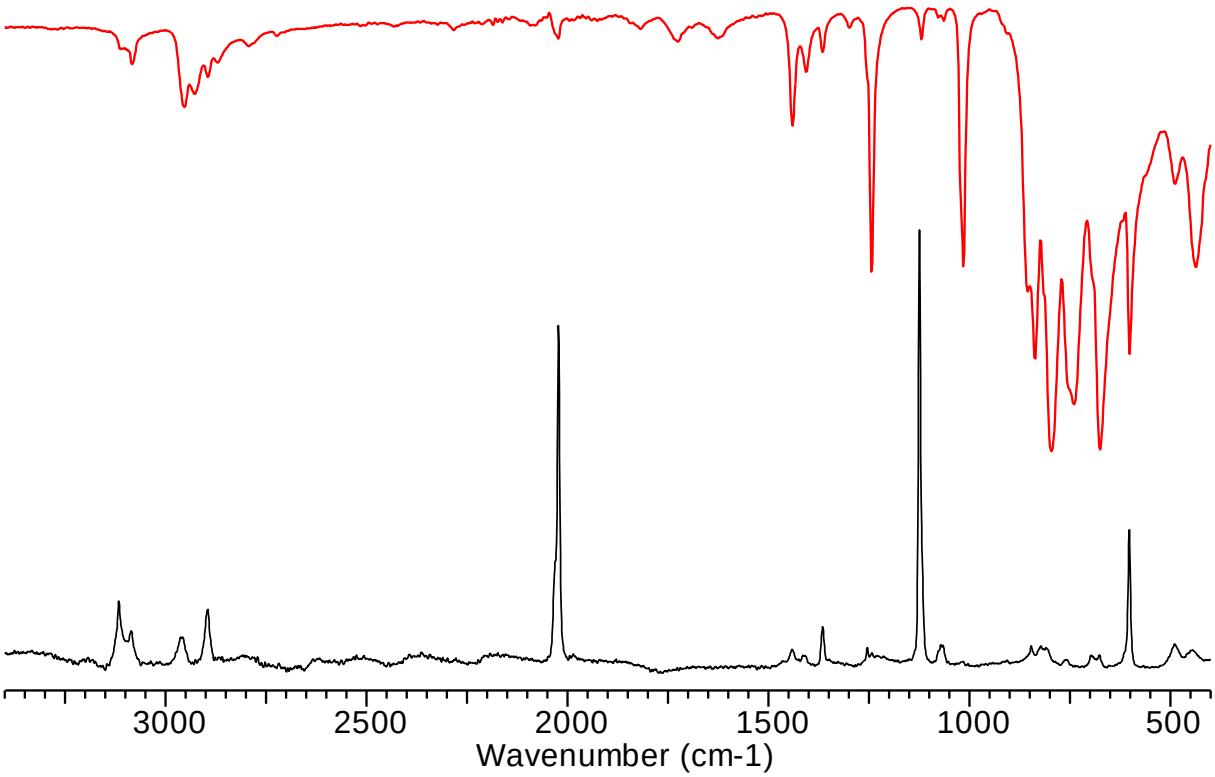

Figure S93. IR (red) and Raman (black) spectrum of complex **11**

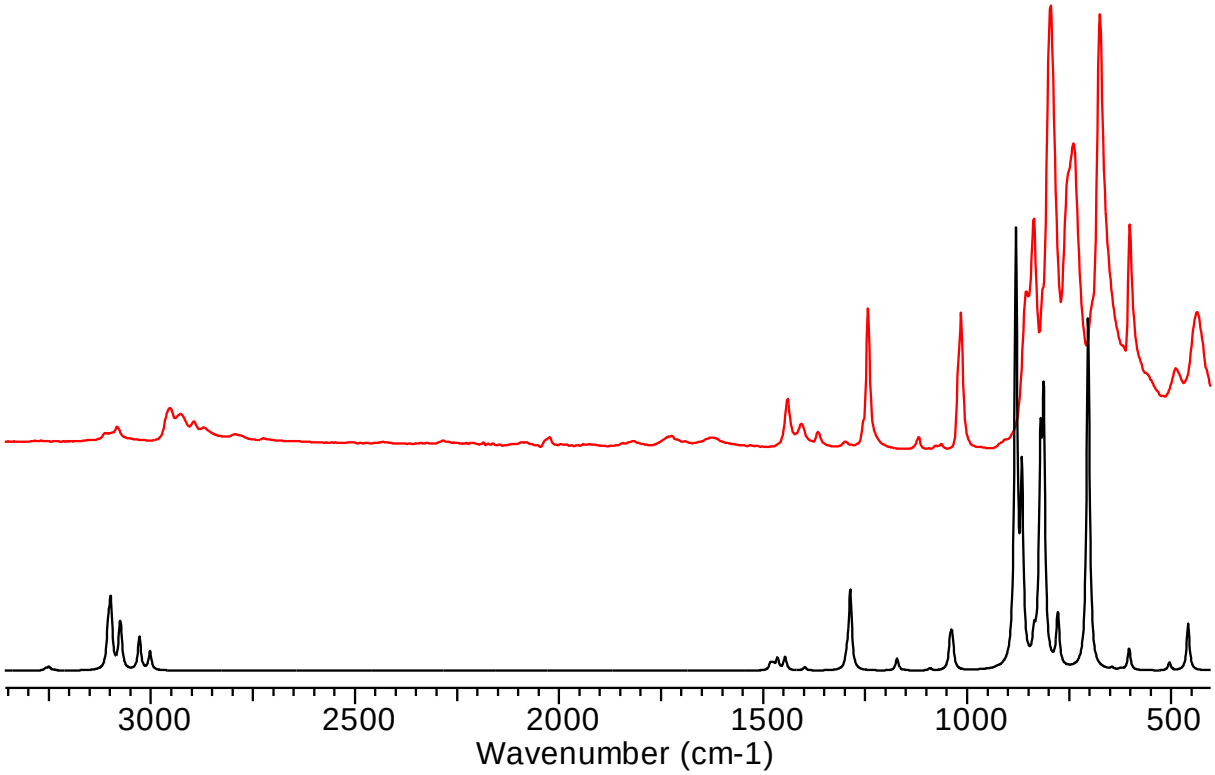

Figure S94. Calculated (black, B3LYP/GD3BJ/def2tzvp) and experimental (red) IR spectrum of **11**.

6. Computational details

All calculations were carried out with the Gaussian 09 package of molecular orbital program.[2] In our calculations, we have used the real-size molecules. First calculations were performed with the pure density functional (DF) BP86[3] in combination with the LANL2DZ[4] basis set and corresponding effective core potential (ECP) at Zr and the TZVP[5] basis set on all other atoms. During a series of unsatisfied calculations, we realised that might be the usage of dispersion correction is more feasibly for the optimization of transition state structures as described before for the mechanistic elucidation of the dehydrocoupling of $H_3B{\cdot}NMe_2H$ using titanocene as catayst.[6] Therefore we switched to the famous hybrid functional density functional method B3LYP[3,7] in combination with basis set def2tzvp[8] and the empirical dispersion correction GD3BJ[9] for all other calculations described herein. Vibrational frequencies were also computed, to include zero-point vibrational energies in thermodynamic parameters and to characterise all structures as minima on the potential energy surface. In order to identify minimum isomeric structures, we carried out relaxed potential energy scans (PES) using BP86 or B3LYP Method and LANL2DZ or def2svp basis set to identify the conformers with the lowest energy. Transition states were proved to be correct using intrinsic reaction coordinates calculation in both directions. Some of these results are presented as selected examples in the following chapter. Our goal was to compare the structures and energetics of all examined reactions of the zirconium complexes. On the basis of the calculated Gibbs free energy we confirmed the observed reaction behaviour. To get an easier access to the calculated structures we have created a multiple xyz file for all optimised structures. This file can be loaded separately as supporting information and opened with e.g. Mercury.[10]

6.1. Investigation of the metal free dehydrogenation of amine boranes and formation of amino boranes and diborazanes

In this chapter the main results of our calculations on metal-free dehydrogenation and formation of the observed products are described. We evaluated these reactions, corresponding transition states and energy values to compare these directly with the calculated values for the metal-centred reactions at the same level of theory.

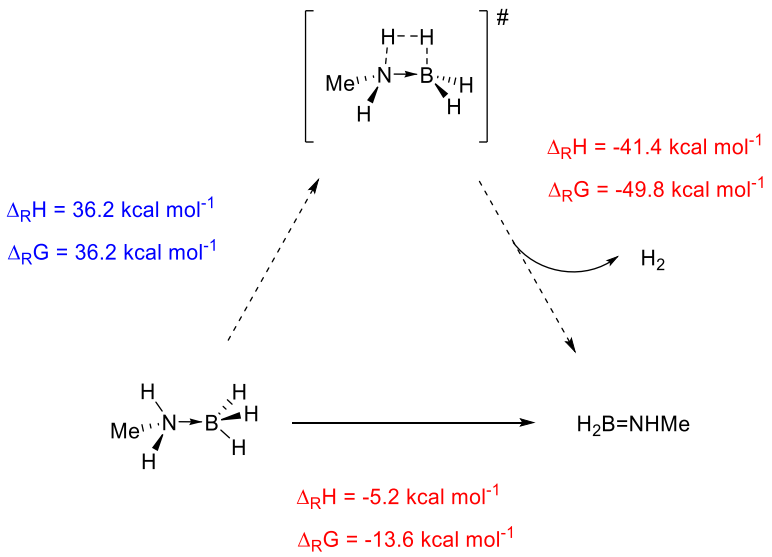

Figure S95. Calculated energies for metal-free intramolecular dehydrogenation of $H_3B{\cdot}NMeH_2$.

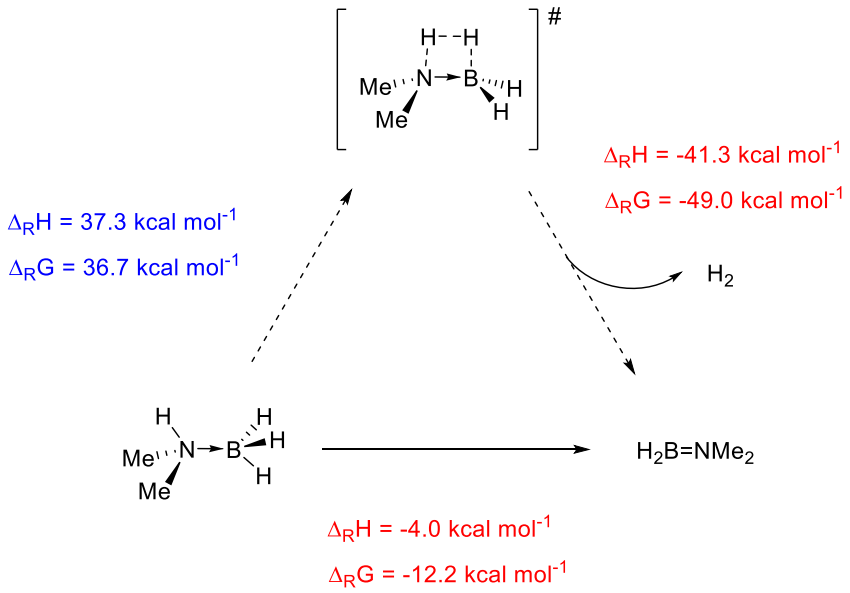

Figure S96. Calculated energies for metal-free intramolecular dehydrogenation of $H_3B{\cdot}NMe_2H$.

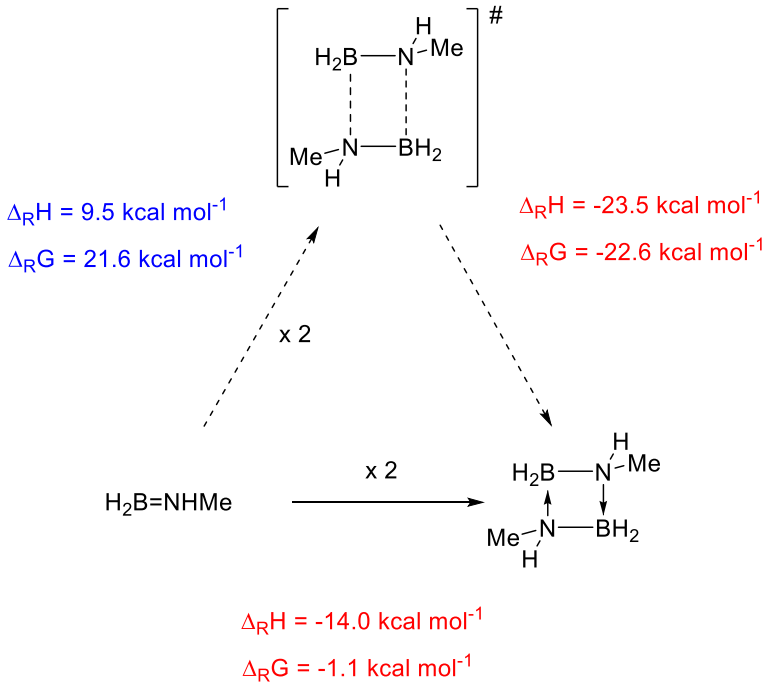

Figure S97. Calculated energies for metal-free formation of $(H_2BNMeH)_2$.

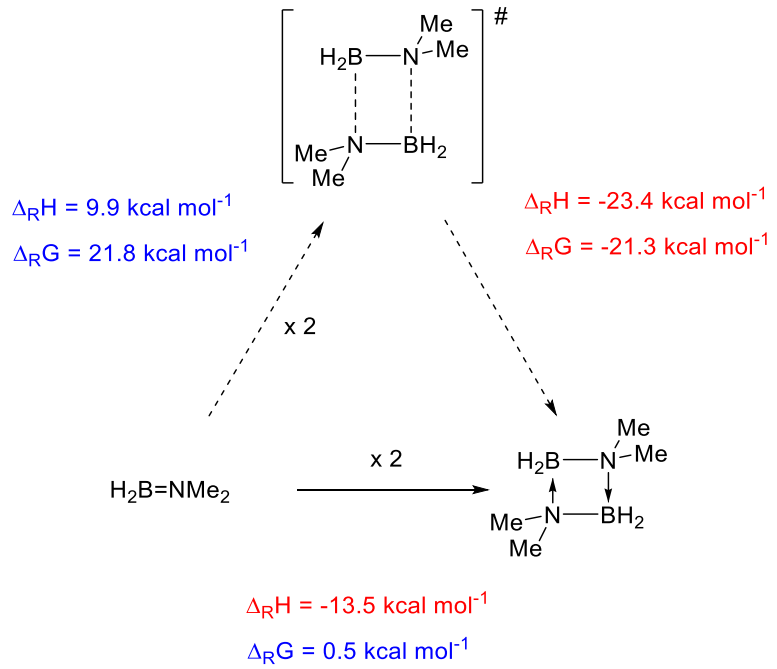

Figure S98. Calculated energies for metal-free formation of $(H_2BNMeH)_2$.

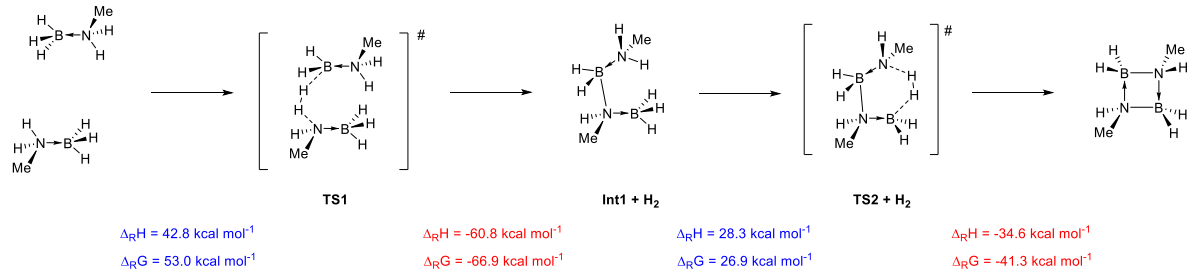

Figure S99. Calculated energies of metal-free intermolecular dehydration of $H_3B{\cdot}NMeH_2$.

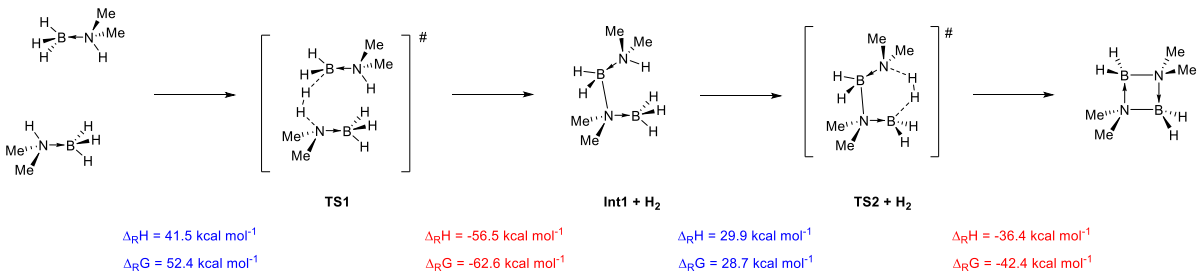

Figure S100. Calculated energies of metal-free intermolecular dehydrocoupling of $H_3B{\cdot}NMe_2H$.

6.2. Investigationgation of the formation of linear diborazane by reaction of amino borane and amin borane

For this study, the 2D potentential energy surface (2D-PES) was calculated for the convergence of amine borane to amino borane. With the help of the three-dimensional representation two main reaction paths were identified. A more careful analysis revealed that along the first reaction path an additional thermodynamic basin was found. This corresponds to the formation of the μ-aminodiborane and free amine, which were also observed experimentally.

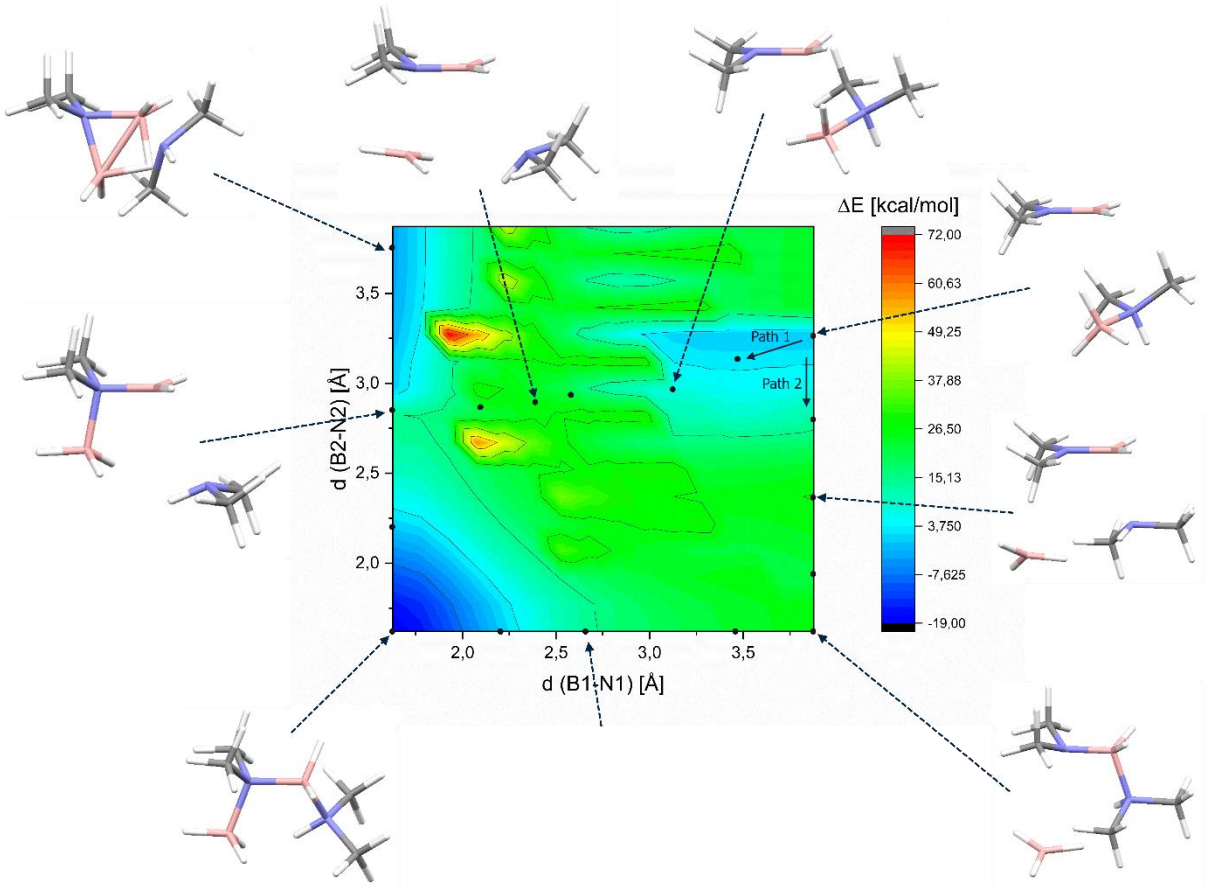

Figure S101. Calculated 2D PES of the convergence of $H_3B{\cdot}NMe_2H$ to H_2BNMe_2.

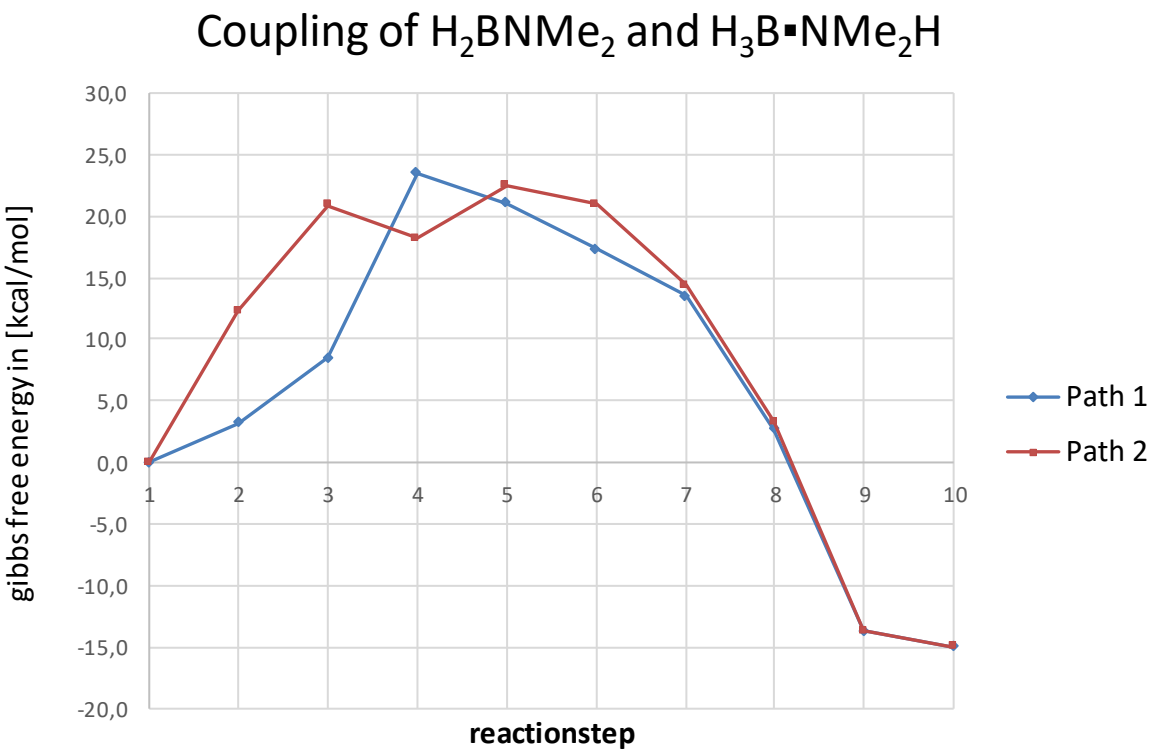

Figure S102. Calculated energy profile of the two different calculated reaction paths.

6.3. Investigation of the on-metal dehydrogenation of amine borane

In this chapter the main results of our calculations of on-metal dehydrogenation and formation of the observed products are described. Furthermore, we tried to investigate the interconversion process from the postulated dihydrate complex [Zr_2H_2] to the experimentally observed complexes **7** and **9**.

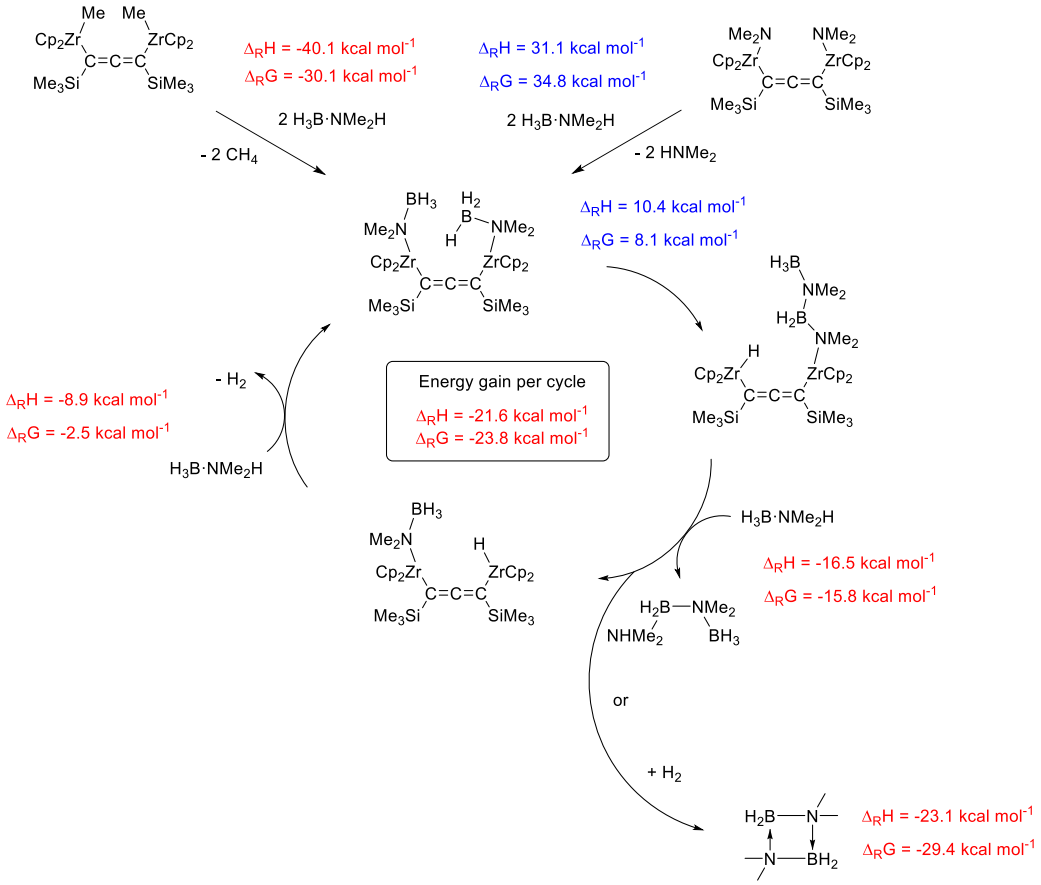

Figure S103. Proposed reaction sequence for dehydrogenation and formation of cyclic diborazane at the allenediide bridged catalyst system.

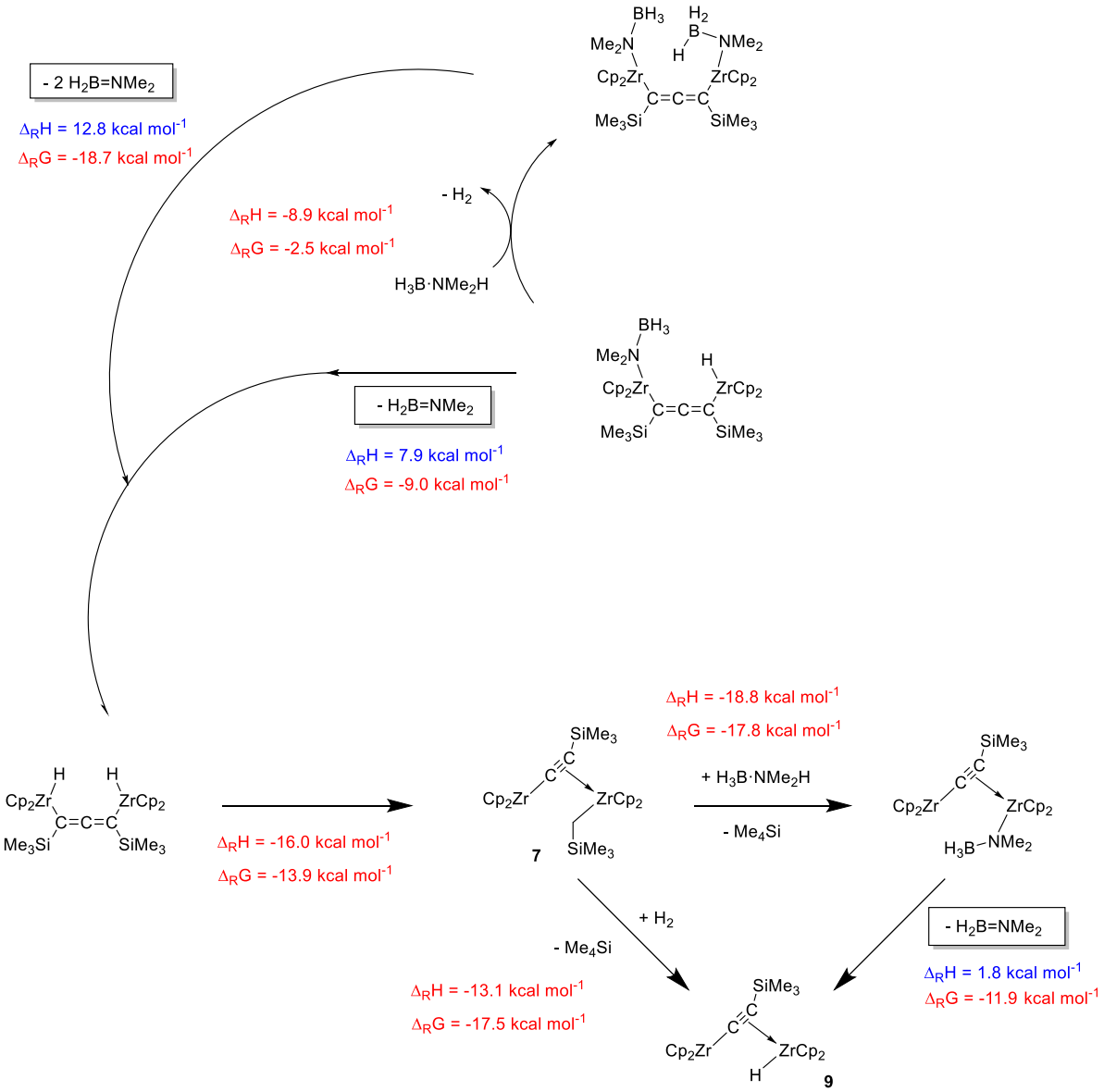

Figure S104. Thermodynamic consideration of a possible conversion of the alleediide bridged catalyst system into the complexes **7** and **9**.

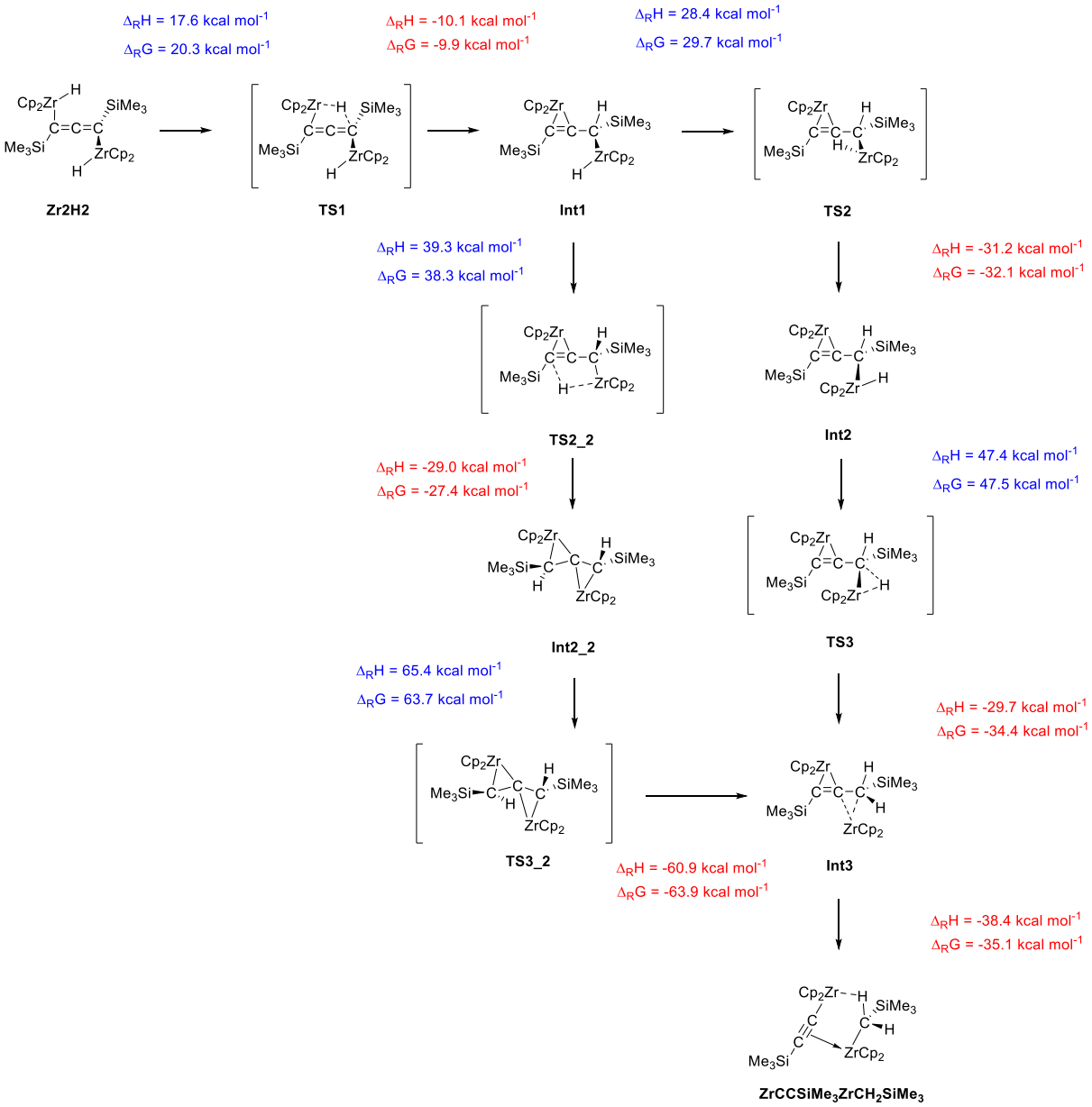

Figure S105. Details of calculations for the transformation of the assumed [Zr_2H_2] complex into the complex **7** including transition state structures. The high energy barriers along both considered pathways reveal that the observed reaction must follow a herein unconsidered pathway.

6.4. Investigation of the bond situation in complexes 7, 9 and 10

As we describe in the main section "Discussion of the bond situation in dinuclear complexes **7**, **9**, and **10** and possible implications for catalysis" of this Paper we first calculated the gibbs free energies of the different connectivity modes as well as their transition state energies of **7** and **10**.

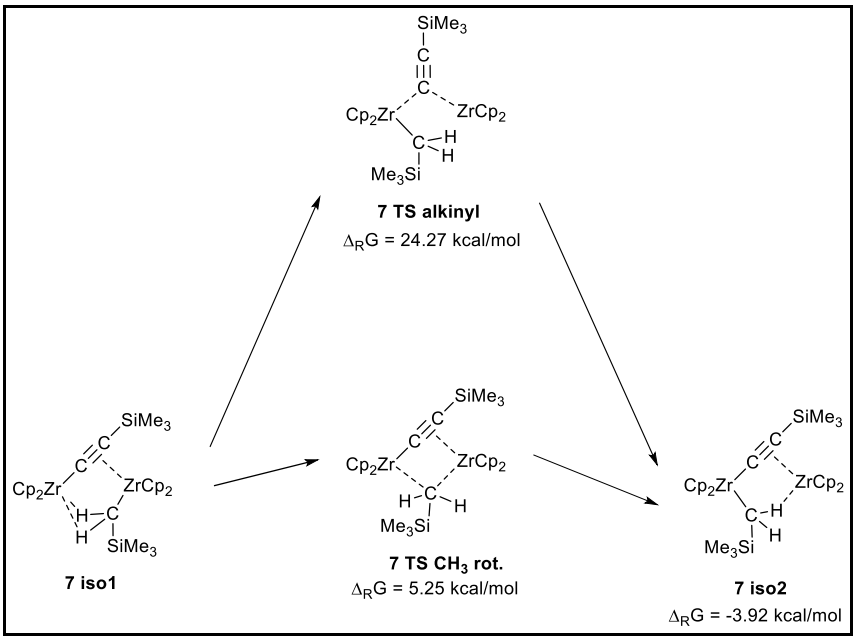

Figure S106. Gibbs free energies of different isomers of **7** as well as their transition states at B3LYP/GD3BJ/def2tzvp level of theory (All energies are referred to **7 iso1**).

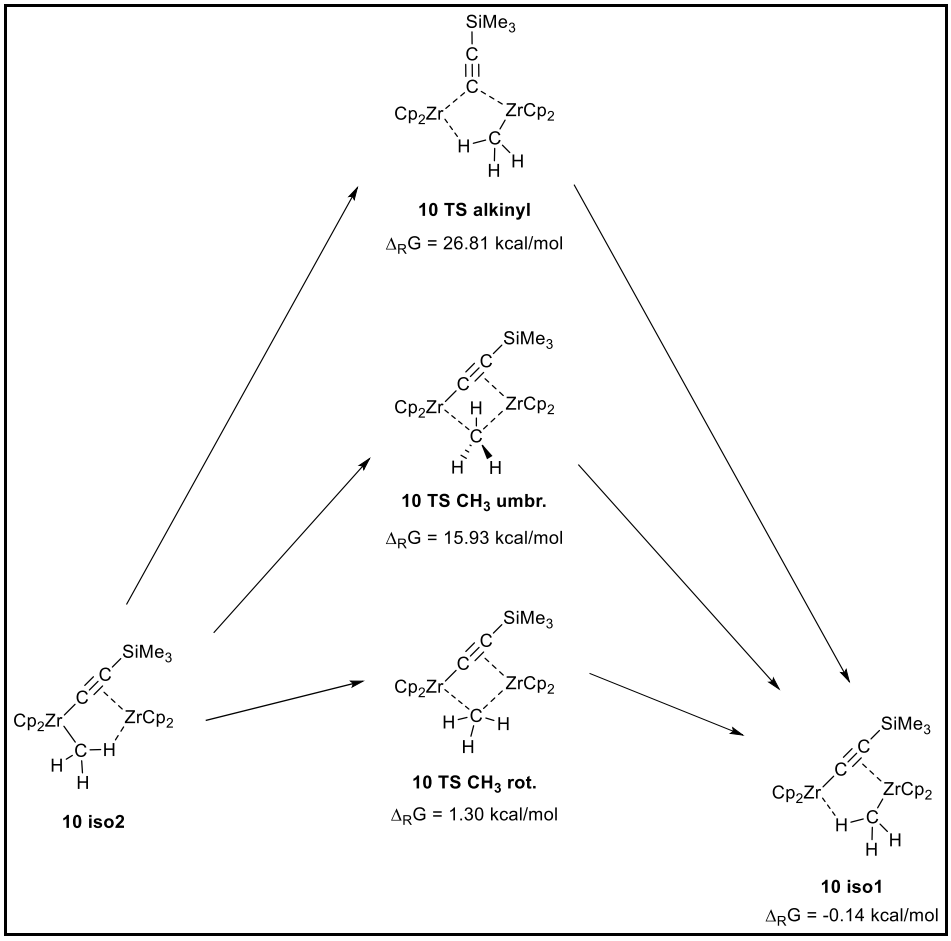

Figure S107. Gibbs free energies of different isomers of **10** as well as their transition states at B3LYP/GD3BJ/def2tzvp level of theory (All energies are referred to **10 iso2**).

Followed by this we had a briefly look on the electronical situation of these Complexes. Therefore, we proofed the stability of the wave functions with respect to restricted/unrestricted Hartree-Fock RHF/UHF or restricted/unrestricted Kohn-Sham RKS/UKS instabilities, in order to analyse the potential binuclear Zr(III/III) complexes. In this context we proofed the different optimized structures (B3LYP/GD3BJ/def2tzvp) of the both connectivity motives Zr(IV/II) and Zr(III/III) of **7** and **10**. While the KS wave function based on the hybrid DF (B3LYP), for all four structures, showed no instabilities, the HF solution exhibited a low-lying, "broken-symmetry" open-shell singlet state for both Zr(III/III) motif of **7** and **9**. While the structures that were optimised using the B3LYP functional show good agreement with experimental structures the electronic energy should only be considered as a rough approximation due to incorrect treatment of the non-dynamic correlation. With a closer look on the HF spin density plots (Figures S106-108) of these Zr(III/III) complexes **7**, **9** and **10** they are best described as ligand assisted ($CCSiMe_3$) antiferromagnetic coupled binuclear zirconium (III) complexes.

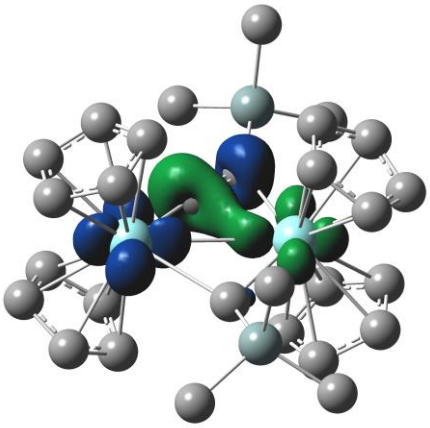

Figure S108. Plot of the spin density of complex **7** at HF/def2tzvp level of theory (iso0.007).

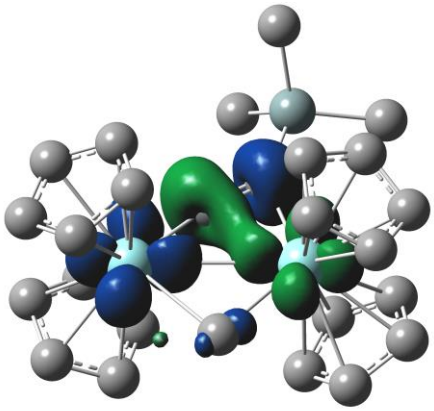

Figure S109. Plot of the spin density of complex **9** at HF/def2tzvp level of theory (iso0.007).

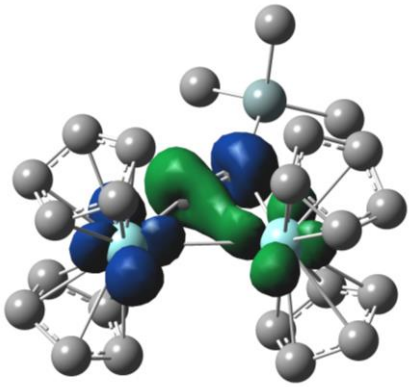

Figure S110. Plot of the spin density of complex **10** at HF/def2tzvp level of theory (iso0.007).

6.5. Summary of thermodynamic values for all calculated molecular structures

Table S2. Caclulated values for all optimised structures. The energetically lowest isomer was marked with a star and its energies were used for the thermodynamic calculations.

Compound	Nimag	HF	ZPE [kcal/mol]	H_{tot} [a.u.]	G_{tot} [a.u.]	Method	Basisset	min. Iso
hydrogen	0	-1.177586	6.174720	-1.164441	-1.179255	BP86	TZVP	*
hydrogen	0	-1.179790	6.315280	-1.166421	-1.181216	B3LYP-GDBJ	def2tzvp	*
methane Td	0	-40.529900	27.335680	-40.482518	-40.503674	BP86	TZVP	*
methane Td	0	-40.539445	27.988260	-40.491030	-40.512156	B3LYP-GDBJ	def2tzvp	*
tetramtehylsilane Td	0	-449.265859	89.967320	-449.112077	-449.152750	BP86	TZVP	*
tetramtehylsilane Td	0	-449.314979	92.142700	-449.157868	-449.198267	B3LYP-GDBJ	def2tzvp	*
dimethylamin	0	-135.2083552	56.113770	-135.113517	-135.144447	BP86	TZVP	*
Borane D3h	0	-26.6252078	16.458580	-26.595150	-26.616524	B3LYP-GDBJ	def2tzvp	
methylaminborane	0	-122.5888307	61.790720	-122.484573	-122.516355	B3LYP-GDBJ	def2tzvp	
dimethylaminborane	0	-161.8752203	77.290660	-161.745093	-161.779939	BP86	TZVP	*
dimethylaminborane	0	-161.9163385	79.494870	-161.782803	-161.817481	B3LYP-GDBJ	def2tzvp	*
TS dehyd. methylaminborane	1	-122.5240219	57.342420	-122.426820	-122.458704	B3LYP-GDBJ	def2tzvp	
TS dehyd. Dimethylaminborane	1	-161.8148850	72.598780	-161.691898	-161.727843	BP86	TZVP	
TS dehyd. Dimethylaminborane	1	-161.8496369	74.728310	-161.723435	-161.758932	B3LYP-GDBJ	def2tzvp	
MeHNBH2	0	-121.4081214	48.001700	-121.326382	-121.356845	B3LYP-GDBJ	def2tzvp	
Me2NBH2 C2V	0	-160.6944934	63.699980	-160.586542	-160.619686	BP86	TZVP	*
Me2NBH2 C2V	0	-160.7336574	65.606910	-160.622769	-160.655736	B3LYP-GDBJ	def2tzvp	*
linear diborazane iso1	0	-322.5841544	143.640980	-322.343075	-322.390613	BP86	TZVP	
linear diborazane iso2	0	-322.5841545	143.6405	-322.343076	-322.390614	BP86	TZVP	*
linear diborazane iso2	0	-322.6712157	148.28239	-322.423079	-322.470053	B3LYP-GDBJ	def2tzvp	
linear diborazane Int1	0	-322.6712158	148.28347	-322.423077	-322.470052	B3LYP-GDBJ	def2tzvp	
cyclic diborazane	0	-242.8431560	100.11565	-242.675116	-242.715384	B3LYP-GDBJ	def2tzvp	
cyclic dimethyl diborazane C2v	0	-321.4089583	131.03279	-321.189039	-321.233442	BP86	TZVP	*

cyclic dimethyl diborazane C2v	0	-321.4932799	135.24129	-321.267042	-321.310625	B3LYP-GDBJ	def2tzvp	*
TS to cyclic diborazane via CA	1	-242.8023918	97.49872	-242.637628	-242.679338	B3LYP-GDBJ	def2tzvp	
TS to cyclic dimethyl diborazane via CA	1	-321.3683997	128.62801	-321.15138	-321.198947	BP86	TZVP	
TS to cyclic dimethyl diborazane via CA	1	-321.45292	132.70243	-321.229705	-321.276682	B3LYP-GDBJ	def2tzvp	
TS1 dehydrogenation of 2 MAB sp Step3	1	-245.1007104	117.91028	-244.900978	-244.948233	B3LYP-GDBJ	def2tzvp	
TS1 dehydrogenation of 2 MAB 2H2 at once	1	-245.1131206	115.91495	-244.917162	-244.963015	B3LYP-GDBJ	def2tzvp	
Int1 dehydrogenation of 2 MAB	0	-244.0213506	113.09108	-243.831506	-243.873629	B3LYP-GDBJ	def2tzvp	
TS2 dehydrogenation of 2 MAB	1	-243.9674273	107.06032	-243.786457	-243.83073	B3LYP-GDBJ	def2tzvp	
TS1 dehydrogenation of 2 DMAB	1	-323.7577075	153.09982	-323.499478	-323.55146	B3LYP-GDBJ	def2tzvp	
TS2 dehydrogenation of 2 DMAB	1	-322.6145704	141.97784	-322.375494	-322.424324	B3LYP-GDBJ	def2tzvp	
ZrClZrCl iso1 Cl inin		not	converged			B3LYP-GDBJ	def2tzvp	
ZrClZrCl iso2 Cl inout	0	-2722.576683	365.05853	-2721.951059	-2722.069612	B3LYP-GDBJ	def2tzvp	
ZrClZrCl iso3 Cl outout	0	-2722.576404	365.30846	-2721.950469	-2722.068421	B3LYP-GDBJ	def2tzvp	
ZrClZrMe iso1 Me inin	0	-2302.200271	386.36967	-2301.540154	-2301.6583	B3LYP-GDBJ	def2tzvp	
ZrClZrMe iso2 inout	0	-2302.194764	386.18525	-2301.534775	-2301.654533	B3LYP-GDBJ	def2tzvp	
ZrMeZrCl iso3 inout	0	-2302.194549	386.13773	-2301.534612	-2301.654024	B3LYP-GDBJ	def2tzvp	
ZrMeZrCl iso4 outout	0	-2302.194218	386.77812	-2301.533719	-2301.651438	B3LYP-GDBJ	def2tzvp	
ZrHZrH iso1 H inin	0	-1801.9464423	358.46668	-1801.331793	-1801.451657	BP86	TZVP/LANL2DZ	*
ZrHZrH iso1 H inin	0	-1803.1386609	371.43105	-1802.505463	-1802.61952	B3LYP-GDBJ	def2tzvp	
ZrHZrH iso2 H outin	0	-1801.9457936	358.4967	-1801.331155	-1801.451288	BP86	TZVP/LANL2DZ	
ZrHZrH iso3 H inout	0	-1801.9457986	358.58546	-1801.331082	-1801.450551	BP86	TZVP/LANL2DZ	
ZrHZrH iso4 H outout	0	-1801.9390522	359.13216	-1801.324091	-1801.440304	BP86	TZVP/LANL2DZ	
ZrMeZrMe iso1 Me inin	0	-1880.5956336	393.08804	-1879.92156	-1880.048073	BP86	TZVP/LANL2DZ	*
ZrMeZrMe iso1 Me inin sing. point	0	-1881.8079262	405.07715	-1881.119925	-1881.230412	B3LYP-GDBJ	def2tzvp	
ZrMeZrMe iso1 Me inin opt	0	-1881.8181913	407.4314	-1881.12387	-1881.242601	B3LYP-GDBJ	def2tzvp	*
ZrMeZrMe iso2 Me outin	0	-1880.5923380	393.38829	-1879.917945	-1880.044316	BP86	TZVP/LANL2DZ	
ZrMeZrMe iso2 Me outin sing. Point	0	-1881.8017101	405.21062	-1881.113558	-1881.223959	B3LYP-GDBJ	def2tzvp	
ZrMeZrMe iso2 Me outin opt	0	-1881.8118475	406.86068	-1881.117896	-1881.23997	B3LYP-GDBJ	def2tzvp	*
ZrMeZrMe iso3 Me outout	0	-1880.5918287	394.01732	-1879.917063	-1880.040566	BP86	TZVP/LANL2DZ	

ZrMeZrMe iso3 Me outout	0	-1881.8118148	407.26656	-1881.117664	-1881.237504	B3LYP-GDBJ	def2tzvp	
ZrNMe2ZrNMe2 iso1	0	-2070.0143888	450.872680	-2069.244149	-2069.377813	BP86	TZVP/LANL2DZ	*
ZrNMe2ZrNMe2 iso1	0	-2071.2755485	466.624380	-2070.482260	-2070.610521	B3LYP-GDBJ	def2tzvp	*
ZrNMe2ZrNMe2 iso2	0	-2070.0060475	451.000790	-2069.235608	-2069.369263	BP86	TZVP/LANL2DZ	
ZrNMe2ZrNMe2 iso3	0	-2070.0055196	451.305470	-2069.235037	-2069.365251	BP86	TZVP/LANL2DZ	
ZrNMe2ZrNMe2 iso4	0	-2070.0105908	450.341930	-2069.240871	-2069.374804	BP86	TZVP/LANL2DZ	
ZrNMe2BH3ZrH iso1 inin	0	-1962.6375533	425.849350	-1961.910415	-1962.036385	BP86	TZVP/LANL2DZ	*
ZrNMe2BH3ZrH iso1 inin	0	-1963.8909117	441.799910	-1963.140821	-1963.260887	B3LYP-GDBJ	def2tzvp	*
ZrNMe2BH3ZrH iso2 inin	0	-1962.6368989	426.520670	-1961.908938	-1962.034424	BP86	TZVP/LANL2DZ	
ZrNMe2BH3ZrH iso3 inin	0	-1962.6317081	426.199420	-1961.904138	-1962.031027	BP86	TZVP/LANL2DZ	
ZrNMe2BH3ZrH iso4 B outin	0	-1962.6372628	425.834110	-1961.910073	-1962.036756	BP86	TZVP/LANL2DZ	
ZrNMe2BH3ZrH iso5 B inout	0	-1962.6329203	426.453920	-1961.905013	-1962.030812	BP86	TZVP/LANL2DZ	
ZrNMe2BH3ZrH iso6 outout	0	-1962.6336454	426.213270	-1961.905819	-1962.033910	BP86	TZVP/LANL2DZ	
ZrHZrH_DMAB_Int1	0	-1965.0763241	451.767710	-1964.307568	-1964.438697	B3LYP-GDBJ	def2tzvp	
ZrNMe2BH3ZrNMe2BH3 iso1 inin	0	-2123.3294084	493.036700	-2122.489258	-2122.627112	BP86	TZVP/LANL2DZ	*
ZrNMe2BH3ZrNMe2BH3 iso1 inin	0	-2124.6382645	511.689720	-2123.771317	-2123.901208	B3LYP-GDBJ	def2tzvp	
ZrNMe2BH3ZrNMe2BH3 iso1 int1	0	-2124.6418511	510.351160	-2123.776477	-2123.908455	B3LYP-GDBJ	def2tzvp	
ZrNMe2BH3ZrNMe2BH3 iso1 int2	0	-2124.6295349	510.035030	-2123.764708	-2123.897360	B3LYP-GDBJ	def2tzvp	
ZrNMe2BH3ZrNMe2BH3_2mz_sp_Int3_tzvp2	0	-2124.6322023	506.218530	-2123.776711	-2123.899317	B3LYP-GDBJ	def2tzvp	
ZrNMe2BH3ZrNMe2BH3_2mz_opt_Int3_tzvp3	0	-2124.6397435	508.540650	-2123.776347	-2123.913194	B3LYP-GDBJ	def2tzvp	*
ZrNMe2BH3ZrNMe2BH3_ZrHB_bonded_opt_freq_Int1	0	-2124.6267561	507.768990	-2123.764455	-2123.900896	B3LYP-GDBJ	def2tzvp	
ZrNMe2BH3ZrNMe2BH3_ZrHB_bonded-b3lyp_opt_freq	1	-2124.6204000	508.812510	-2123.757703	-2123.889987	B3LYP-GDBJ	def2tzvp	
ZrNMe2BH3ZrNMe2BH3_b3lyp_opt_freq_abcleavInt2	0	-2124.6295349	510.035030	-2123.764708	-2123.897360	B3LYP-GDBJ	def2tzvp	
ZrNMe2BH3ZrNMe2BH3_b3lyp_opt_freq_abcleavTS1	1	-2124.6166876	509.472530	-2123.752974	-2123.884888	B3LYP-GDBJ	def2tzvp	
ZrHZrH_2DMAB_b3lyp_freq_iso1	0	-2127.0145433	532.417620	-2126.109749	-2126.258306	B3LYP-GDBJ	def2tzvp	
ZrNMe2BH3ZrNMe2BH3 iso2 inin	0	-2123.3258207	494.033280	-2122.484690	-2122.620251	BP86	TZVP/LANL2DZ	
ZrNMe2BH3ZrNMe2BH3 iso3 outin	0	-2123.3264888	493.225700	-2122.486250	-2122.623257	BP86	TZVP/LANL2DZ	
ZrNMe2BH3ZrNMe2BH3 iso4 outout	0	-2123.3262390	493.973960	-2122.485374	-2122.619952	BP86	TZVP/LANL2DZ	

ZrNMe2BH3ZrNMe2BH3 iso5 inin	0	-2123.3243420	493.796580	-2122.483617	-2122.618958	BP86	TZVP/LANL2DZ	
ZrNMe2BH3ZrNMe2BH3 iso6 inin	0	-2123.3185933	494.283260	-2122.477599	-2122.610812	BP86	TZVP/LANL2DZ	
ZrDiDMABZrH iso 1	0	-2123.3112398	491.73454	-2122.472965	-2122.615033	BP86	TZVP/LANL2DZ	
ZrDiDMABZrH iso2	0	-2123.3139841	492.04464	-2122.475464	-2122.614604	BP86	TZVP/LANL2DZ	*
ZrDiDMABZrH iso2	0	-2124.6192868	509.92556	-2123.754743	-2123.888349	B3LYP-GDBJ	def2tzvp	*
ZrCCSiMe3ZrCH2SiMe3 sing	0	-1801.9810779	362.127210	-1801.360945	-1801.476921	BP86	TZVP/LANL2DZ	*
ZrCCSiMe3ZrCH2SiMe3 sing	0	-1803.1695811	375.095900	-1802.530892	-1802.641671	B3LYP-GDBJ	def2tzvp	
ZrCCSiMe3ZrCH2SiMe3 trip	0	-1801.9373784	360.97108	-1801.318057	-1801.441395	BP86	TZVP/LANL2DZ	
ZrCCSiMe3ZrCH2SiMe3 sing iso2	0	-1803.1729651	374.32702	-1802.535010	-1802.64791	B3LYP-GDBJ	def2tzvp	
ZrCCSiMe3ZrCH2SiMe3 iso2 TS CH3_1wrongTS	1	-1803.1689955	374.40746	-1802.531812	-1802.641643	B3LYP-GDBJ	def2tzvp	
ZrCCSiMe3ZrCH2SiMe3 iso2 TS CH2TMS rot.	1	-1803.1605963	374.49170	-1802.523170	-1802.633302	B3LYP-GDBJ	def2tzvp	
ZrCCSiMe3ZrCH2SiMe3 iso2 TS alkinyl	1	-1803.1250976	373.07566	-1802.489228	-1802.602995	B3LYP-GDBJ	def2tzvp	
ZrCCSiMe3ZrCH2SiMe3_H2_TS2	1	-1804.316733	383.101560	-1803.663672	-1803.778891	B3LYP-GDBJ	def2tzvp	
ZrCCSiMe3ZrCH2SiMe3_H2_Int2	0	-1804.324105	385.14723	-1803.66814	-1803.783559	B3LYP-GDBJ	def2tzvp	
ZrCCSiMe3ZrDMAB iso 1	0	-1514.5794360	348.26695	-1513.985283	-1514.09279	BP86	TZVP/LANL2DZ	
ZrCCSiMe3ZrDMAB iso 2	0	-1514.6188310	349.02625	-1514.023532	-1514.130243	BP86	TZVP/LANL2DZ	*
ZrCCSiMe3ZrDMAB iso 2	0	-1515.7996463	361.72586	-1515.185845	-1515.289202	B3LYP-GDBJ	def2tzvp	*
ZrCCSiMe3ZrH iso1 sing	0	-1353.9396980	282.693690	-1353.456036	-1353.552025	BP86	TZVP/LANL2DZ	*
ZrCCSiMe3ZrH iso1 sing	0	-1355.0583114	292.663250	-1354.560246	-1354.652465	B3LYP-GDBJ	def2tzvp	*
ZrCCSiMe3ZrH iso2 sing	0	-1353.9394425	282.561520	-1353.455922	-1353.552181	BP86	TZVP/LANL2DZ	
ZrCCSiMe3ZrH trip	0	-1353.9081220	281.590810	-1353.425597	-1353.524795	BP86	TZVP/LANL2DZ	
ZrCCCHZr TS1	1	-1803.1092222	371.202960	-1802.477398	-1802.587197	B3LYP-GDBJ	def2tzvp	
ZrCCCHZr Int1	0	-1803.1290998	373.565800	-1802.493422	-1802.602950	B3LYP-GDBJ	def2tzvp	
ZrCCCHZr TS2	1	-1803.0835794	373.919130	-1802.448163	-1802.555603	B3LYP-GDBJ	def2tzvp	
ZrCCCHZr TS2_2	1	-1803.0641057	371.944400	-1802.430770	-1802.541842	B3LYP-GDBJ	def2tzvp	
ZrCCCHZr Int2	0	-1803.1339716	373.934190	-1802.497961	-1802.606710	B3LYP-GDBJ	def2tzvp	
ZrCCCHZr Int2_2	0	-1803.1141298	374.442650	-1802.477024	-1802.585440	B3LYP-GDBJ	def2tzvp	
ZrCCCHZr TS3	1	-1803.0574056	373.424450	-1802.422438	-1802.530991	B3LYP-GDBJ	def2tzvp	
ZrCCCHZr TS3_2	1	-1803.0044991	370.728230	-1802.372795	-1802.484007	B3LYP-GDBJ	def2tzvp	

ZrCCCHZr Int3	0	-1803.1073663	373.959160	-1802.469770	-1802.585760	B3LYP-GDBJ	def2tzvp	
ZrNMe2BH3ZrNMe2BH3 iso2 inin	0	-2122.8245002	511.572440	-2121.957939	-2122.088209	B3LYP-GDBJ	def2svp	
ZrNMe2BH3ZrNMe2BH3 iso2 TS1	1	-2122.7662449	507.116070	-2121.906400	-2122.035415	B3LYP-GDBJ	def2svp	
ZrCCSiMe3ZrH_2_DMAB iso 1	0	-1677.386441	453.233320	-1676.617418	-1676.744214	B3LYP-GDBJ	def2svp	*
ZrCCSiMe3ZrH_2_DMAB iso 2	0	-1677.375716	452.946230	-1676.606782	-1676.735301	B3LYP-GDBJ	def2svp	
ZrCCSiMe3ZrH_2_DMAB iso 3	0	-1677.382508	452.915980	-1676.613839	-1676.743501	B3LYP-GDBJ	def2svp	
ZrCCSiMe3ZrH_DMAB_Int1	0	-1516.995146	373.18729	-1516.361164	-1516.470179	B3LYP-GDBJ	def2tzvp	*
ZrCCSiMe3ZrH_DMAB_Int2	0	-1516.973399	369.49668	-1516.345318	-1516.455498	B3LYP-GDBJ	def2tzvp	*
ZrCCSiMe3ZrH3_DMAoB_TS1 sp	0	-1516.968940	368.512200	-1516.345099	-1516.445368	B3LYP-GDBJ	def2tzvp	
ZrCCSiMe3ZrH3_DMAoB_TS1 opt	1	-1516.972909	369.375910	-1516.345930	-1516.452928	B3LYP-GDBJ	def2tzvp	
ZrCCSiMe3ZrH3_DMAoB_TS2 sp	0	-1516.966901	367.968320	-1516.343213	-1516.447374	B3LYP-GDBJ	def2tzvp	
ZrCCSiMe3ZrH3_DMAoB_TS2 opt	1	-1516.971008	368.654450	-1516.344212	-1516.457016	B3LYP-GDBJ	def2tzvp	
ZrCCSiMe3ZrH3_Int3	0	-1356.229746	302.35346	-1355.715222	-1355.811082	B3LYP-GDBJ	def2tzvp	*
ZrCCSiMe3ZrH3_TS3	1	-1356.212137	300.615250	-1355.699847	-1355.796412	B3LYP-GDBJ	def2tzvp	
ZrCCSiMe3ZrCH2SiMe3_H2_TS2	1	-1804.316733	383.101560	-1803.663672	-1803.778891	B3LYP-GDBJ	def2tzvp	
ZrCCSiMe3ZrCH2SiMe3_H2_Int2	0	-1804.324105	385.14723	-1803.66814	-1803.783559	B3LYP-GDBJ	def2tzvp	
Cp2ZrCCSiMe3ZrMe iso1 2Zr3	0	-1394.3867388	310.597640	-1393.858120	-1393.954423	B3LYP/GD3BJ	def2tzvp	*
Cp2ZrCCSiMe3ZrMe iso2 Zr4Zr2	0	-1394.3864998	310.509640	-1393.858009	-1393.954205	B3LYP/GD3BJ	def2tzvp	
Cp2ZrCCSiMe3ZrMe TS-iso1-iso2 CH3 rot	1	-1394.3838625	310.071170	-1393.856325	-1393.952139	B3LYP/GD3BJ	def2tzvp	
Cp2ZrCCSiMe3ZrMe TS-iso1-iso2 CH3 umbr.	1	-1394.359707	309.859630	-1393.832516	-1393.928814	B3LYP/GD3BJ	def2tzvp	
Cp2ZrCCSiMe3ZrMe TS-iso1-iso2 alkinyl	1	-1394.3401941	309.263810	-1393.813703	-1393.911480	B3LYP/GD3BJ	def2tzvp	
ZrCCSiMe3ZrCH3_H2_TS3_2	0	-1395.568022	317.79776	-1395.024413	-1395.129327	B3LYP/GD3BJ	def2tzvp	
ZrCCSiMe3ZrCH3_H2_Int1	0	-1395.567825	317.70989	-1395.024431	-1395.128456	B3LYP/GD3BJ	def2tzvp	
ZrCCSiMe3ZrCH3_H2_Int6_b3lyp_sp_freq_tzvp_step7	1	-1395.568889	321.28122	-1395.021933	-1395.122748	B3LYP/GD3BJ	def2tzvp	
ZrCCSiMe3ZrCH3_H2_scanTS5_sp_tzvp_step10	0	-1395.559231	321.71253	-1395.013969	-1395.105881	B3LYP/GD3BJ	def2tzvp	
ZrCCSiMe3ZrCH3_H2_scanTS5_sp_tzvp_step11	0	-1395.559231	321.71253	-1395.013969	-1395.105881	B3LYP/GD3BJ	def2tzvp	
ZrCCSiMe3ZrCH3_H2_Int5_b3lyp_opt_freq_tzvp	0	-1395.60142	321.31869	-1395.052895	-1395.158128	B3LYP/GD3BJ	def2tzvp	
hyrdogen	0	-1.1795214	5.90726	-1.166803	-1.181649	B3LYP/GD3BJ	def2tzvp/sp	
dimethylaminborane	0	-161.9151723	79.04775	-161.783022	-161.816279	B3LYP/GD3BJ	def2tzvp/sp	

Me2NBH2 C2V	0	-160.7326273	65.2668	-160.622842	-160.655295	B3LYP/GD3BJ	def2tzvp/sp	
ZrHZrH_cat	0	-1803.133015	370.34881	-1802.504882	-1802.607224	B3LYP/GD3BJ	def2tzvp/sp	
ZrHZrH_DMAB_Int1	0	-1965.06945	450.36683	-1964.307122	-1964.424006	B3LYP/GD3BJ	def2tzvp/sp	
ZrHZrH_DMAB_TS1	-1	-1965.008714	448.062	-1964.250895	-1964.364089	B3LYP/GD3BJ	def2tzvp/sp	
ZrHZrH_DMAB_Int2	0	-1965.062178	448.21015	-1964.302922	-1964.417788	B3LYP/GD3BJ	def2tzvp/sp	
ZrHZrH_DMAB_Int3	0	-1963.881297	438.32578	-1963.139526	-1963.251963	B3LYP/GD3BJ	def2tzvp/sp	
ZrHZrH_DMAB_TS2	0	-1963.862091	436.80642	-1963.12278	-1963.235929	B3LYP/GD3BJ	def2tzvp/sp	
ZrHZrH_DMAB_Int4	0	-1963.874597	436.99242	-1963.134039	-1963.249943	B3LYP/GD3BJ	def2tzvp/sp	
ZrHZrH_DMAB_Intx	0	-1965.0637	448.58241	-1964.30406	-1964.418117	B3LYP/GD3BJ	def2tzvp/sp	
ZrHZrH_DMAB_cat	0	-1963.881297	438.32571	-1963.139526	-1963.251963	B3LYP/GD3BJ	def2tzvp/sp	
ZrHZrH_2DMAB_Int1	0	-2125.819701	518.52124	-2124.943571	-2125.069642	B3LYP/GD3BJ	def2tzvp/sp	
ZrHZrH_2DMAB_TS1	-1	-2125.77456	517.19334	-2124.901714	-2125.022267	B3LYP/GD3BJ	def2tzvp/sp	
ZrHZrH_2DMAB_Int2	0	-2125.81529	516.64547	-2124.941471	-2125.067165	B3LYP/GD3BJ	def2tzvp/sp	
ZrHZrH_2DMAB_Int3	0	-2124.632202	506.21853	-2123.776711	-2123.899317	B3LYP/GD3BJ	def2tzvp/sp	
ZrHZrH_2DMAB_TS2	-1	-2124.620293	504.35207	-2123.767904	-2123.890933	B3LYP/GD3BJ	def2tzvp/sp	
ZrHZrH_2DMAB_Int4	0	-2124.622389	504.65338	-2123.768897	-2123.893011	B3LYP/GD3BJ	def2tzvp/sp	
ZrHZrH_DMAB_Int1	0	-1963.290254	451.20558	-1962.522505	-1962.653584	B3LYP/GD3BJ	def2svpp	
ZrHZrH_DMAB_TS1	-1	-1963.229069	449.1853	-1962.465739	-1962.590852	B3LYP/GD3BJ	def2svpp	
ZrHZrH_2DMAB_Int1	0	-2123.848334	520.00643	-2122.965501	-2123.105063	B3LYP/GD3BJ	def2svpp	
ZrHZrH_2DMAB_TS1	-1	-2123.803953	518.34128	-2122.924909	-2123.058285	B3LYP/GD3BJ	def2svpp	

7. References

[1] H. J. Drexler, A. Preetz, T. Schmid, D. Heller, "*Kinetics of Homogeneous Hydrogenations: Measurement and Interpretation*", chapter 10 in "*Handbook of Homogeneous Hydrogenation*", WILEY-VCH, J.G. de Vries , C.J. Elsevier, 257-295, 2007.

[2] Gaussian 09, Revision E.01, M. J. Frisch, G. W. Trucks, H. B. Schlegel, G. E. Scuseria, M. A. Robb, J. R. Cheeseman, G. Scalmani, V. Barone, B. Mennucci, G. A. Petersson, H. Nakatsuji, M. Caricato, X. Li, H. P. Hratchian, A. F. Izmaylov, J. Bloino, G. Zheng, J. L. Sonnenberg, M. Hada, M. Ehara, K. Toyota, R. Fukuda, J. Hasegawa, M. Ishida, T. Nakajima, Y. Honda, O. Kitao, H. Nakai, T. Vreven, J. A. Montgomery, Jr., J. E. Peralta, F. Ogliaro, M. Bearpark, J. J. Heyd, E. Brothers, K. N. Kudin, V. N. Staroverov, T. Keith, R. Kobayashi, J. Normand, K. Raghavachari, A. Rendell, J. C. Burant, S. S. Iyengar, J. Tomasi, M. Cossi, N. Rega, J. M. Millam, M. Klene, J. E. Knox, J. B. Cross, V. Bakken, C. Adamo, J. Jaramillo, R. Gomperts, R. E. Stratmann, O. Yazyev, A. J. Austin, R. Cammi, C. Pomelli, J. W. Ochterski, R. L. Martin, K. Morokuma, V. G. Zakrzewski, G. A. Voth, P. Salvador, J. J. Dannenberg, S. Dapprich, A. D. Daniels, O. Farkas, J. B. Foresman, J. V. Ortiz, J. Cioslowski, and D. J. Fox, Gaussian, Inc., Wallingford CT, **2013**.

[3] A. D. Becke, *Phys. Rev. A,* 1988, **38**, 3098–3100; b) J. P. Perdew, *Phys. Rev. B*, 1986, **33**, 8822–8824.

[4] a) P. J. Hay and W. R. Wadt, *J. Chem. Phys.*, 1985, **82**, 270–283; b) P. J. Hay and W. R. Wadt, *J. Chem. Phys*., 1985, **82**, 299–310.

[5] A. Schäfer, C. Huber and R. Ahlrichs, *J. Chem. Phys*., 1994, **100**, 5829–5835.

[6] J. Zhu, E.-L. Zins and M. E. Alikhani, *Phys. Chem. Chem. Phys.*, 2018, **20**, 15687-15695.

[7] a) S. H. Vosko, L.Wilk and M. Nusair, *Can. J. Phys*., 1980, **58**, 1200–1211; b) C. Lee, W. Yang and R. G. Parr, *Phys. Rev. B*, 1988, **37**, 785–789; c) B. Miehlich, A. Savin, H. Stoll and H. Preuss, *Chem. Phys. Lett*., 1989, **157**, 200–206; d) A. D. Becke, *J. Chem. Phys.*, 1993, **98**, 5648–5652.

[8] F. Weigend and R. Ahlrichs, *Phys. Chem. Chem. Phys.*, 2005, **7**, 3297–3305.

[9] S. Grimme, S. Ehrlich and L. Goerigk, *J. Comp. Chem.*, 2011, **32**, 1456-1465.

[10] https://www.ccdc.cam.ac.uk/support-and-resources/Downloads/